FE ANALYSIS OF PLASTIC BUCKLING OF PLATES WITH INITIAL IMPERFECTIONS AND SIMULATION OF EXPERIMENTS

By

Bing Liu

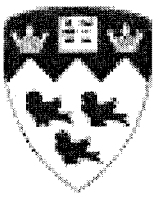

Department of Civil Engineering and Applied Mechanics
McGill University. Montreal, Quebec, Canada

A thesis submitted to the Faculty of Graduate and Postdoctoral Studies
in partial fulfillment of the requirements for the degree of
Master of Engineering

Your file Votre référence
ISBN: 978-0-494-51439-9
Our file Notre référence
ISBN: 978-0-494-51439-9

Abstract

The general problem of plastic buckling of flat metal plates is a fundamental area of investigation in mechanics not only because of its intrinsic importance in the design of engineering structures, but also because it still has not been settled in a satisfying manner. Which theory of plasticity is the correct one to predict the buckling loads in the plastic range is a long-argued problem.

This thesis presents finite element analyses of plastic buckling and postbuckling behaviour of columns and plates, taking into account the presence of initial out-of-plane imperfections. The FE programs constructed by the author for this purpose are used to analyze the imperfection growth of such columns and plates under axial loading and simply supported edge conditions. The material behaviour is modeled according to both the incremental and the deformation theories of strain-hardening plasticity. The programs combine both the geometric and material nonlinearities to trace the load-deflection behaviours of these structures in prebuckling (up to the maximum load) as well as postbuckling ranges. The results of the analyses for plates show the extreme sensitivity of the incremental theory, and the relative insensitivity of the deformation theory, to the initial imperfections.

The programs are used to simulate the plastic buckling experiments on Aluminum tubes, taking into account their measured imperfections. The imperfection growth analyses demonstrate that the maximum load predictions of the incremental theory are quite close to those recorded in the experiments.

Résumé

Le problème du flambage plastique des plaques minces métalliques est un sujet de recherche important en mécanique, non seulement dû à son importance pour la conception des structures, mais également parce qu'il n'a toujours pas été résolu adéquatement. Laquelle des théories de plasticité est correcte pour prédire les charges de flambage dans le domaine plastique ne fait pas l'unanimité.

Cette thèse présente une analyse d'éléments finis du comportement post-flambage de colonnes et de plaques, simplement appuyées, comprimées par une charge uniaxiale. Des analyses prenant en compte les imperfections initiales hors-plan sont effectuées à partir de théories élémentaires avec les suppositions cinématiques appropriées. Les résultats sont obtenus pour les deux théories de plasticité - théories incrémentale et de déformation - afin de les comparer. Les programmes d'éléments finis élaborés à cet effet combinent les non-linéarités géométriques et matérielles pour tracer le comportement charge-déformation dans les phases pré-flambage, flambage et post-flambage.

La propagation des imperfections initiales hors-plan, telle qu'enregistrée par des expériences, est simulée par le programme d'éléments finis. Les résultats sont comparés aux résultats expérimentaux.

Acknowledgments

I wish to express sincere appreciation to my research advisor Professor Suresh Shrivastava of the Department of Civil Engineering and Applied Mechanics, McGill University, for his support and guidance throughout the project.

I take this opportunity to thank my husband Bo Sun, for his moral support and love.

Dedicated to the most important person in my life

my mother, Yuzhen Jiang,

to whom I owe everything I am and I will be.

Table of Contents

Abstracts i
Resume (French) ii
Acknowledgments iii
Table of Contents v
List of Figures viii
List of Tables x
List of Symbols xi

Chapter 1. Introduction and Literature review 1
1.1 Motivation 1
1.2 Previous work at McGill University 3
1.3 Objective of the Present Study 3
1.4 Literature Review 4
1.5 Organization of the thesis 6

Chapter 2 Theory of Plastic Buckling and Postbuckling 8
2.1 Theory of Plasticity 8
2.1.1 Basic Assumptions of the Phenomenological Theories of Plasticity 8
2.1.2 Incremental Theory of Plasticity 10
2.1.3 Deformation Theory of Plasticity 14
2.1.4 Incremental Relations for Deformation Theory of Plasticity 16
2.2 Formulation of Finite Element Equilibrium Equations 18
2.2.1 Basic Assumptions of Finite Element Formulation 18
2.2.2 Total Strain Finite Element Formulation for Deformation Theory 18
2.2.3 Incremental Strain Formulation for Incremental Theory 21
2.3 Exact Analysis for Plastic Bifurcation Buckling of Axially Compressed SS Plates 23

Chapter 3 Plastic Buckling and Postbuckling of Columns 26
3.1 Strain-Displacement Relations 27
3.2 Elastic Column with Imperfections 30
3.3 Uniaxial Elastic-Plastic Stress-Strain Relations 31
3.4 Stiffness Matrix Formulation 32
3.4.1 Stiffness Matrix for Incremental Analysis — J_2 Incremental Theory 34

3.4.2 Stiffness Matrix for Total Analysis — J_2 Deformation Theory 35
3.5 Numerical Integration 36
3.6 Solution Procedure for Incremental Analysis 38
3.6.1 Elastic Buckling and Postbuckling..... 39
3.6.2 Plastic Buckling and Postbuckling, Increemental Theory 41
3.7 Plastic Buckling and Postbuckling, Deformation Theory 45
3.8 Comparison and Conclusions 46

Chapter 4 Plastic Buckling and Postbuckling of Plates 49
4.1 Strain-Displacement Relations 49
4.2 Stiffness Matrix Formulation..... 51
4.2.1 Stiffness Matrix for Incremental Analysis J_2 Incremental Theory 55
4.2.2 Stiffness Matrix for Total Analysis J_2 Deformation Theory 56
4.3 Numerical Integration 57
4.4 Solution Procedures..... 58
4.4.1 Solution Procedure for Incremental Load-Displacement Method 58
4.4.2 Solution Procedure for Total Load-Displacement Method 61
4.5 Results of Imperfection Sensitivity Analyses in Plastic Range 63
4.5.1 Elastic Buckling and Postbuckling of Square Plates 65
4.5.2 Elastic Buckling and Postbuckling of Rectangular Plates 67
4.5.3 Plastic Buckling and Postbuckling of Square Plates..... 70
4.5.3.1 Numerical Results for the Incremental Theory..... 71
4.5.3.2 Numerical Results for the Deformation Theory 73
4.5.4 Plastic Buckling and Postbuckling of Rectangular Plates..... 74
4.5.4.1 Numerical Results for the Incremental Theory..... 75
4.5.4.2 Numerical Results for the Deformation Theory 76
4.6 Comparison and Conclusion 78

Chapter 5 Comparison with the Experimental Results 83
5.1 Finite Element Simulation of Realistic Experimental Cases..... 83
5.1.1 Material Properties 83
5.1.2 Stress-Strain Relation 84
5.1.3 Initial Geometrical Imperfections 85
5.1.4 Boundary Conditions 85
5.1.5 Load Application 87
5.2 Representation of Initial Imperfections 87

5.3 Numerical Results 91
5.4 Discrepancy Analysis 97
5.4.1 Effect of material properties 97
5.4.2 Geometric Imperfections 98
5.4.3 Effects of boundary conditions 98
5.4.4 Effects of Eccentricity 99

Chapter 6 Conclusions and Future Work 100
6.1 Conclusions 100
6.2 Future Works 102

References 103

List of Figures

page

Fig. 2.1 Idealized uniaxial stress-strain curve 9
Fig. 2.2 Von Mises yield surface 10
Fig. 2.3 Uniaxially compressed plate simply supported at all four edges 24
Fig. 3.1 Bernoulli-Euler displacement model 28
Fig. 3.2 An initially curved beam element 29
Fig. 3.3 The six degrees of freedom of a beam element 33
Fig. 3.4 The distribution of 3×3 Gauss points in an element 37
Fig. 3.5 Elastic postbuckling behaviour of simply supported columns 40
Fig. 3.6 Plastic postbuckling of columns by incremental theory ($n = 5$)..... 44
Fig. 3.7 Plastic postbuckling of columns by incremental theory ($n = 10$) 44
Fig. 3.8 Plastic postbuckling of columns by deformation theory ($n = 5$) 45
Fig. 3.9 Plastic postbuckling of columns by deformation theory ($n = 10$) 46
Fig. 3.10Effect of initial imperfection on maximum load 48
Fig. 4.1 Kirchhoff thin plate deformation model 50
Fig. 4.2 Element geometry and nodal degrees of freedom 51
Fig. 4.3 Element nondimensional coordinate system and node numbering 52
Fig. 4.4 Location of Gauss points in an element 57
Fig. 4.5 Load condition and finite element mesh employed 66
Fig. 4.6 A symmetrical quater of the simply supported plate of Fig. 4.5 66
Fig. 4.7 Elastic postbuckling of a simply supported square plates 67
Fig. 4.8 FE mesh for elastic imperfection behaviour of a rect. plate ($L/B = 5$) 68
Fig. 4.9 Elastic postbuckling of rectangular plate ($L/B = 5$) 69
Fig. 4.10Plastic postbuckling of square plates by incremental theory ($B/t = 23$) 72
Fig. 4.11Plastic postbuckling of square plates by incremental theory ($B/t = 18$) 72
Fig. 4.12Plastic postbuckling of square plates by deformation theory ($B/t = 23$) 73
Fig. 4.13Plastic postbuckling of square plates by deformation theory ($B/t = 18$) 74
Fig. 4.14FE mesh for plastic imperfection behaviour of a rect. plate ($L/B = 5$) 75
Fig. 4.15Plastic postbuckling of rectangular plate ($L/B = 5$, $B/t = 23$)
by incremental theory 75
Fig. 4.16Plastic postbuckling of rectangular plates ($L/B = 5, B/t = 18$),
by incremental theory 76
Fig. 4.17Plastic postbuckling of rectangular plates ($L/B = 5$, $B/t = 23$)
by deformation theory 77

Fig. 4.18Plastic postbuckling of rectangular plates ($L/B = 5$, $B/t = 18$) by deformation theory 77
Fig. 4.19Numerical result comparision of square plates ($B/t = 23$) 78
Fig. 4.20Numerical result comparision of square plates ($B/t = 18$) 79
Fig. 4.21Numerical result comparision of rect. plates ($L/B = 5$, $B/t = 23$) 79
Fig. 4.22Numerical result comparision of rect. plates ($L/B = 5$, $B/t = 18$) 80
Fig. 5.1 Bilinear stress-strain relation 84
Fig. 5.2 Cross-section of a buckled hollow square tube 86
Fig. 5.3 Simply supported plate under uniform compression 86
Fig. 5.4 Initial imperfection profile of specimen 03 86
Fig. 5.5 Initial imperfection profile of specimen 04 89
Fig. 5.6 Initial imperfection profile of specimen 08 89
Fig. 5.7 Initial imperfection profile of specimen 11 89
Fig. 5.8 Initial imperfection profile of specimen 14 90
Fig. 5.9 Imperfection growth curves for specimen 03 91
Fig. 5.10Imperfection growth curves for specimen 04 92
Fig. 5.11Imperfection growth curves for specimen 08 93
Fig. 5.12Imperfection growth curves for specimen 11 94
Fig. 5.13Imperfection growth curves for specimen 14 95
Fig. 5.14Friction force along the loaded edges 98

List of Tables

		page
Table 3.1	Abscissae and weights of Gauss points for a column element	37
Table 3.2	Effect of Gauss points along x direction (mesh 3×5)	42
Table 3.3	Effect of Gauss points along z direction (mesh 3×3)	43
Table 3.4	Effect of Gauss points along z direction (mesh 3×2)	43
Table 3.5	Maximum loads by incremental and deformation theories ($n = 5$)	47
Table 3.6	Maximum loads by incremental and deformation theories ($n = 10$)	47
Table 3.7	Reduction in maximum loads	47
Table 4.1	Abscissae and weights of 2×2 Gauss points in $\xi\eta$ plane	58
Table 4.2	Abscissae and weights of Gauss points along ζ axis	58
Table 4.3	Maximum loads; effect of Gauss points in one element	71
Table 4.4	Maximum stress comparison (square plate $B/t = 23$)	80
Table 4.5	Maximum stress comparison (square plate $B/t = 18$)	81
Table 4.6	Maximum stress comparison (rect. plate $L/B = 5$, $B/t = 23$)	81
Table 4.7	Maximum stress comparison (rect. plate $L/B = 5$, $B/t = 18$)	81
Table 5.1	Comparison of incremental theory maximum stresses with experimental results	96
Table 5.2	Comparison of deformation theory maximum stresses with experimental results	96

List of Symbols

a, b	length and width of a typical plate finite element
$e = E/E_s - 1$	quantity used in J_2 deformation theory
h	the factor characterizing strain hardening of the material
l	length of a column element
m	number of buckled half waves in the x direction
n	number of buckled half waves in the y direction
n	exponent in the function describing the uniaxial stress-strain curve
q_i	nodal displacements
s_{ij}	deviatoric stress tensor
ds_{ij}	increment of deviatoric stress tensor
t	plate thickness or columns depth
u, v, w	middle plane displacements in x, y, z directions respectively
$\overline{u}, \overline{v}, \overline{w}$	displacements at a distance z from the middle plane
u_o, v_o, w_o	middle plane initial displacements in x, y, z directions respectively
u_i	three displacement variables in the three coordinate directions x_i
$u_{i,j}$	nine displacement gradients with respect to undeformed coords x_j
δu_i	virtual change in current displacements
w_0	initial imperfection function
x, y, z	Cartesian coordinates
$\alpha = \dfrac{3\,(\lambda - 1)}{4J_2}$	quantity used in J_2 incremental theory
$\beta = \dfrac{3(\gamma - 1)}{4J_2}$	quantity used in J_2 deformation theory
$\gamma = \dfrac{E_s}{E_t}$	quantity used in J_2 deformation theory
ε_{ij}	Green strain tensors, $\varepsilon_{ij} = \dfrac{1}{2}(u_{i,j} + u_{j,i} + u_{k,i}\,u_{k,j})$
$\delta\varepsilon_{ij}$	virtual change in Green strain tensor
$\delta\varepsilon_{ij}$	$= \dfrac{1}{2}(\delta u_{i,j} + \delta u_{j,i} + \delta u_{k,i}\,u_{k,j} + u_{k,i}\,\delta u_{k,j})$
ε^p_{ij}	plastic strain tensor
ε^e_{ij}	elastic strain tensor
ε	total strain in uniaxial test
ε^e	elastic strain in uniaxial test
ε^p	plastic strain in uniaxial test

ε_e^p	equivalent plastic strain
ε_L	linear part of strain
ε_N	nonlinear part of strain
$d\varepsilon_{ij}^p$	increment of plastic strain tensor
$d\varepsilon_{ij}^e$	increment of elastic strain tensor
ε_{ij}^o	initial strain associated with zero stress
ε_{ij}^T	total strain
ξ, η, ζ	non-dimensional coordinates
κ	strain hardening parameter
$\lambda = \dfrac{E}{E_t}$	quantity used in J_2 incremental theories
ν	Poisson's ratio
$\nu_s = \dfrac{E-(1-2\nu)E_s}{2E}$	effective Poisson's ratio in J_2 deformation theory
ρ	parameter related to imperfection magnitude
σ	stress in uniaxial test
σ_{ij}	Kirchhoff stress tensor
σ_{kk}	$\sigma_{kk} = \sigma_{xx} + \sigma_{yy} + \sigma_{zz}$
$d\sigma_{ij}$	increment of stress tensor
σ_{cr}	bifurcation buckling stress
σ_e	the von Mises equivalent stress
$\sigma_{\text{cr}}^{\text{def}}$	bifurcation stress of the J_2 deformation theory
$\sigma_{\text{cr}}^{\text{inc}}$	bifurcation buckling stress of the J_2 incremental theory
$\sigma_{\text{max}}^{\text{exp}}$	maximum experimental stress
$\sigma_{\text{max}}^{\text{def}}$	maximum stress of the J_2 deformation theory
$\sigma_{\text{max}}^{\text{inc}}$	maximum stress of the J_2 incremental theory
σ_Y	initial yield stress obtained from uniaxial stress-strain curve
σ_Y'	current yield, as a result of strain hardening
$\theta = \dfrac{\partial w}{\partial x}, \phi = \dfrac{\partial w}{\partial y}$	slopes along x, y directions respectively
φ	scalar used in J_2 deformation theory constitutive relations
A	arbitrary amplitude of the sinusoidal buckling mode
B	plate width
$A_1, B_1, C_1, D_1, F_1, R_1$	elastic/plastic moduli for exact plastic bifurcation analysis
$A_s, B_s, C_s, D_s,$ F_s, F_{s1}, F_{s2}	elastic/plastic moduli in J_2 deformation theory

A_t, B_t, C_t, D_t, F_t, F_{t1}, F_{t2}	elastic/plastic moduli in J_2 incremental theory
E	Young's modulus of elasticity
E_s	secant modulus
E_t	tangent modulus
F	yield function
G	shear modulus
H'	the slope of the uniaxial stress-plastic strain curve
J_2	the second invariation of deviatoric stress tensor
dJ_2	increment in J_2
L	column, or plate length
M_{xx}	moment stress resultant per unit length due to buckling in xz plane
M_{yy}	moment stress resultant per unit length due to buckling in yz plane
M_{xy}	moment stress resultant per unit length due to buckling in xy plane
P_{cr}	bifurcation load for the perfect column
P_i	externally applied nodal forces
W_i	weight coefficient in Gauss integration
$\{a\}$	the vector normal to the yield surface in the stress space
$\{u\}$	the vector of displacement variables
$\{q\}$	the vector of appropriate nodal displacements
$\{\delta q\}$	virtual displacements
$\{\sigma_L\}$	the stress vector arising from the linear strain
$\{\sigma_N\}$	the stress vector arising from the nonlinear strain
$[B]$	incremental strain-displacement matrix
$[B_L]$	linear part of the $[B]$ matrix
$[B_N]$	nonlinear part of the $[B]$ matrix
$[D]$	matrix of elastic moduli
$[D_s]$	matrix of secant elastic-plastic moduli in deformation theory
$[D_t]$	matrix of tangent elastic-plastic moduli in incremental theory
$[D_s^t]$	matrix of tangent elastic-plastic moduli in deformation theory
$[G]$	geometry matrix connecting rotations to nodal displacements
$[K_T]$	tangent stiffness matrix
$[K_S]$	secant stiffness matrix
$[K_L]$	small displacement stiffness matrix

$[K_N]$	large displacement stiffness matrix
$[K_\sigma]$	geometric stiffness matrix
$[N]$	the matrix of shape functions
$[N_1], [N_2]$	symmetric nonlinear stiffness matrix of secant stiffness matrix
$\{P\}$	external force vector
$\{\overline{P}\}$	internal force vector
$\{\Delta R\}$	out-of-balance force vector

Chapter 1

Introduction and Literature Review

1.1 Motivation

Plastic Buckling of plates is a subject of continuing interest due to not only its relevance in the design of technologically important structures, such as ships, bridges, and airplanes, but also because it continues to remain a "paradox" for researchers in this topic.

Historically, there have been two theories of strain-hardening plasticity in widespread use. One is the deformation theory of plasticity, and the other is the incremental theory. The incremental theory is accepted as the correct theory of plasticity from both theoretical and experimental points of view. On the other hand, the deformation theory, although simpler than the incremental theory, is generally considered to be an invalid theory of plasticity. However, the predictions of bifurcation loads of perfectly plane plates based on the incremental theory are unrealistically higher than the experimental results [1, 2]. On the other hand, paradoxically, the bifurcation loads predicted by the 'unacceptable' deformation theory are close to the buckling loads determined experimentally [1, 2]. The bifurcation loads for a cruciform column calculated by the two theories best illustrate the above-mentioned discrepancy. The basic difference between the two theories is that whereas the incremental theory is strain-path dependent, the deformation theory is not. In particular, the deformation theory does not take into account the elastic unloading of the material from a state of plasticity. This is important, because of the influence of elastic unloading on the postbuckling behaviour. In plastic buckling, the bifurcation occurs under increasing load, as was shown experimentally by Shanley [3]. Therefore, the maximum load is obtained after bifurcation, though quite soon. Elastic unloading begins after the maximum load [4] and the additional buckling deflections occur under decreasing load. This paradox has prompted researchers to find ways to lower the predictions of the incremental theory to realistic levels. Onat and Drucker [5] showed that the maximum loads predicted by the incremental theory are very sensitive to initial geometric imperfections of plates. They analyzed the buckling of a cruciform column (which models the buckling of a long rectangular plate under uniaxial

compression with three edges simply supported) and showed that the maximum load is much lower than the bifurcation load even for small 'unavoidable' imperfections.

Later, the plastic buckling paradox was examined by Sewell [6, 7]. He obtained somewhat lower buckling loads by using an incremental theory which allowed a corner in the yield surface and hence a variation in the direction of the normal at the corner; the normal represents the direction of the vector of the plastic strain increments. In a subsequent study, Sewell [8] illustrated that use of the Tresca yield surface, which has corners unlike the smooth Mises yield surface, brings about significant reduction in the buckling loads. Neale [9] demonstrated the sensitivity of the maximum load predictions of simply supported rectangular plates to initial geometric imperfections, using the J_2 incremental theory and a semi-analytical method. Needleman and Tvergaard [10] performed a purely numerical study on the effect of in-plane boundary conditions for square plates loaded in uniaxial compression. An extensive discussion of the buckling paradox, together with several examples, was given by Hutchinson [4] who did not rule out the use of the deformation theory by arguing that it can be regarded as an incremental theory allowing the development of a corner on its yield surface. He also stated that Sewell's [8] use of Tresca yield surface does not provide a generally applicable answer, since it would not, for example, lead to any improvement in the bifurcation load of the cruciform column. The experimental evidence concerning the existence of sharp corners on yield surfaces is not conclusive. Thus, generally, imperfection sensitivity provides a widely accepted explanation for the buckling paradox.

As indicated previously, in plastic buckling, the maximum load, even for a perfect plate, is only slightly higher than the bifurcation buckling load [4, 11]. Therefore, it can be expected that the inclusion of realistic out-of-plane imperfections would reduce the theoretical maximum loads of the incremental theory to values less than the bifurcation loads of the deformation theory. Indeed, in the experiments of Berrada [12], the observed maximum loads of the imperfect plates were sometimes higher than the bifurcation loads predicted by the deformation theory. Therefore, it is unlikely that an imperfection growth analysis carried out by using the deformation theory for simply supported plates, could increase the theoretical maximum load to those observed in the experiments. On the other hand, since the incremental theory is imperfection-sensitive, the predicted maximum loads for the tested specimens could well be close to the experimental loads. Such results would then provide the much needed experimental validation of the incremental theory, so far demonstrated only by hypothetical numerical examples.

1.2 Previous work at McGill University

An experimental study of the plastic buckling of plane rectangular aluminum plates under uniaxial compression and simply supported edge conditions was performed by Berrada [12] in 1985. The plates were simulated by the four sides of hollow square tubes. In all, twenty-one tubes were tested incorporating a wide range of width to thickness ratios for buckling in the plastic range. All specimens in the experiment were annealed in an effort to approach the ideal elastic-plastic material properties postulated in the theories of plasticity. The behaviour of the specimens during the tests was monitored by recording the out-of-plane displacements, average stress-strain curves, and the axial load. The experimental buckling load was taken to be the maximum load. On the other hand, the theoretical buckling loads were computed as the bifurcation buckling loads according to both, the J_2 incremental and J_2 deformation theories of plasticity. These results were determined using the average stress-strain curves of each specimen. Based on the above definitions of experimental and theoretical buckling loads, it was found that neither of the theories provided close correlation with experiments. In particular, the bifurcation buckling loads based on the J_2 incremental theory were found to be totally unrealistic in being too high. In contrast, the results of the J_2 deformation theory were found to be generally lower than the experimental results.

1.3 Objectives of the Present Study

In order to find agreement with the experimental results, an imperfection growth analysis using the J_2 incremental theory is needed. In this study, the main objective is to use the finite element method to analyze the plastic buckling and postbuckling behaviours of simply supported columns and plates based on both the J_2 incremental and J_2 deformation theories of plasticity. It should be noted that in the context of the imperfection analysis, buckling is identified with reaching the maximum load, and hence the postbuckling with the load-displacement behaviour after the occurrence of the maximum load.

Three main objectives are pursued:

(1) To perform imperfection growth analyses using the J_2 incremental theory of plasticity for columns and plates.

(2) To perform imperfection growth analyses using the J_2 deformation theory of plasticity for columns and plates.

(3) To compare the maximum load predictions of the two theories against each other, and whenever possible, compare the numerical results of the two theories with experiments.

To achieve these objectives, in a transparent and flexible manner, finite element programs were constructed by the author using the *Mathematica* software. This required taking into account material as well as geometric nonlinearities. The effect of imperfections, large deflections, and strain-hardening plastic behaviour were included in the programs.

1.4 Literature Review

In order to predict the load-deflection paths of imperfect columns and plates in the elastic/plastic regime of material behaviour, analyses including the effects of geometric as well as material nonlinearities are conducted in this thesis. In this section, previous investigations on nonlinear analyses are discussed, along with a brief introduction to the present approaches to these topics.

1.4.1 Geometrically Nonlinear Finite Element Analysis

The first work on the extension of the finite element procedure to geometrically nonlinear structures is attributed to Turner et al [13]. Most of the earlier analyses were concerned with linear elastic buckling problems [14, 15, 16, 17]. Although a linear stability analysis is convenient from a mathematical viewpoint, it is quite restrictive in practical applications. For predicting realistic nonlinear load-deflection behaviours of a structure, incremental approaches were first adopted [13,18]. These approaches involved formulating the nonlinear stiffness matrices related to the rotations of the material elements, and continual updating of the geometry of the deforming structure. Mallet and Marcal [19] showed that for elastic structures, a total Lagrangian approach could be adopted if an 'initial displacement' matrix was added to the formulation. This approach was more efficient than the updating approach, and gave better solutions when a small number of elements were used [20].

In using the incremental approach, great care must be exercised to prevent an unacceptable buildup of errors. To minimize this problem, Newton-Raphson iteration method can be adopted [19, 21]. In general, for problems involving instability, it is some times difficult to achieve convergence to the true equilibrium state. For this reason, combination of incremental and iterative methods were developed by a number of investigators, see for example References [22, 23]. Incremental stiffness procedure is used for a certain number of load steps, and equilibrium correction is then applied by performing the Newton-Raphson iterations. Murray and Wilson [22] determined the imbalance in the nodal forces at the end of a load increment, and used an iterative approach to reduce the imbalance to zero. For problems involving instability, however, updating of the stiffness matrix is essential.

1.4.2 Materially Nonlinear Finite Element Analysis

Nonlinear effects due to plasticity have been tackled either by the tangent modulus or the secant modulus approach. The tangent modulus approach is an incremental approach, and requires constitutive relations relating the incremental stresses to the incremental strains. For thin plate elements, because of the assumption that the strain/stress components in the thickness direction can be ignored, the finite element may be regarded as a multi-layered system with each layer in a state of plane stress. The material nonlinearity is included by allowing each layer to have variable mechanical properties as the state of the material changes in the loading process. The secant modulus approach, on the other hand, requires constitutive relations relating the total stresses to the total strains. The total Lagrangian method may therefore be used in such cases.

For the incremental theory of plasticity, because of its incremental nature, the tangent modulus approach is followed [24]. Some researchers, however, adopted a modified Newton-Raphson approach [25, 26] to solve such problems. Since the elastic-plastic moduli in the tangent modulus approach are functions of the current stress levels, small load increments must be used in the incremental analyses.

For the deformation theory, both approaches are possible. A finite element analysis using the tangent moduli derived from the total moduli with the effect of the initial stress included, was performed by El-Ghazaly, Dubey and Sherbourne [27]. The secant modulus approach has been used in the present study, as it is the easier approach in the present context.

1.4.3 Combined Geometrically and Materially Nonlinear Finite Element Analysis

Early works in the field of combined nonlinearities were concerned with the buckling of plates [28, 29] using the Stowell-Ilyshin [30, 31] plastic buckling theory. An approximate combination of geometric and material nonlinearities was given by Murray and Wilson [32] who extended their earlier work on large elastic deflection analysis [22]. They used the deformation theory for the material nonlinearity. The investigation of the postbuckling behaviour and imperfection sensitivity of a simply supported square plate under axial compression was carried out by Needleman and Tvergaard [10]. The imperfection sensitivity was studied through an analytical asymptotic analysis of the behaviour of the hypoelastic plate, the material model that results from neglecting the effect of elastic unloading. The results of the asymptotic analyses were compared with the results of the incremental numerical analysis based on a combined finite element-Rayleigh Ritz method.

Numerical integration plays a very important role in nonlinear finite element analysis. The integration process within the element is considered in some detail by Stricklin et al [33]. The trapezoidal rule was initially used for integration through the depth of the plate, but Simpson's rule was later adopted. This change led to more accurate results with a smaller number of integration stations. Simpson's rule was preferred to Gaussian quadrature since the latter does not account for the zero surface stresses in plate problems. However, this restriction is not of a major importance from the viewpoint of predicting buckling loads. For example, Crisfield [34] adopted Gauss integration method to analyze elastic-plastic buckling of plates, and obtained satisfactory results.

1.5 Organization of the Thesis

In Chapter 2, a presentation is made of the two plasticity theories, J_2 incremental and J_2 deformation, required for imperfection-growth analyses, and finite element formulation of the present nonlinear problems.

In Chapters 3 and 4, the buckling behaviours of simply supported columns and simply supported plates with initial imperfections, subjected to uniaxial compressive forces are examined by means of the finite element method. The detailed procedures including

stiffness matrix formulation, numerical integration, and stress updating for the one-dimensional column problems and the two-dimensional plate problem are illustrated in these two chapters respectively. The two J_2 plasticity theories are used to calculate the maximum loads of imperfect columns and plates, and a comparison is made between the results. The load-deflection curves, before and after the maximum load, are traced by using the Newton-Raphson method of solving nonlinear algebraic equations, in conjunction with the displacement control option. Sensitivity of the buckling behaviour to imperfection magnitudes is also studied.

In Chapter 5, the FE programs developed in accordance with the two plasticity theories in Chapter 4 are applied to the task of imperfection analysis of the specimens tested by Berrada [12]. Load displacement paths, up to and beyond the maximum load points, are calculated using the initial imperfections measured for the test specimens. These maximum loads predictions for the two theories are compared with the experimental results, as well as with the predictions of the bifurcation loads of the two theories.

Conclusions and suggestions for future work form the contents of Chapter 6.

Chapter 2

Theory of Plastic Buckling and Postbuckling

This chapter presents parts of the plasticity theory required for imperfection-buckling analyses, and also an outline of the finite element formulation needed for such analyses.

2.1 Theories of Plasticity

2.1.1 Basic Assumptions of the Phenomenological Theories of Plasticity

The constitutive relations for commonly used phenomenological theories of plasticity for ductile metals are based upon the following basic assumptions. For a thorough presentation, the reader may consult standard book on this subject [35].

(1) The material is initially isotropic and homogeneous, and remains so during the elastic-plastic deformations. Thus, no Bauschinger effect is considered to be present.

(2) There is no volume change associated with the plastic strains.

(3) The strain components remain small in comparison to unity.

(4) Only the isothermal, time-independent, plastic behaviour is considered.

A suitable plasticity theory is assumed to incorporate the following characteristics of the uniaxial (tension or compression) stress-strain behaviour, Fig. 2.1. The straight line AB represents the linear elastic response with B denoting the yield point, which marks the beginning of the plastic deformations. The line BC and its extension correspond to strain-hardening elastic-plastic behaviour. At a stress level σ on this line, the elastic strain, recoverable by unloading to zero stress, is equal to $\varepsilon^e = \sigma/E$ where E is the Young's modulus, assumed to remain unchanged. The plastic part, or the irrecoverable part of strain is therefore $\varepsilon^p = \varepsilon - \sigma/E$ where ε is the total strain. In a subsequent reloading from D, the response is elastic until the previous stress (from which unloading was effected), is reached, here denoted by point C. Therefore, there is an increase in

yield stress with increase in plastic strain. The yield stress is thus a function of the plastic strain present in the material, i.e., $\sigma_y = \sigma(\varepsilon^p)$.

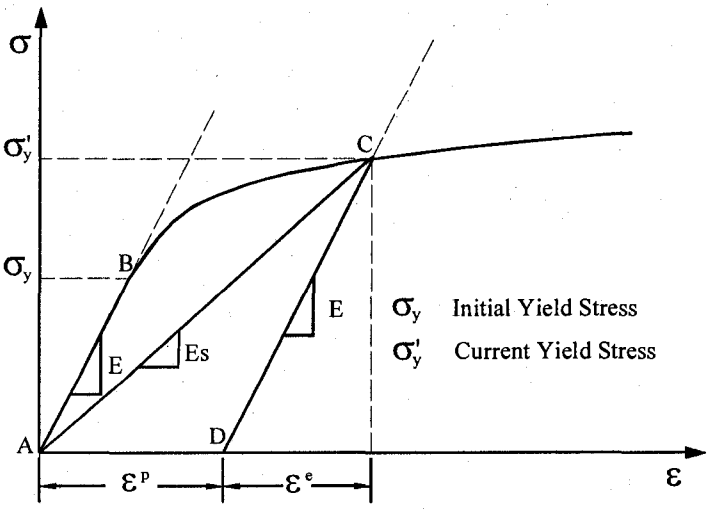

Fig. 2.1 Idealized uniaxial stress-strain curve

In the general three dimensional stress conditions, yielding is determined by a yield criterion taking into account the interaction of the stress components present. The usual assumption made is that the yield criterion is direction independent, and is therefore a function of the invariants of the stress tensor and the accumulated plastic strain. The yield criterion is represented by a yield surface in the stress space. This yield surface evolves with the amount of plastic deformation (i.e., the accumulated plastic strain) beginning with the initial yield surface. The yield surface is assumed to expand uniformly with increasing plastic strain in accordance with the isotropic hardening assumption of material behaviour. The current stress point may lie either inside or on the current yield surface. If it lies inside, then any infinitesimal change in stress components will result only in additional infinitesimal elastic strains, If it lies on the yield surface, then such a change might take the stress point outside the current yield surface to a new surface, keep it on the current surface, or bring it inside. These changes are termed loading, neutral loading, and unloading respectively. Plastic deformations are produced only when loading takes place. Neutral loading and unloading produce only elastic strains.

In this study, the material is assumed to obey the J_2, i.e., the von Mises yield criterion, and the corresponding yield surface is assumed to undergo uniform expansion in the

stress space with increasing plastic deformations, Fig. 2.2. The yield function can be expressed as:

$$F = \sigma_e - \sigma'_Y = \sqrt{3J_2} - \sigma'_Y(\varepsilon_{ep}) \tag{2.1}$$

where $J_2 = \frac{1}{2}s_{ij}s_{ij}$ is the second invariant of the deviatoric stress $s_{ij} = \sigma_{ij} - \frac{1}{3}\sigma_{kk}\delta_{ij}$. By definition, $\sigma_e = \sqrt{\frac{3}{2}s_{ij}s_{ij}} = \sqrt{3J_2}$ is the von Mises equivalent stress, and σ'_Y is the largest value of σ_e reached in the previous plastic straining. The equivalent plastic strain increment is defined as $d\varepsilon_{ep} = \sqrt{\frac{2}{3}d\varepsilon^p_{ij}\,d\varepsilon^p_{ij}}$ and the accumulated equivalent plastic strain as $\varepsilon_{ep} = \int d\varepsilon_{ep}$, where the integral is along the strain path the particular material element has been subjected to. In a uniaxial test, $\sigma_e = \sigma, \varepsilon_{ep} = \varepsilon^p$. Elastic response is predicted when $F < 0$, and the possibility of plastic straining (i.e., yielding) when $F = 0$. The concepts of equivalent stress and equivalent strain are useful in establishing the connection of general states of stress and strain to uniaxial stress and strain, as will be seen subsequently.

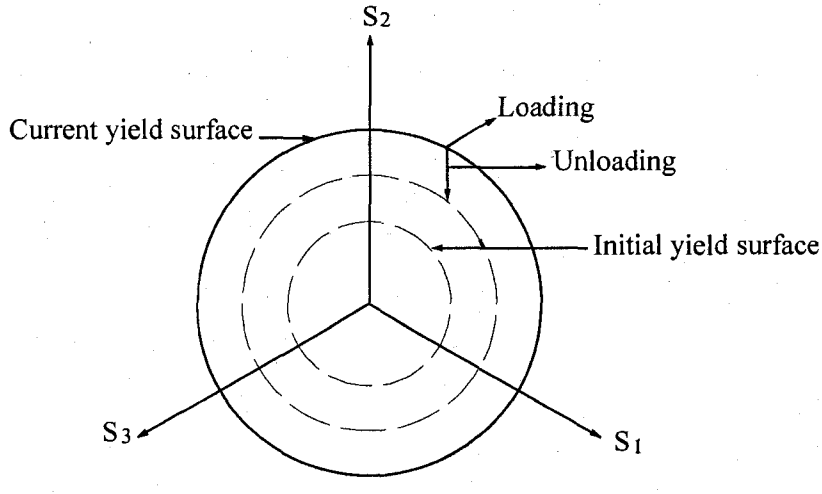

Fig. 2.2 von Mises yield surface

2.1.2 Incremental Theory of Plasticity

During plastic deformations, the yield criterion $F = 0$ must continue to hold. Hence, from Eq. (2.1) one obtains, for stress increments corresponding to yielding, the condition

$$dF = \frac{\partial F}{\partial \{\sigma\}}\{d\sigma\} + \frac{\partial F}{\partial \sigma'_Y}\frac{\partial \sigma'_Y}{\partial \varepsilon_{ep}} d\varepsilon_{ep} = \{a\}^T\{d\sigma\} - A' d\varepsilon_{ep} = 0 \tag{2.2}$$

where $\{a\}^T = \dfrac{\partial F}{\partial \{\sigma\}}$ is the vector normal to the yield surface in the stress space, and A' is related to the hardening characteristic of the material as represented by its uniaxial stress-strain curve. For associative incremental theory of plasticity, the plastic strain increments are postulated to be proportional to this vector so that

$$\{d\varepsilon^p\} = h\,\{a\} \tag{2.3}$$

where the proportionality factor h is related to hardening characteristic of the material. This equation is known as the flow rule. Employing the index notation, the vector $\{a\}$ for the von Mises yield condition is the deviatoric stress tensor s_{ij}, and the flow rule may be written as

$$d\varepsilon^p_{ij} = h\, s_{ij} \tag{2.4}$$

Now, the incremental yield condition can be expressed as

$$d\sigma_e - A' d\varepsilon_{ep} = 0 \tag{2.5}$$

Applying this condition to a uniaxial test, for which $d\sigma_e = d\sigma,\ d\varepsilon_{ep} = d\varepsilon_p$, one obtains

$$A' = \frac{d\sigma_e}{d\varepsilon_{ep}} = \frac{d\sigma}{d\varepsilon_p} = \frac{1}{(\frac{1}{E_t} - \frac{1}{E})} \tag{2.6}$$

On the other hand, using the flow rule, one obtains

$$\frac{1}{\sqrt{\frac{3}{2}s_{ij}s_{ij}}}\frac{3}{2}\frac{d\varepsilon^p_{ij}}{h} ds_{ij} - A' d\varepsilon_{ep} = 0 \tag{2.7}$$

for which the uniaxial test gives

$$\frac{3}{2\sigma}\frac{d\sigma}{h} - A' = 0 \tag{2.8}$$

hence

$$h = \frac{3\,d\sigma}{2A'\sigma} = \frac{3(E - E_t)d\sigma_e}{2E\,E_t\sigma_e} \tag{2.9}$$

The flow rule may therefore be written as

$$d\varepsilon_{ij}^p = (\frac{1}{E_t} - \frac{1}{E})\frac{3\,dJ_2}{4\,J_2}s_{ij} = \frac{3\,(\lambda - 1)\,dJ_2}{4\,EJ_2}s_{ij} \tag{2.10}$$

where $\lambda = \dfrac{E}{E_t}$.

Now for the plate problems to be considered here, it will be assumed that insofar as the constitutive relations are concerned, the state of stress is that of plane stress. Accordingly the relevant stress and strain components are only σ_{11}, σ_{22}, σ_{12} and ε_{11}, ε_{22}, ε_{12} and their increments. One has therefore

$$J_2 = \frac{1}{2}(s_{11}^2 + s_{22}^2 + s_{33}^2 + 2s_{12}^2) = s_{11}^2 + s_{22}^2 + s_{11}\,s_{22} + s_{12}^2 \tag{2.11}$$

$$dJ_2 = s_{11}d\sigma_{11} + s_{22}d\sigma_{22} + 2s_{12}d\sigma_{12} \tag{2.12}$$

Hence, the plastic strain increments are

$$\begin{bmatrix} d\varepsilon_{11}^p \\ d\varepsilon_{22}^p \\ 2d\varepsilon_{12}^p \end{bmatrix} = \frac{3(\lambda - 1)}{4\,EJ_2}\begin{bmatrix} s^2{}_{11} & s_{11}s_{22} & 2s_{11}s_{12} \\ s_{22}s_{11} & s^2{}_{22} & 2s_{22}s_{12} \\ 2s_{12}s_{11} & 2s_{12}s_{22} & 4\,s^2{}_{12} \end{bmatrix}\begin{bmatrix} d\sigma_{11} \\ d\sigma_{22} \\ d\sigma_{12} \end{bmatrix} \tag{2.13}$$

On the other hand, the elastic strains increments, are taken as the incremental form of the standard Hooke's law for isotropic materials, i.e.,

$$d\varepsilon_{ij}^e = \frac{1+\nu}{E}d\sigma_{ij} - \frac{\nu}{E}d\sigma_{kk}\delta_{ij} \tag{2.14}$$

Or, explicitly as

$$\begin{bmatrix} d\varepsilon_{11}^e \\ d\varepsilon_{22}^e \\ 2d\varepsilon_{12}^e \end{bmatrix} = \frac{1}{E}\begin{bmatrix} 1 & -\nu & 0 \\ -\nu & 1 & 0 \\ 0 & 0 & 2+2\,\nu \end{bmatrix}\begin{bmatrix} d\sigma_{11} \\ d\sigma_{22} \\ d\sigma_{12} \end{bmatrix} \tag{2.15}$$

The total strain increments, taken as the sum of the elastic and plastic parts, are

$$d\varepsilon_{11} = \{1 + \frac{3(\lambda-1)}{4J_2}s_{11}^2\}\frac{d\sigma_{11}}{E} + \{-\nu + \frac{3(\lambda-1)}{4J_2}s_{11}s_{22}\}\frac{d\sigma_{22}}{E} + \frac{3(\lambda-1)}{4J_2}2s_{11}s_{12}\frac{d\sigma_{12}}{E}$$

$$d\varepsilon_{22} = \{-\nu + \frac{3(\lambda-1)}{4J_2}s_{11}s_{22}\}\frac{d\sigma_{11}}{E} + \{1 + \frac{3(\lambda-1)}{4J_2}s_{22}^2\}\frac{d\sigma_{22}}{E} + \frac{3(\lambda-1)}{4J_2}2s_{22}s_{12}\frac{d\sigma_{12}}{E} \qquad (2.16)$$

$$2d\varepsilon_{12} = \frac{3(\lambda-1)}{4J_2}2s_{11}s_{12}\frac{d\sigma_{11}}{E} + \frac{3(\lambda-1)}{4J_2}2s_{22}s_{12}\frac{d\sigma_{22}}{E} + \{2 + 2\nu + \frac{3(\lambda-1)}{4J_2}4s_{12}^2\}\frac{d\sigma_{12}}{E}$$

The inverted relations required for the finite element application can now be obtained in closed form by using the *Mathematica* software. For simplifying the presentation, the inverted relations can be expressed as

$$\begin{bmatrix} d\sigma_{11} \\ d\sigma_{22} \\ d\sigma_{12} \end{bmatrix} = \begin{bmatrix} B_t & C_t & F_{t1} \\ C_t & D_t & F_{t2} \\ F_{t1} & F_{t2} & F_t \end{bmatrix} \begin{bmatrix} d\varepsilon_{11} \\ d\varepsilon_{22} \\ 2d\varepsilon_{12} \end{bmatrix} \qquad (2.17)$$

where

$$B_t = \frac{1}{A_t}[\alpha\{2s_{12}^2 + s_{22}^2(1+\nu)\} + (1+\nu)]$$

$$C_t = \frac{1}{A_t}[\alpha\{2\nu s_{12}^2 - (1+\nu)s_{11}s_{22}\} + \nu(1+\nu)\}$$

$$D_t = \frac{1}{A_t}[\alpha\{2s_{12}^2 + s_{11}^2(1+\nu)\} + (1+\nu)]$$

$$F_t = \frac{1}{2A_t}[\alpha\{(s_{11}^2 + s_{22}^2) + 2\,\nu\, s_{11}s_{22}\} + (1-\nu^2)] \qquad (2.18)$$

$$F_{t1} = -\frac{\alpha}{A_t}(s_{12}s_{11} + \nu s_{12}s_{22})$$

$$F_{t2} = -\frac{\alpha}{A_t}(s_{12}s_{22} + \nu s_{12}s_{11})$$

and where

$$A_t = \frac{(1+\nu)}{E}[\alpha\{s_{11}^2 + s_{22}^2 + 2s_{12}^2 + 2\,\nu(s_{11}s_{22} - s_{12}^2)\} + 1 - \nu^2],$$

$$\alpha = \frac{3\,(\lambda - 1)}{4J_2}, \text{ and } \lambda = \frac{E}{E_t}.$$

When $\lambda = 1$, the above relations collapse to those for purely elastic behaviour. In the following, the above relations will be referred to in a symbolic form as

$$\{d\sigma\} = [D_t]\{d\varepsilon\} \tag{2.19}$$

where $[D_t]$ will be called the matrix of the tangent moduli.

2.1.3 Deformation Theory of Plasticity

The deformation theory postulates relations between total stress and total strain. It may be considered suitable for simple deformation processes. There is no elastic unloading, and there is no dependency of stress on the strain path. The stresses are uniquely related to strains like in nonlinear elasticity with deformation dependent moduli. For J_2 deformation theory, the plastic strains are postulated to be proportional to the deviatoric stress

$$\varepsilon_{ij}^p = \varphi\, s_{ij} \tag{2.20}$$

where s_{ij} is the deviatoric stress tensor defined previously, and φ is a proportionality factor. This relation ensures that the plastic volume change is zero. If the above equation is contracted with itself, one obtains

$$\varepsilon_{ij}^p \varepsilon_{ij}^p = \varphi^2 s_{ij} s_{ij} \tag{2.21}$$

The factor φ is therefore given by

$$\varphi = \frac{\sqrt{\varepsilon_{ij}^p\, \varepsilon_{ij}^p}}{\sqrt{s_{ij}s_{ij}}} = \frac{3\varepsilon_e^p}{2\sigma_e} = \frac{3}{2}\left(\frac{E - E_s}{EE_s}\right) \tag{2.22}$$

where the equivalent stress is according to the previous definition, $\sigma_e = \sqrt{\frac{3}{2}s_{ij}s_{ij}}$, and the equivalent strain is obtained as $\varepsilon_e^p = \sqrt{\frac{2}{3}\varepsilon_{ij}^p\varepsilon_{ij}^p}$. Also, $E_s = \frac{\sigma_e}{\varepsilon_e}$ is the secant modulus

obtained from a uniaxial stress-strain σ-ϵ curve at stress level $\sigma = \sigma_e$. Hence the plastic part of the stain can be written as

$$\varepsilon_{ij}^{p} = \frac{3}{2}\left(\frac{E - E_s}{EE_s}\right)s_{ij} = \frac{3e}{2E}(\sigma_{ij} - \frac{\sigma_{kk}}{3}\delta_{ij}) \tag{2.23}$$

where

$$e = \frac{E}{E_s} - 1$$

The elastic strains are related to the stress tensor and are given by Hooke's law for an isotropic materials as

$$\varepsilon_{ij}^{e} = \frac{1+\nu}{E}\sigma_{ij} - \frac{\nu}{E}\sigma_{kk}\delta_{ij} \tag{2.24}$$

The total strain tensor, $\varepsilon_{ij} = \varepsilon_{ij}^{e} + \varepsilon_{ij}^{p}$, is the sum of the elastic and plastic parts

$$\varepsilon_{ij} = \frac{2 + 2\nu + 3e}{2E}\sigma_{ij} - \frac{2\nu + e}{2E}\sigma_{kk}\delta_{ij} \tag{2.25}$$

Now, as previously, it will be assumed that $\varepsilon_{13} = \varepsilon_{23} = \sigma_{13} = \sigma_{23} = \sigma_{33} = 0$, and ε_{33} ignored. These stress and strain components therefore do not enter into the constitutive equations corresponding to the plane stress assumption for plate behaviour. Accordingly,

$$\begin{bmatrix} \varepsilon_{11} \\ \varepsilon_{22} \\ 2\varepsilon_{12} \end{bmatrix} = \frac{1}{2E}\begin{bmatrix} 2+2e & -(2\nu+e) & 0 \\ -(2\nu+e) & 2+2e & 0 \\ 0 & 0 & 2(2+2\nu+3e) \end{bmatrix}\begin{bmatrix} \sigma_{11} \\ \sigma_{22} \\ \sigma_{12} \end{bmatrix} \tag{2.26}$$

The desired constitutive relations for use in finite element formulation are the inverted ones, expressing stress in terms of strain. They are found to be

$$\begin{bmatrix} \sigma_{11} \\ \sigma_{22} \\ \sigma_{12} \end{bmatrix} = \frac{2E}{\Delta}\begin{bmatrix} 2+2e & (2\nu+e) & 0 \\ (2\nu+e) & 2+2e & 0 \\ 0 & 0 & \dfrac{(2-2\nu+e)}{2} \end{bmatrix}\begin{bmatrix} \varepsilon_{11} \\ \varepsilon_{22} \\ 2\varepsilon_{12} \end{bmatrix} \tag{2.27}$$

where

$$\Delta = (2 - 2\nu + e)(2 + 2\nu + 3e)$$

For elastic behaviour, $E_s = E$, or equivalently $e = 0$ in the above relations. When needed in the sequel, the above relations will be referred to in a symbolic form as

$$\{\sigma\} = [D_s]\{\varepsilon\} \tag{2.28}$$

and $[D_s]$ will be called the matrix of the secant moduli.

2.1.4 Incremental Relations for Deformation Theory of Plasticity

One may also obtain the incremental form of the deformation theory constitutive law. These relations follow upon differentiating the above total relations, and are expressible as

$$\begin{aligned}
d\varepsilon_{11} &= \{1 + \frac{3(\gamma-1)}{4J_2}s^2{}_{11}\}\frac{d\sigma_{11}}{E_s} + \{-\nu_s + \frac{3(\gamma-1)}{4J_2}s_{11}s_{22}\}\frac{d\sigma_{22}}{E_s} + \frac{3(\gamma-1)}{4J_2}2s_{11}s_{12}\frac{d\sigma_{12}}{E_s} \\
d\varepsilon_{22} &= \{-\nu_s + \frac{3(\gamma-1)}{4J_2}s_{11}s_{22}\}\frac{d\sigma_{11}}{E_s} + \{1 + \frac{3(\gamma-1)}{4J_2}s^2{}_{22}\}\frac{d\sigma_{22}}{E_s} + \frac{3(\gamma-1)}{4J_2}2s_{22}s_{12}\frac{d\sigma_{12}}{E_s} \\
d\varepsilon_{12} &= \frac{3(\gamma-1)}{4J_2}2s_{11}s_{12}\frac{d\sigma_{11}}{E_s} + \frac{3(\gamma-1)}{4J_2}2s_{22}s_{12}\frac{d\sigma_{22}}{E_s} + \{2 + 2\nu_s + \frac{3(\gamma-1)}{4J_2}4s^2{}_{12}\}\frac{d\sigma_{12}}{E_s}
\end{aligned} \tag{2.29}$$

where

$$\gamma = \frac{E_s}{E_t} = \frac{\lambda}{e+1}, \nu_s = \frac{E-(1-2\nu)E_s}{2E} = \frac{e+2\nu}{2(e+1)}$$

These relations are seen to become those for the incremental theory when E_s is replaced by E, or equivalently $e = 0$. Then, $\gamma = \lambda$, and $\nu_s = \nu$. Hence, correspondingly, the inverted incremental relations for the deformation theory are obtained by replacing λ by γ and ν by ν_s in the relations of the incremental theory. The applicable equations are

$$\begin{bmatrix} d\sigma_{11} \\ d\sigma_{22} \\ d\sigma_{12} \end{bmatrix} = \begin{bmatrix} B_s & C_s & F_{s1} \\ C_s & D_s & F_{s2} \\ F_{s1} & F_{s2} & F_s \end{bmatrix} \begin{bmatrix} d\varepsilon_{11} \\ d\varepsilon_{22} \\ 2d\varepsilon_{12} \end{bmatrix} \tag{2.30}$$

$$B_s = \frac{1}{A_s}[\beta\{2s_{12}^2 + s_{22}^2(1+\nu_s)\} + (1+\nu_s)]$$

$$C_s = \frac{1}{A_s}[\beta\{2\nu_s s_{12}^2 - (1+\nu_s)s_{11}s_{22}\} + \nu_s(1+\nu_s)\}$$

$$D_s = \frac{1}{A_s}[\beta\{2s_{12}^2 + s_{11}^2(1+\nu_s)\} + (1+\nu_s)]$$

$$F_s = \frac{1}{2A_s}[\beta\{(s_{11}^2 + s_{22}^2) + 2\,\nu_s\, s_{11}s_{22}\} + (1-\nu_s^2)] \tag{2.31}$$

$$F_{s1} = -\frac{\beta}{A_s}(s_{12}s_{11} + \nu_s s_{12}s_{22})$$

$$F_{s2} = -\frac{\beta}{A_s}(s_{12}s_{22} + \nu_s s_{12}s_{11})$$

and where

$$A_s = \frac{(1+\nu_s)}{E}[\beta\{s_{11}^2 + s_{22}^2 + 2s_{12}^2 + 2\nu_s(s_{11}s_{22} - s_{12}^2)\}+1-\nu_s^2],$$

$$\beta = \frac{3(\gamma-1)}{4J_2}, \gamma = \frac{E_s}{E_t} = \frac{\lambda}{e+1}, \text{ and } \nu_s = \frac{e+2\nu}{2(e+1)}$$

In this thesis, only the total relations, Eqs. (2.27), are used to determine the buckling behaviour according to the deformation theory of plasticity (and not the incremental relations, Eqs. (2.31), given above). However, the above relations are needed if a bifurcation analysis is to be performed, for example in [36].

It should be noted that the above relations, Eqs. (2.31), are quite general, and include relations of the incremental theory as well as those of the elastic theory. Substitution of $E_s = E$ (or $e = 0$, $\gamma = \lambda$) leads to the former, whereas substitution of $E_s = E_t = E$ (or $e = 0$, $\lambda = 1$) leads to the elastic relations. These general relations will be denoted subsequently as

$$\{d\sigma\} = [D_s^t]\{d\varepsilon\} \tag{2.32}$$

and $[D_s^t]$ will be called the matrix of the tangent moduli of the deformation theory.

2.2 Formulation of Finite Element Equilibrium Equations

2.2.1 Basic Assumptions of Finite Element Formulation

An outline of the general method of finite element analysis will now be presented. Procedures for carrying out such analyses by employing constitutive relations of the two plasticity theories are outlined. The formulation using the deformation theory of plasticity is based on the option of total strain formulation. On the other hand, the formulation using the incremental theory is necessarily an incremental strain formulation. Both formulations take into account geometric nonlinearity by employing nonlinear strain-displacement relations. However, these effects are considered to be primarily due to the rotation of the material elements. Therefore strains are assumed to remain small, i.e., much smaller than unity.

2.2.2 Total Strain Finite Element Formulation for Deformation Theory

First, stiffness matrices using the deformation theory of plasticity, are derived. The total stress-strain relations applicable to the plate problems, derived above, will be used. The starting point is the principle of virtual work, written with respect to the undeformed configuration:

$$\int_{V_o} \delta\varepsilon_{ij}\,\sigma_{ij}\,dV_o - \delta q_i\,P_i = 0 \tag{2.33}$$

where summation convention is employed. With reference to finite element formulation, V_o is the original volume of the element, and where

u_i = the three displacement variables in the three fixed coordinate directions x_i.

$u_{i,j}$ = the nine displacement gradients with respect to the undeformed coordinates x_j.

ε_{ij} = Green strain tensor, $\varepsilon_{ij} = \frac{1}{2}(u_{i,j} + u_{j,i} + u_{k,i}\,u_{k,j})$

q_i = nodal displacements

δu_i = virtual change in current displacements

$\delta\varepsilon_{ij}$ = virtual change in Green strain tensor,
$= \frac{1}{2}(\delta u_{i,j} + \delta u_{j,i} + \delta u_{k,i}\,u_{k,j} + u_{k,i}\,\delta u_{k,j})$

σ_{ij} = Kirchhoff stress tensor.

P_i = externally applied nodal forces.

Although the Kirchhoff stress is not the stress which is usually used in experimental determination and specification of the stress-strain law, it is assumed, in view of the small strain restriction, that the specified stress-strain relations are indeed those between the Kirchhoff stress and the Green strain components.

For finite element approximation, one chooses appropriate shape functions and writes

$$\{u\} = [N]\{q\} \tag{2.34}$$

where $\{u\}$ is the vector of displacement variables, appropriate for the problem at hand, $\{q\}$ is the vector of appropriate nodal displacements, and $[N]$ is the matrix of shape functions. Arranging the strain components as a column matrix, and employing their definition as functions of displacement gradients, one may write

$$\{\varepsilon\} = [B_L]\{q\} + \frac{1}{2}[B_N]\{q\} \tag{2.35}$$

where $[B_L]$ is derived from the linear part of the definition, and $[B_N]$ from the nonlinear one. Consequently, $[B_N]$ depends on $\{q\}$ but $[B_L]$ is independent of $\{q\}$. The stress $\{\sigma\}$ is assumed related to the above strain by the matrix of secant moduli $[D_s]$ as

$$\{\sigma\} = [D_s]\{\varepsilon\} = [D_s][B_L]\{q\} + \frac{1}{2}[D_s][B_N]\{q\} = \{\sigma_L\} + \{\sigma_N\} \tag{2.36}$$

where $\{\sigma_L\}$ is the stress arising from the linear strain, and $\{\sigma_N\}$from the nonlinear one.

Now, let the virtual displacements be $\{\delta q\}$, as variations on $\{q\}$. Then, the corresponding virtual strain, in accordance with the definition given above, is expressible as

$$\{\delta\varepsilon\} = [B_L]\{\delta q\} + [B_N]\{\delta q\} \tag{2.37}$$

where $[B_N]$ is exactly the same matrix as before, dependent on $\{q\}$, but now multiplied with a factor 1 (rather than 1/2). The virtual work equation is therefore expressible as

$$\int_{V_o} \{\delta q\}^T ([B_L]^T + [B_N]^T)[D_s]([B_L] + \frac{1}{2}[B_N])\{q\} dV = \{\delta q\}^T \{P\} \tag{2.38}$$

The equations of equilibrium for the element follow from the arbitrary character of $\{\delta q\}$ and one may write

$$[K_S]\ \{q\}\ = \{P\} \tag{2.39}$$

where the element secant stiffness matrix is

$$[K_S] = \int_{V_o} [B_L]^T [D_s][B_L] dV_o + \frac{1}{2}\int_{V_o} [B_N]^T [D_s][B_N] dV_o + \frac{1}{2}\int_{V_o} [B_L]^T [D_s][B_N] dV_o + \int_{V_o} [B_N]^T [D_s][B_L] dV_o \tag{2.40}$$

This secant stiffness matrix is unsymmetric because of the last term. However, following reference [37], an exactly equivalent form can be obtained, by introducing symmetric matrices $[N_1]$ and $[N_2]$ defined as follows:

$$[N_1] = \int_{V_o} ([B_L]^T [D_s][B_N] + [B_N]^T [D_s][B_L] + [G]^T [\sigma_L][G]) dV_o \tag{2.41}$$

$$[N_2] = \int_{V_o} ([B_N]^T [D_s][B_N] + [G]^T [\sigma_N][G]) dV_o \tag{2.42}$$

where $[G]$ is a (geometry) matrix connecting rotations to the nodal displacements, and where $[\sigma_L]$ and $[\sigma_N]$ are the same as $\{\sigma_L\}$ and $\{\sigma_N\}$ defined above but written as a two dimensional matrix to show symmetry of the terms. With this change, the secant stiffness matrix $[K_S]$ is symmetric in form and is expressible as

$$[K_S] = [K_L] + \frac{1}{2}[N_1] + \frac{1}{3}[N_2] \tag{2.43}$$

where $[K_L] = \int_{V_o} [B_L]^T [D_s][B_L] dV_o$ is the stiffness matrix due to linear strain.

The definition of the $[G]$ matrix appropriate for columns and for plates will be given in Chapter 3 and Chapter 4 respectively.

The assembled equations to be solved are $[K_S]^G\{q\}^G = \{P\}^G$ where $[K_S]^G = \sum[K_S]$ is the system stiffness matrix, $\{q\}^G$ is the system displacement vector, and $\{P\}^G$ is the system load vector.

2.2.3 Incremental Finite Element Formulation for Incremental Theory

For implementing the incremental theory of plasticity, an incremental FE formulation is required. Increments of displacements $\{dq\}$ are to be found at each stage of the increment of load. The total displacements, strains, and stresses are accumulated at different points of the structure with respect to a fixed set of axes, as the load is increased incrementally. Using matrix notation, the equilibrium requires that

$$\int_{V_o} \{\delta\varepsilon\}^T\{\sigma\}dV_o - \{\delta q\}^T\{P\} = 0 \tag{2.44}$$

or.

$$\int_{V_o} \{\delta q\}^T([B_L]^T + [B_N]^T)\{\sigma\}dV_o - \{\delta q\}^T\{P\} = 0 \tag{2.45}$$

where $\{P\}$ are element nodal loads, $\{\delta q\}$ are element virtual displacements, and $\{\delta\varepsilon\} = ([B_L] + [B_N])\{\delta q\}$ are the corresponding virtual strains. For any other state of deformation, one similarly has

$$\int_{V_o} \{\delta q\}^T([B'_L]^T + [B'_N]^T)\{\sigma'\}dV_o - \{\delta q\}^T\{P'\} = 0 \tag{2.46}$$

where a prime refers to nodal displacements $\{q'\}$ at this other state. Note however that $[B'_L] = [B_L]$ since they are independent of $\{q\}$ or $\{q'\}$. Now, let $\{P'\} = \{P\} + \{dP\}$, $\{q'\} = \{q\} + \{dq\}, \{\sigma'\} = \{\sigma\} + \{d\sigma\}$. Then, on subtracting (2.45) from (2.46) one obtains, by virtue of $\{\delta q\}$ being arbitrary

$$\int_{V_o}[B_L]^T\{d\sigma\}dV_o + \int_{V_o}[B'_N]^T\{d\sigma\}dV_o + \int_{V_o}([B'_N]^T - [B_N]^T)\{\sigma\}dV_o = \{dP\} \tag{2.47}$$

The nonlinear matrix $[B_N]$ can be expressed as

$$[B_N] = [R][G] \tag{2.48}$$

where $[R]$ and $[G]$ are matrices to be defined appropriately for columns and plates in Chapter 3 and Chapter 4 respectively. Matrix $[G]$ involves first derivatives of the shape functions and is therefore independent of $\{q\}$. Matrix $[R]$ on the other hand involves $\{q\}$ in a linear way. Therefore,

$$[B'_N] - [B_N] = ([R'] - [R])[G] \tag{2.49}$$

and $[R'] - [R]$ is proportional to $\{dq\}$. The last term of Eq. (2.47) can therefore be written as

$$\int_{V_o} ([B'_N]^T - [B_N]^T)\{\sigma\}dV_o = \int_{V_o} [G]^T([R']^T - [R]^T)\{\sigma\}dV_o \tag{2.50}$$

It will be seen subsequently, for columns and for plates, that the above term can be written in a symmetric form by changing the notation for stress from a column matrix to a square matrix. Then, it can be shown that, the last term can be expressed as [38]

$$\int_{V_o} [G]^T([R']^T - [R]^T)\{\sigma\}dV_o = \int_{V_o} [G]^T[\sigma][G]\{dq\}dV_o \tag{2.51}$$

Obviously this term is independent of the moduli, but depends on the prevailing stress. Now the constitutive relations of the incremental theory require

$$\{d\sigma\} = [D_t]\{d\varepsilon\} = [D_t][B_L]\{dq\} + [D_t][B_N]\{dq\} \tag{2.52}$$

Hence the first term of Eq. (2.47) becomes

$$\int_{V_o} [B_L]^T\{d\sigma\}dV_o = \int_{V_o} ([B_L]^T[D_t][B_L] + [B_L]^T[D_t][B_N])\{dq\}dV_o \tag{2.53}$$

and the second one becomes

$$\int_{V_o} [B'_N]^T\{d\sigma\}dV_o = \int_{V_o} ([B_N]^T[D_t][B_L]\{dq\} + [B_N]^T[D_t][B_N])\{dq\}dV_o \tag{2.54}$$

where the second order quantities in $\{dq\}$ have been neglected by taking $[B'_N] = [B_N]$. in Eq. (2.54). Using the notation

$$[K_L] = \int_{V_o} [B_L]^T [D_t][B_L]\, dV_o \tag{2.55}$$

$$[K_N] = \int_{V_o} ([B_N]^T [D_t][B_L] + [B_L]^T [D_t][B_N] + [B_N]^T [D_t][B_N]) dV_o \tag{2.56}$$

$$[K_\sigma] = \int_{V_o} [G]^T [\sigma][G]\, dV_o \tag{2.57}$$

Eq. (2.47) can be written as

$$([K_L] + [K_N] + [K_\sigma])\{dq\} = \{dP\} \tag{2.58}$$

Invoking the compatibility of the displacement increments, the assembled incremental equilibrium equations can be written as

$$[K_T]^G \{dq\}^G = \{dP\}^G \tag{2.59}$$

where

$$[K_T]^G = \sum([K_L] + [K_N] + [K_\sigma]) \tag{2.60}$$

and the summation is over all the elements. Thus $[K_T]^G$ is the system tangent stiffness matrix, $\{dP\}^G$ is the vector of the incremental applied nodal loads, and $\{dq\}^G$ is the corresponding vector of incremental nodal displacements of the system.

2.3 Exact Analysis of Plastic Buckling of Axially Compressed SS Plates

For comparison purpose in the latter part of the thesis, the following analysis presents formulas for the plastic bifurcation buckling stress for simply supported plates subjected to uniform axial stress $\sigma_{xx} = -\sigma$. The analysis is exact, and rather well known, see for example [36]. Therefore, the presentation is kept quite brief.

The differential equation governing plastic bifurcation buckling of a rectangular plate under $\sigma_{xx} = -\sigma$, Fig. 2.3, on the basis of Kirchhoff kinematic hypothesis, and Shanley's concept of bifurcation under increasing load, is

$$B_1 \frac{\partial^4 w}{\partial x^4} + 2(C_1 + 2F_1) \frac{\partial^4 w}{\partial x^2 \partial y^2} + D_1 \frac{\partial^4 w}{\partial y^4} = -\frac{12\sigma}{t^2} \frac{\partial^2 w}{\partial x^2} \tag{2.61}$$

where w is the out-of-plane displacement due to buckling of the plate, t is the thickness , and B_1, C_1, D_1 and F_1 are the incremental elastic-plastic moduli (listed below) corresponding to the stress state $\sigma_{xx} = -\sigma$ at bifurcation. These moduli can be specialized to J_2 deformation and J_2 incremental theories, and also to the elastic case.

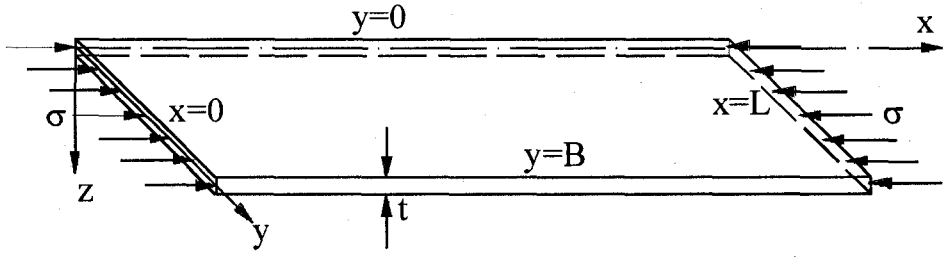

Fig. 2.3 Uniaxially compressed plate simply supported at all four edges

The boundary conditions corresponding to simple supports are defined as

$$w = 0,\ M_{xx} = -\frac{t^3}{12}(B_1 \frac{\partial^2 w}{\partial x^2} + C_1 \frac{\partial^2 w}{\partial y^2}) = 0 \text{ at } x = 0, L \tag{2.62}$$

and,

$$w = 0;\ Myy = -\frac{t^3}{12}(A_1 \frac{\partial^2 w}{\partial x^2} + D_1 \frac{\partial^2 w}{\partial y^2}) = 0 \text{ at } y = \pm \frac{B}{2} \tag{2.63}$$

where L and B are respectively the length and width of the plate. M_{xx} and M_{yy} are the moment stress resultants per unit length due to buckling in the xz and yz planes, respectively. A bifurcation buckling solution of Eq.(2.61) subjected to Eqs. (2.62) and (2.63) can be taken as a sinusoidal mode

$$w = A \sin\frac{m\pi x}{L} \sin\frac{n\pi y}{B} \tag{2.64}$$

where m is the number of half waves in the x direction, n is the number of half waves in the y direction, and A is an arbitrary scale factor. For $m = n = 1$, the bifurcation buckling stress of a square plate is [36]:

$$\sigma_{cr} = \frac{\pi^2}{12}\left(\frac{t}{B}\right)^2 \{B_1 + D_1 + 2(C_1 + 2F_1)\} \tag{2.65}$$

For an 'infinitely' long plate ($\frac{L}{B} \gg 1$), the bifurcation buckling stress is [36]:

$$\sigma_{\text{cr}} = \frac{\pi^2}{12}\left(\frac{t}{B}\right)^2 \{2\sqrt{B_1 D_1} + 2(C_1 + 2F_1)\} \tag{2.66}$$

The number of sine waves along longitudinal direction for a long plate can be determined from the following equation [36]:

$$(mB/L)^2 = \sqrt{D_1/B_1} \tag{2.67}$$

The moduli in Eq.(2.65) and Eq.(2.66) are given by the following relations suitable for deformation theory [36]:

$$\begin{aligned} A_1 &= \frac{E}{\lambda(5 - 4\nu + 3e) - (1 - 2\nu)^2} \\ B_1 &= A_1(\lambda + 3 + 3e) \\ C_1 &= 2A_1(\lambda - 1 + 2\nu) \\ D_1 &= 4A_1\lambda \end{aligned} \tag{2.68}$$

$$F_1 = \frac{E}{(2 + 2\nu + 3e)}$$

where $e = \dfrac{E}{E_S} - 1$ and $\lambda = \dfrac{E}{E_t}$.

In fact, these moduli are exactly the same (except for the notation) as those derived for the incremental stress-strain behaviour for both theories of plasticity, when they are specialized for the present case of uniaxial prebuckling stress (with $s_{11} = -2\sigma/3$, $s_{22} = s_{33} = \sigma/3$, $s_{12} = 0$). The incremental theory results are obtained by putting $e = 0$ in the above relations, whereas those for the elastic case are obtained by substituting $e = 0$ and $\lambda = 1$.

Chapter 3

Plastic Buckling and Postbuckling of Columns

In this chapter, the buckling behaviour of simply supported columns with initial imperfections, subjected to centrally applied compressive forces, is examined by means of the finite element method. A detailed procedure including stiffness matrix formulation, numerical integration, and stress updating for the present one-dimensional problem is illustrated in this chapter. The two J_2 plasticity theories are used to calculate the maximum loads of imperfect columns, and a comparison is made between the results. The load-deflection curves, before and after the maximum load, are traced by using the Newton-Raphson method of solving nonlinear algebraic equations, in conjunction with the displacement control option. Sensitivity of the buckling behaviour to imperfection magnitudes is also studied.

3.1 Strain-Displacement Relations

The nonlinear strain in the x direction, required for the present analysis is the Green strain (see Chapter 2):

$$\varepsilon_{xx} = \frac{du}{dx} + \frac{1}{2}\left(\frac{du}{dx}\right)^2 + \frac{1}{2}\left(\frac{dw}{dx}\right)^2 \tag{3.1}$$

in which $\frac{du}{dx}$ is the gradient of the axial displacement, and $\frac{dw}{dx}$ is the slope arising due to transverse displacement w. Since $\frac{du}{dx} \ll 1$, $\frac{1}{2}\left(\frac{du}{dx}\right)^2$ can be neglected in comparison, and Eq. (3.1) can be written as

$$\varepsilon_{xx} = \frac{du}{dx} + \frac{1}{2}\left(\frac{dw}{dx}\right)^2 \tag{3.2}$$

In the present analysis the column is assumed to poss a uniform rectangular cross-section of width b and depth t. The x direction is the centroidal line of the perfect (straight) column of length L. The support at $x = 0$ is assumed to be on rollers, while that at $x = L$

is assumed a hinge. The plane of bending is the xz principal plane. Small changes in L due to loading or imperfections are neglected.

According to the usual Bernoulli-Euler kinematic assumption of the beam theory, plane sections remain plane and perpendicular to the column centroidal axis during deformation. The displacement $\overline{u}$ in the x direction at a distance z from the centroid, Fig. 3.1, is

$$\overline{u}(x,\, z) = u - z\,\frac{dw}{dx} \tag{3.3}$$

where $u = u(x)$ is the displacement of the centroid, and $\dfrac{dw}{dx}$ is the rotation of the cross-section.

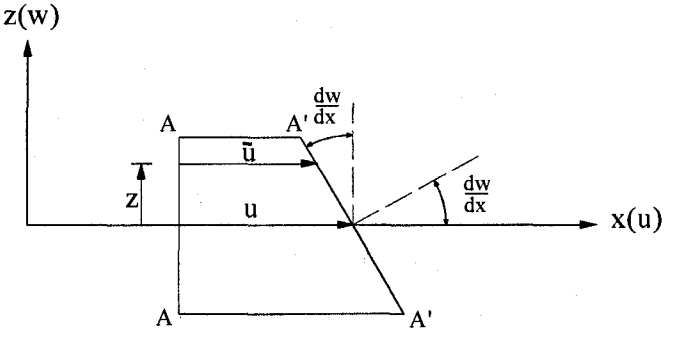

Fig. 3.1 Bernoulli-Euler displacement model

Combining Eqs. (3.2) and (3.3), gives

$$\varepsilon_{xx} = \frac{du}{dx} + \frac{1}{2}\left(\frac{d\,w}{d\,x}\right)^2 - z\,\frac{d^2w}{dx^2} \tag{3.4}$$

For a column with initial imperfection $w_0(x)$, Fig. 3.2, the initial strain associated with zero stress is

$$\varepsilon^o_{xx} = \frac{1}{2}\left(\frac{d\,w_o}{d\,x}\right)^2 - z\,\frac{d^2w_o}{dx^2} \tag{3.5}$$

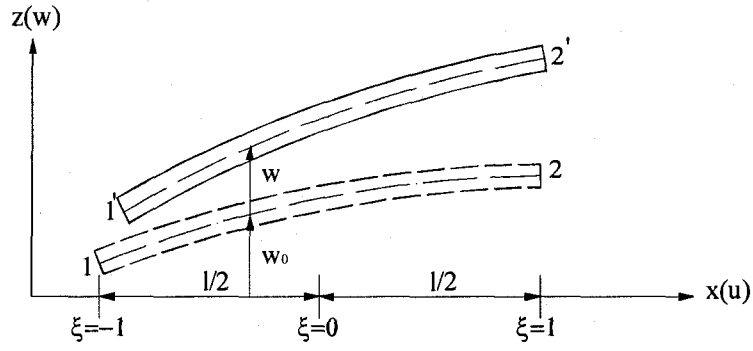

Fig. 3.2 An initially curved beam element

If $u(x)$ and $w(x)$ are the additional displacements arising due to loading of the column then the total strain is

$$\varepsilon_{xx}^{T} = \frac{du}{dx} + \frac{1}{2}\left(\frac{d\,(w+w_o)}{d\,x}\right)^2 - z\,\frac{d^2\,(w+w_o)}{dx^2} \tag{3.6}$$

Hence the strain induced due to loading is $\varepsilon_{xx}^{T} - \varepsilon_{xx}^{o} = \varepsilon_{xx}$, i.e.,

$$\varepsilon_{xx} = \frac{du}{dx} - z\,\frac{d^2w}{dx^2} + \frac{1}{2}\left(\frac{d\,w}{d\,x}\right)^2 + \frac{dw}{dx}\,\frac{dw_o}{dx} \tag{3.7}$$

This expression of strain used in the virtual work principle leads to the following differential equation of transverse equilibrium:

$$\frac{d^2M}{dx^2} + P\frac{d^2w}{dx^2} = -P\frac{d^2w_o}{dx^2} \tag{3.8}$$

where

$$M = -\int_A z\,\sigma_{xx}dA, \text{ and } P = -\int_A \sigma_{xx}dA \tag{3.9}$$

are respectively the bending moment and the axial compressive force.

3.2 Elastic Column with Imperfections

For small-strain elastic behaviour, stress is related to linear strain by $\sigma_{xx} = E(\frac{du}{dx} - z\frac{d^2w}{dx^2})$. Accordingly, for a column with uniform properties, the above differential equation becomes

$$EI\frac{d^4w}{dx^4} + P\frac{d^2w}{dx^2} = -P\frac{d^2w_0}{dx^2} \tag{3.10}$$

For a perfect column, $w_0 = 0$, and the above equation reduces to $EI\frac{d^4w}{dx^4} + P\frac{d^2w}{dx^2} = 0$. For a simply supported column, as is well known, one then has an eigenvalue problem, with eigenvalues $P = \frac{m^2\pi^2EI}{L^2}$ and eigenmodes $w = A_m \sin\frac{m\pi x}{L}$, $m = 1, 2, 3, ...$ The eigenvalues are the bifurcation loads. The smallest of such loads, is the critical bifurcation load, and the corresponding mode is the critical bifurcation mode. Here $m = 1$ gives

$$P_{cr} = \frac{\pi^2EI}{L^2},\ w_{cr} = A_1 \sin\frac{\pi x}{L}. \tag{3.11}$$

For an imperfect column, one should use a representation of the known imperfections in terms of the eigenmodes of the corresponding eigenvalue problem, the reason for which will become apparent shortly. For the simply supported column, let

$$w_o(x) = w_o^1 \sin\frac{\pi x}{L} + w_o^2 \sin\frac{2\pi x}{L} + w_o^3 \sin\frac{3\pi x}{L} + ... \tag{3.12}$$

where the Fourier components w_o^m of $w_o(x)$, $m = 1,\ 2, 3, ...$ are obtained from the standard formula

$$w_o^m = \frac{2}{L}\int_0^L w_o(x)\sin\frac{m\pi x}{L}dx \tag{3.13}$$

Substitution of this representation in the differential equation gives

$$EI\frac{d^4w}{dx^4} + P\frac{d^2w}{dx^2} = P\{w_o^1\frac{\pi^2}{L^2}\sin\frac{\pi x}{L} + w_o^2\frac{4\pi^2}{L^2}\sin\frac{2\pi x}{L} + w_o^3\frac{9\pi^2}{L^2}\sin\frac{\pi x}{L} + ...\} \tag{3.14}$$

and hence the solution as

$$w(P,x) = \frac{PL^2 w_o^1}{\pi^2 EI - PL^2}\sin\frac{\pi x}{L} + \frac{PL^2 w_o^2}{4\pi^2 EI - PL^2}\sin\frac{2\pi x}{L} + \frac{PL^2 w_o^3}{9\pi^2 EI - PL^2}\sin\frac{3\pi x}{L} + \ldots \tag{3.15}$$

As P is increased from zero, each term of $w(P,x)$ begins to grow. It is clear however that the fastest growth occurs in the term corresponding to the critical mode, here the first term. This term grows unbounded as P approaches the critical bifurcation load $\frac{\pi^2 EI}{L^2}$, while all the other terms remain small. Hence, to perform an efficient imperfection growth analysis, the given imperfection should be represented as a Fourier expansion employing the eigenmodes of the corresponding bifurcation problem. This will be taken as a general guiding principle, to be employed elsewhere in this thesis, both for the elastic and plastic imperfection growth analyses.

3.3 Uniaxial Elastic-Plastic Stress-Strain Relations

For a strain hardening material, the typical σ-ϵ stress-strain curve in a uniaxial test (say tension test with $\sigma = \sigma_{xx}$), is like that shown previously in Fig. 2.1. The incremental stress-strain relationship for loading $(\Delta\sigma_{xx} > 0)$ beyond the elastic limit can be expressed as

$$\Delta\sigma_{xx} = E_t\, \Delta\varepsilon_{xx} \tag{3.16}$$

where $E_t = E_t(\sigma)$ is the tangent modulus, which is the slope $\frac{d\sigma}{d\varepsilon}$ of the stress-strain curve at the stress level σ. For unloading $(\Delta\sigma_{xx} < 0)$, the applicable modulus is the elastic modulus E.

The relationship between the total stress and total strain, assuming no unloading, can be expressed as

$$\sigma_{xx} = E_s\, \varepsilon_{xx} \tag{3.17}$$

where $E_s = E_s(\sigma)$ is the secant modulus, which is equal to $\frac{\sigma}{\varepsilon}$ on the stress-strain curve at a given stress level σ. In elastic range E_s is equal to the elastic modulus E.

In this work, the following power-law representation of the uniaxial stress-strain curve, used by Tvergaard and Needleman [39] is adopted

$$\varepsilon = \begin{cases} \dfrac{\sigma}{E} & |\sigma| \leq \sigma_Y' \\ \dfrac{\sigma_Y}{E}\left[\dfrac{1}{n}\left(\dfrac{\sigma}{\sigma_Y}\right)^n + 1 - \dfrac{1}{n}\right] & |\sigma| > \sigma_Y' \end{cases} \tag{3.18}$$

In the above, σ_Y is the initial yield stress and σ_Y' is the current yield stress; the exponent n of the power law can be looked upon as a strain-hardening parameter. For such a curve

$$\frac{1}{E_t} = \frac{1}{E}\left(\frac{\sigma}{\sigma_Y}\right)^{n-1}, \quad \frac{1}{E_s} = \frac{1}{E}\left\{\frac{1}{n}\left(\frac{\sigma}{\sigma_Y}\right)^{n-1} + \left(1 - \frac{1}{n}\right)\left(\frac{\sigma_Y}{\sigma}\right)\right\} \tag{3.19}$$

It follows from the above expressions that a higher value of n implies smaller hardening moduli. For example, $E_t(n = 10) < E_t(n = 5)$, and also $E_s(n = 10) < E_s(n = 5)$.

For the present one dimensional problem, the equivalent stress is

$$\sigma_e = \sqrt{3J_2} = \sigma_{xx} \tag{3.20}$$

and the yield function, Eq. (2.1), becomes simplified as:

$$F = \sigma_{xx} - \sigma_Y'(\varepsilon_{xx}^p) \tag{3.21}$$

where σ_Y' is the current yield stress and ε_{xx}^p is the accumulated plastic strain. Purely elastic behaviour is predicted when $F < 0$, and elastic-plastic behaviour when $F = 0$. After initial yielding, loading (i.e. strain-hardening) is signified by $d\sigma_{xx} > 0$ and unloading (i.e. elastic behaviour) by $d\sigma_{xx} < 0$.

3.4 Stiffness Matrix Formulation

A typical beam element with nodes $i = 1$ and $j = 2$ is shown in Fig. 3.3. Each of the two nodes of this element has 3 degrees of freedom: u_1, w_1, θ_1 and u_2, w_2, θ_2 corresponding to axial and transverse displacements, and slopes of the column centroidal axis due to loading.

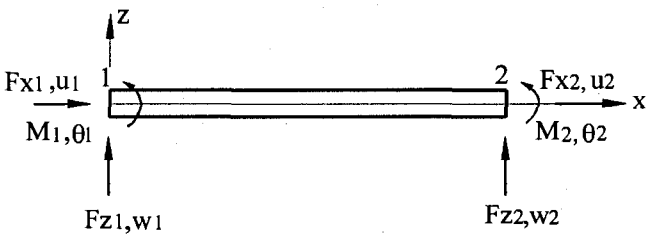

Fig. 3.3 The six degrees of freedom of a beam element

For finite element formulation, the axial displacement u is taken as a linear function of x with parameters u_1, u_2. On the other hand, the transverse displacement w is considered as a cubic function of x with parameters w_1, θ_1 and w_2, θ_2. They are therefore expressible as

$$\begin{bmatrix} u(x) \\ w(x) \end{bmatrix} = \begin{bmatrix} N_1 & 0 & 0 & N_2 & 0 & 0 \\ 0 & H_1 & H_2 & 0 & H_3 & H_4 \end{bmatrix} \begin{bmatrix} u_1 \\ w_1 \\ \theta_1 \\ u_2 \\ w_2 \\ \theta_2 \end{bmatrix} \tag{3.22}$$

where

$$N_1 = 1 - \frac{x}{l},\ N_2 = \frac{x}{l}$$

$$H_1 = \frac{(l-x)^2\,(l+2x)}{l^3}, H_2 = \frac{(l-x)^2\,x}{l^2},\ H_3 = \frac{(3l-2x)\,x^2}{l^3},\ H_4 = \frac{(x-l)\,x^2}{l^2} \tag{3.23}$$

are identified as the shape functions. Now, following the usual procedure in formulating the stiffness matrices, the total strain, Eq. (3.4), is considered as composed of linear and nonlinear parts:

$$\varepsilon = \varepsilon_L + \varepsilon_N \tag{3.24}$$

The linear part is

$$\varepsilon_L = u_x - z\,w_{xx} + w_x w_{ox} \tag{3.25}$$

and the nonlinear one is

$$\varepsilon_N = \frac{1}{2} w_x^2 \tag{3.26}$$

where $u_x = \frac{du}{dx}$, $w_x = \frac{dw}{dx}$, $w_{xx} = \frac{d^2w}{dx^2}$, $w_{ox} = \frac{dw_o}{dx}$. It is apparent that whereas the linear part involves both u and w, the nonlinear part is dependent only on w. The change in the linear part, due to a change in nodal displacements and rotations can be expressed as

$$d\varepsilon_L = < B_L > \{dq\} = (< B_{L1} > + < B_{L2} > + < B_{L3} >)\{dq\} \tag{3.27}$$

where $< B_{L1} >$, $< B_{L2} >$ and $< B_{L3} >$ in accordance with Eq.(3.27), are

$$< B_{L1} > = < N_{1,x} \quad 0 \quad 0 \quad N_{2,x} \quad 0 \quad 0 > \tag{3.28}$$

$$< B_{L2} > = < 0 \quad -z\,H_{1,xx} \quad -zH_{2,xx} \quad 0 \quad -z\,H_{3,xx} \quad -z\,H_{4,xx} > \tag{3.29}$$

$$< B_{L3} > = w_{ox} < G > \tag{3.30}$$

$$< G > = < 0 \quad H_{1,x} \quad H_{2,x} \quad 0 \quad H_{3,x} \quad H_{4,x} > \tag{3.31}$$

$$< dq > = < du_1 \quad dw_1 \quad d\theta_1 \quad du_2 \quad dw_2 \quad d\theta_2 > \tag{3.32}$$

The change in the nonlinear part can be written as

$$d\varepsilon_N = < B_N > \{dq\} \tag{3.33}$$

where

$$< B_N > = w_x < G > = [R] < G > \tag{3.34}$$

Here, in the notation of Chapter 2, $[R]$ is a 1×1 matrix, and $[G]$ is a 1×6 row matrix. $\{q\} = \sum\{dq\}$ are the accumulated displacements in the incremental loading of the imperfect column.

3.4.1 Stiffness Matrix for Incremental Analysis — J_2 Incremental Theory

For the incremental analysis, necessary for the J_2 incremental theory, the applicable modulus at a material point is either the tangent modulus E_t or the Young's modulus E depending upon the strain increment. One may recall from Chapter 2, the following expressions for the tangent stiffness matrix for the column finite element:

$$[K_T] = [K_L] + [K_N] + [K_\sigma] \tag{3.35}$$

where, assuming loading everywhere

$$[K_L] = \int_{V_o} E_t \{B_L\} < B_L > dV_o \tag{3.36}$$

$$[K_N] = \int_{V_o} E_t \Big(\{B_L\} < B_N > + \{B_N\} < B_L > + \{B_N\} < B_N > \Big) dV_o \tag{3.37}$$

$$[K_\sigma] = \int_{V_o} \sigma_{xx} \{G\} < G > dV_o \tag{3.38}$$

where in the present one dimensional problem, $< B_{L1} >$, $< B_{L2} >$, $< B_{L3} >$ are 1×6 row matrices defined above by Eqs. (3.28), (3.29), and (3.30) respectively. The sum of these matrices, $< B_L >$ is defined by Eq. (3.27). The matrix $< B_N >$ needed for evaluating $[K_N]$, is again a 1×6 row matrix, defined by Eq. (3.34). The 1×6 row matrix $< G >$ required for determining $[K_\sigma]$ has been defined by Eq. (3.31).

In actual calculations, a sweep must be made over all integration points (here Gauss points) to determine whether the appropriate modulus should be E_t or E. The iterative process of correctly revising the moduli is explained in Section 3.5.2 dealing with plastic buckling using the incremental theory. For elastic buckling, since $E_t = E$ at all times, this need does not arise.

3.4.2 Stiffness Matrix for Total Analysis — J_2 Deformation Theory

The analysis based on the total constitutive relations was adopted for the J_2 deformation theory here. The secant stiffness matrix $[K_S]$, as may be recalled from Chapter 2, may be constructed by the following formulas:

$$[K_S] = [K_L] + \frac{1}{2}[N_1] + \frac{1}{3}[N_2] \tag{2.43}$$

where

$$[K_L] = \int_{V_o} E_s \{B_L\} < B_L > dV_o \tag{3.39}$$

$$[N_1] = \int_{V_o} \Big(E_s(\{B_L\} < B_N > + \{B_N\} < B_L >) + \sigma_L \{G\} < G > \Big) dV_o \qquad (3.40)$$

$$[N_2] = \int_{V_o} \Big(E_s \{B_N\} < B_N > + \sigma_N \{G\} < G > \Big) dV_o \qquad (3.41)$$

$$\sigma_L = E_s < B_L > \{q\} \qquad (3.42)$$

$$\sigma_N = \frac{1}{2} E_s < B_N > \{q\} \qquad (3.43)$$

where σ_L is the linear stress vector corresponding to linear strain; σ_N is the nonlinear stress corresponding to nonlinear strain.

In this case of deformation theory, the moduli are only stress dependent. There are no loading-unloading considerations. The stress at an integration point determines the corresponding E_s which can be used in formulating the secant stiffness matrices.

3.5 Numerical Integration

In the present analysis, the stiffness matrix is a function of the element nodal degrees of freedom, and also of the stresses and strains at different points along the column length, and also along the depth of its cross-section. Therefore, in order to obtain the applicable material moduli at each stage of deformation, one must accumulate the strain and stress histories at different points (here Gauss points) of the column. Specifically, from the stored stresses and plastic strains, one can compute the current tangent and secant moduli, E_t and E_s.

The Gauss quadrature method has been employed to obtain the element stiffness matrices and the internal force vector. By this numerical integration approach, a polynomial of degree $(2n-1)$ can be integrated exactly with n Gauss points. The tangent stiffness matrix contains terms up to degree 8 in x. Accordingly, Burgoynne and Crisfield [40] have suggested a 5×5 integration mesh through the xz plane. However, in this work a 3×3 integration mesh, Fig. 3.4, has been adopted for faster computations. That such a mesh yields sufficiently accurate results for the present problems will be demonstrated in

a later section. Table 3.1 gives the location and weights of the Gauss points for a 3 × 3 mesh, which are well known [41].

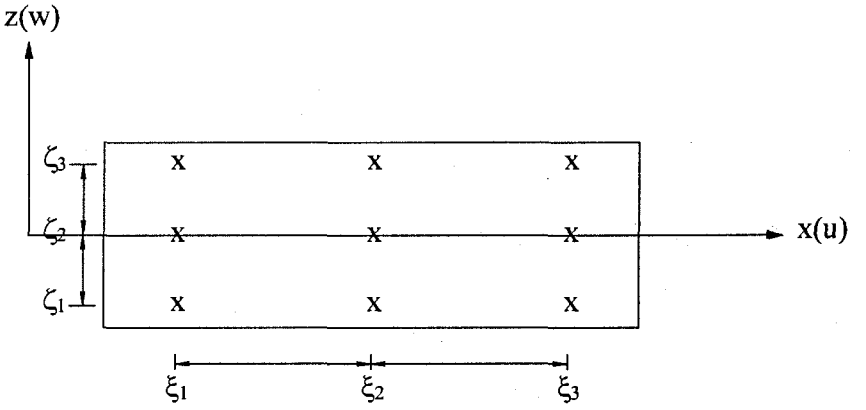

Fig. 3.4 The distribution of 3 × 3 Gauss points in an element

Table 3.1 Abscissae and weights for 3 point Gauss quadrature

$i(j)$	$\xi_i(\zeta_j)$	$W_i(W_j)$
1	$-\sqrt{3/5}$	5/9
2	0	8/9
3	$+\sqrt{3/5}$	5/9

At each grid point, the uniaxial strain ε_{xx} is calculated and then the corresponding stress σ_{xx} and the moduli E_s and E_t. Consider for example, the integration to obtain the linear stiffness matrix given by

$$[K_L] = b\int_0^l \int_{-\frac{t}{2}}^{\frac{t}{2}} E_t \{B_L\} < B_L > dzdx \tag{3.44}$$

where t is depth of cross-section, b is width of cross-section, l is one element length. By introducing $x = \dfrac{(1+\xi)l}{2}$, $z = \dfrac{\zeta t}{2}$, $[K_L]$ can be written as

$$[K_L] = \frac{btl}{4}\int_{-1}^{1}\int_{-1}^{1} E_t \{B_L\} < B_L > d\zeta d\xi \tag{3.45}$$

First, the integrand is evaluated by obtaining each term in closed form

$$[Q] = E_t \{B_L\} < B_L > \tag{3.46}$$

These terms are functions of (ξ, ζ) and element constitutive coefficients $[E_t]$. The matrix $[K_L]$ is then obtained by numerically integration of $[Q]$ by Gauss quadrature

$$[K_L] = \frac{btl}{4} \sum_{i=1}^{3} \sum_{j=1}^{3} W_i \times W_j \times [Q(\xi_i, \zeta_j)] \tag{3.47}$$

3.6 Solution Procedure for Incremental Analysis

Newton-Raphson method combined with displacement control has been used to solve the assembled incremental equilibrium equations:

$$[K_T]^G \{\Delta q\}^G = \{\Delta P\}^G + \{P\}^G - \{\overline{P}\}^G \tag{3.48}$$

in which $[K_T]^G = \sum [K_T]$ is the assembled global (i.e., system) tangent stiffness matrix, $\{\Delta q\}^G$ is the vector of global incremental displacements and rotations, $\{P\}^G$ is the external force vector, $\{\Delta P\}^G$ is its specified increment, and $\{\overline{P}\}^G$ is the internal force vector given by:

$$\{\overline{P}\}^G = \sum \int_{V_o} \sigma_{xx} \left(\{B_L\} + \{B_N\}\right) dV_o \tag{3.49}$$

The residual $\{\Delta R\}^G = \{P\}^G - \{\overline{P}\}^G$ may be considered as an out-of-balance force vector. The iterative numerical procedure must ensure that the magnitude of this vector is rendered close to zero by the convergence criterion, before the next load increment is applied. Here, loading of the column was effected by specifying the increments of mid-span lateral deflection Δw, rather than the increments of the axial load. The corresponding axial load P is obtained as a reaction force. This device, called the displacement control, is necessary in order to negotiate the maximum load point on the load deflection curve. The solution consists in obtaining correctly updated $\{q\}^G$ corresponding to $\{P\}^G$ which then enables one to plot the load-deflection curve.

The above incremental procedure has been applied first to the elastic buckling and postbuckling of columns, and then to the case of material behaviour according to the J_2 incremental theory of plasticity.

3.6.1 Elastic Buckling and Postbuckling

Elastic buckling of columns with inertial imperfection was dealt with analytically in Section 3.2. Here the same problem is solved by the above incremental numerical procedure. As discussed previously, to determine the buckling and postbuckling behaviour of a column, an initial geometric imperfection of the same shape as the critical bifurcation mode of the perfect column should be assumed. For a simply-supported column the critical mode is a half-sine wave. Hence, the initial imperfection for the present numerical analysis was also assumed as a half-sine wave:

$$w_o = \rho L \sin\frac{\pi x}{L} \tag{3.50}$$

where ρL is the imperfection magnitude at the centre of the column. The corresponding critical bifurcation load for the perfect column is

$$P_{cr} = \frac{\pi^2 EI}{L^2} \tag{3.51}$$

which is taken as the reference load for comparison purposes. In the finite element analysis, four elements were used along the half length of the column, with the properties: rectangular cross section with $\frac{b}{t} = \frac{1}{2}$, $\frac{L}{t} = 20$, and $E = 70,000\,\text{MPa}$ (Aluminum). The load-deflection curves of perfect and imperfect structure are shown in the Fig. 3.5 for various imperfection magnitudes.

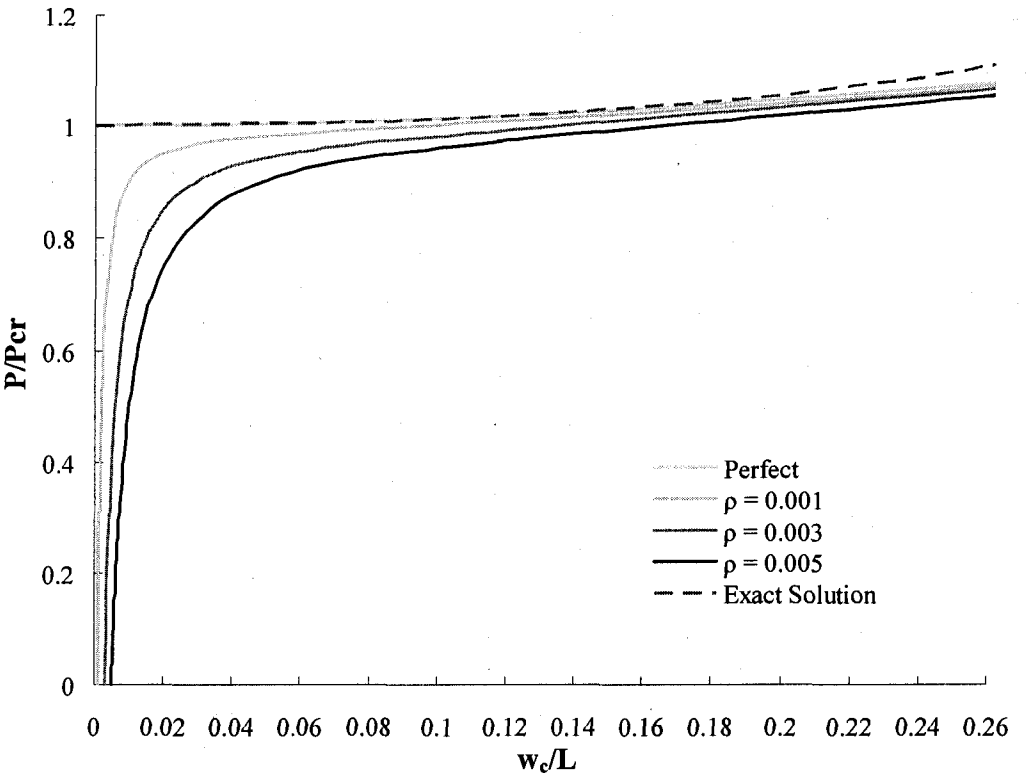

Fig. 3.5 Elastic postbuckling behaviour of simply supported columns

The dotted line shown in Fig. 3.5 is the well known exact solution [42] for elastic buckling of a column in terms of the Elliptic functions. There is almost no difference between the numerical result for a "perfect" column and the present theoretical result when w_c/L is less than 0.2%. From a study of Fig. 3.5 it is concluded that:

1. The axial load keeps on increasing after the bifurcation point. The load-deflection curves have positive slopes, and therefore signify stable postbuckling behaviour. For the perfect column the slope is zero at the bifurcation point. For imperfect columns, the slope decreases rapidly near the bifurcation point. The slopes begin to increase after the column has acquired some significant deflection.

2. The postbuckling behaviour of elastic columns is not very sensitive to the initial imperfections. At relatively large deflections, beyond the bifurcation point, the load-deflection curves begin to come close to each other regardless of the amount of initial

imperfections, although as expected, for greater imperfections the attained loads are smaller for the same deflection w_c/L.

3.6.2 Plastic Buckling and Postbuckling, Incremental Theory

In elastic analysis the stress is uniquely determined by the strain. Total stress σ or the incremental stress $\Delta\sigma$ can therefore be computed from the total strains ε or the incremental strain $\Delta\varepsilon$ by multiplying with E. However, for the elastic-plastic material, the stress must be computed incrementally, taking into account loading or unloading.

In the actual calculations, to obtain the element stiffness matrices $[K_T]$, a sweep must be made over all Gauss points to determine whether the appropriate modulus should be E_t or E. At each Gauss point the current stress σ^i and the current yield stress σ'^i_Y are stored. If $\|\sigma^i\| = \sigma'^i_Y$ then the stress at this Gauss point is on the strain-hardening part of the stress-strain curve with potential for either further yielding or unloadng. The appropriate modulus is taken as E_t as a first trial. If $\|\sigma^i\| < \sigma^i_Y$, the choice is for E since this inequality implies the stress point is below the yield stress. The $[K_T]$ formulated in this way for each element is assembled to obtain the global stiffness matrix $[K_T]^G$, and is used to solve for $\{\Delta q\}^G$ corresponding to a load increment $\{\Delta P\}^G$ from the following equation:

$$[K_T]^G\{\Delta q\}^G = \{\Delta P\}^G + \{\Delta R\}^G \tag{3.52}$$

where $\{\Delta R\}^G$, the residual force vector, may be taken as zero for the first trial. This provisional solution then furnishes, at any Gauss point i, $\Delta\varepsilon^i$ and appropriately $\Delta\sigma^i = E_t\,\Delta\varepsilon^i$ if further plasticity was assumed to occur, or $\Delta\sigma^i = E\,\Delta\varepsilon^i$ if elastic behaviour was assumed. The updated stresses are, again provisionally, $\sigma^i + \Delta\sigma^i$. Now, before accepting the incremental results, a sweep must be made, using the provisionally updated stresses, to revise the assumed choice of modulus at the Gauss points if it is found incorrect. A fresh iteration for determining $\{\Delta q\}^G$ is then made with the revised $[K_T]$ and assembled stiffness matrix $[K_T]^G$, and $\{\Delta R\}^G = \{P\}^G - \{\overline{P}\}^G$. The process is repeated until the two successive trials converge to yield the same moduli and consequently the same $\{\Delta q\}^G$, and $\{\Delta R\}^G \approx \{0\}$, for the specified load increment $\{\Delta P\}^G$.

The converged $\{\Delta q\}^G$ so obtained is then used to find the corresponding $\Delta\varepsilon^i$ and $\Delta\sigma^i$ at all Gauss points. The displacements, strains, stresses, and the yield stresses are then correctly updated at all Gauss points.

Because the buckling mode for a perfect, simply-supported column is the same as that of an elastic column, we assume the same initial imperfection function as for the latter

$$w_o = \rho L \sin\frac{\pi x}{L} \tag{3.50}$$

The corresponding bifurcation load is expressed as

$$P_{\text{cr}} = \frac{\pi^2 E_t I}{L^2} \tag{3.53}$$

where E_t is the tangent modulus at the stress level $\sigma = \sigma_{\text{cr}}$. This fact renders Eq. (3.53) to be a nonlinear relation, since the right side depends on the left side.

For numerical analysis of plastic buckling of an imperfect column, as in the elastic case, four elements were are used along the length of the column. The properties were taken as: $L/t = 20$, $E = 70,000$ MPa, and $\sigma_Y/E = 0.001$. Four schemes of Gauss integration were tried to pick the optimum. For each element, meshes of the sizes 5×5, 3×5, 3×3, and 3×2 were tried. Tables 3.2 to 3.4 list the comparison of the maximum load values and the corresponding transverse displacements at the centre of the column for three increasing imperfection levels $\rho = w_o/L = 0.001, 0.003, 0.005$.

Table 3.2 Effect of number of Gauss points along x direction (mesh 3×5)

Mesh Size	ρ **= 0.001**	ρ **= 0.003**	ρ **= 0.005**
Mesh 5 × 5	(0.0033, 0.9066)	(0.0077, 0.781)	(0.0115, 0.6997)
Mesh 3 × 5	(0.0033 0.908)	(0.0076, 0.7834)	(0.0114, 0.704)
***Error in Displacement**	0%	1.299 %	0.87 %
***Error in Load**	0.066 %	0.128 %	0.243 %

Table 3.3 Effect of number of Gauss points along z direction (mesh 3 × 3)

Mesh Size	$\rho = 0.001$	$\rho = 0.003$	$\rho = 0.005$
Mesh 5 × 5	(0.0033, 0.9066)	(0.0077, 0.781)	(0.0115, 0.6997)
Mesh 3 × 3	(0.00345, 0.908)	(0.0082, 0.7834)	(0.01235, 0.704)
***Error in Displacement**	4.545 %	6.494 %	8.502 %
***Error in Load**	0.154 %	0.307 %	0.615 %

Table 3.4 Effect of number of Gauss points along z direction (mesh 3 × 2)

Mesh Size	$\rho = 0.001$	$\rho = 0.003$	$\rho = 0.005$
Mesh 5 × 5	(0.0033, 0.9066)	(0.0077, 0.781)	(0.0115, 0.6997)
Mesh 3 × 2	(0.0029, 0.905)	(0.0065, 0.7816)	(0.00955, 0.698)
***Error in Displacement**	12.121 %	15.584 %	16.957 %
***Error in Load**	0.176 %	0.008 %	0.243 %

*The error in displacement is relative to the results from the 5 × 5 mesh, and similarly the error in load is relative to the loads corresponding to this mesh.

If the results of a 5 × 5 mesh are considered most accurate, one finds that the errors in maximum loads are all very small (less than 1 %). However, the error in displacements are quite significant. For example, the error in displacement is greater than 16% for a 3 × 2 mesh. The 3 × 2 mesh is therefore unacceptable. The 3 × 3 mesh predicts buckling load higher by 0.61 % and a displacement lower by 8.5 %. These errors are considered acceptable in the present study, and accordingly a choice of three Gauss points depth wise is considered acceptable in all further computations. A finer mesh can always be implemented, but the computational time increases rather exponentially.

The load-deflection curves for various imperfection levels are shown in Fig. 3.6 for a material with strain hardening exponent $n = 5$. The dots on these curves denote the

maximum load points, which are the critical loads for onset of instability. Fig. 3.7 shows similar graphs for a material with strain hardening exponent $n = 10$.

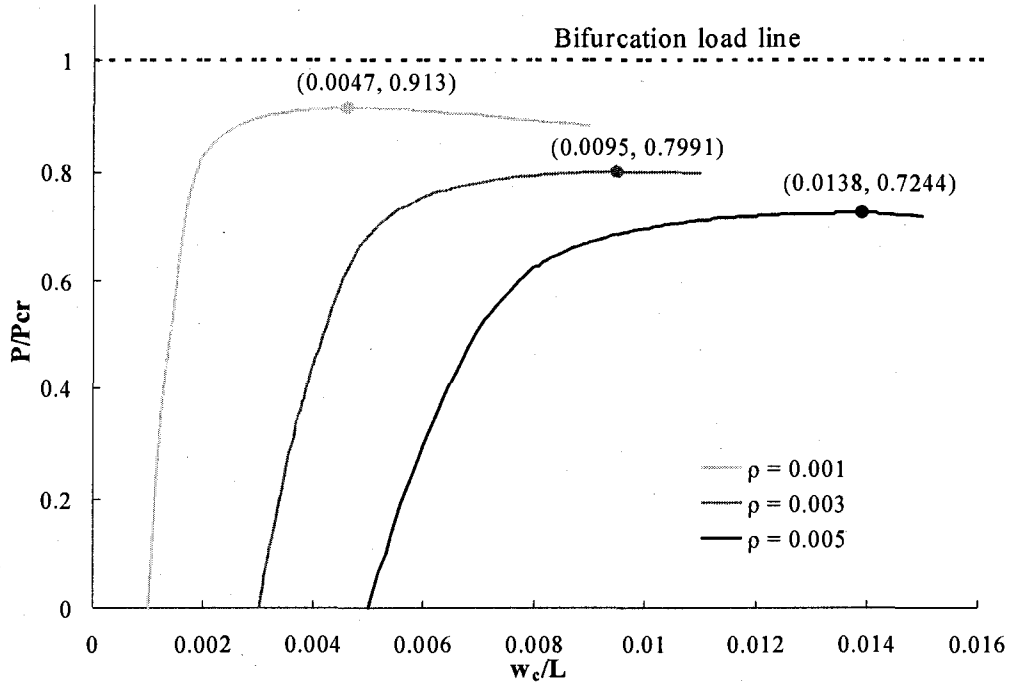

Fig. 3.6 Plastic postbuckling of columns by the incremental theory ($n = 5$)

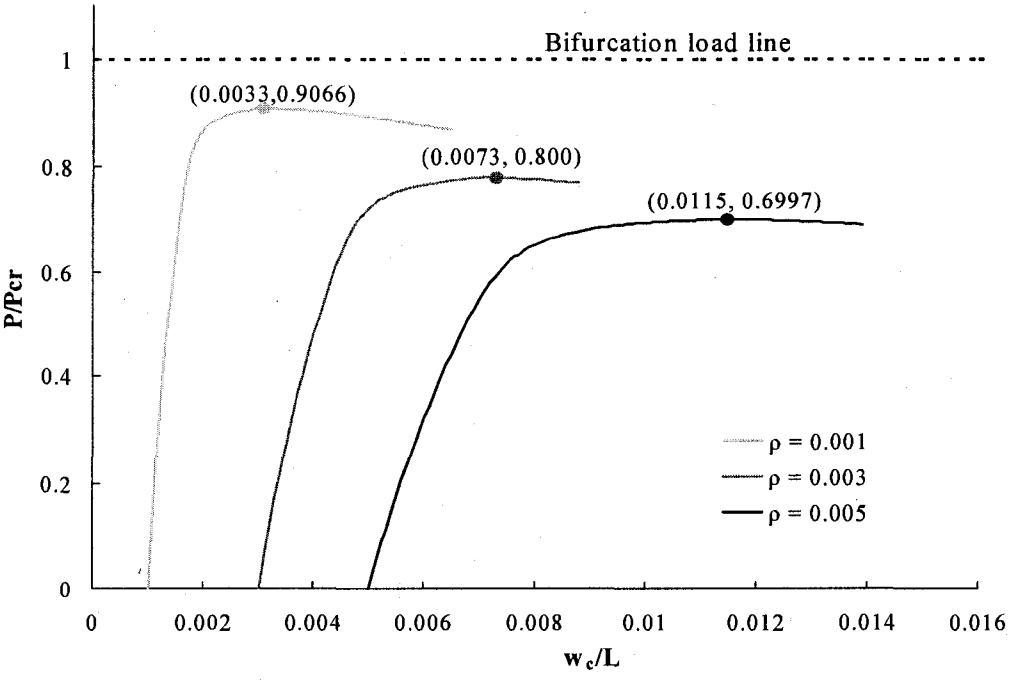

Fig. 3.7 Plastic postbuckling of columns by the incremental theory ($n = 10$)

3.7 Plastic Buckling and Postbuckling, Deformation Theory

The incremental approach is not necessary for this theory of plasticity, as it is not dependent on the strain path. Hence, the nonlinear finite element equations of equilibrium

$$[K_S]^G \{q\}^G = \{P\}^G + \{\Delta R\}^G \tag{3.54}$$

can be solved directly by an iterative method. Starting with suitable initial values of the displacements, the corresponding strains, stresses, and the secant moduli can be determined, and therefore $[K_S]^G = \sum [K_S]$ can be constructed. The above relation is then a set of linear equations, solved easily to find the solution $\{q\}^G$ as the next trial displacement vector. The matrices $[K_S]$ are then updated to correspond with the stresses obtained from the calculated $\{q\}^G$. The procedure is then repeated with revised $[K_S]^G$ until a $\{q\}^G$ is found for which the moduli are consistent, and $\{\Delta R\}^G$ is reduced to a vector close to zero. The success of the method depends largely upon the accuracy of the initial guess values of the displacements.

Using the same properties as for the column of the increment theory, one can trace for a given imperfection, the load-deflection curve, including the unstable part, by the above iterative method combined with displacement control. The results are shown in Figs. 3.8 and 3.9.

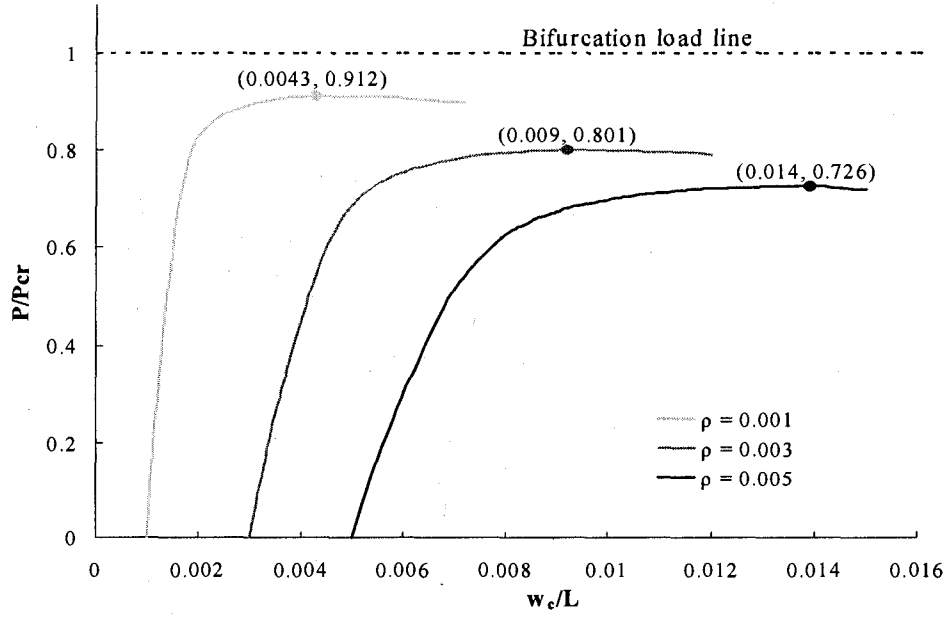

Fig. 3.8 Plastic postbuckling of columns by the deformation theory ($n = 5$)

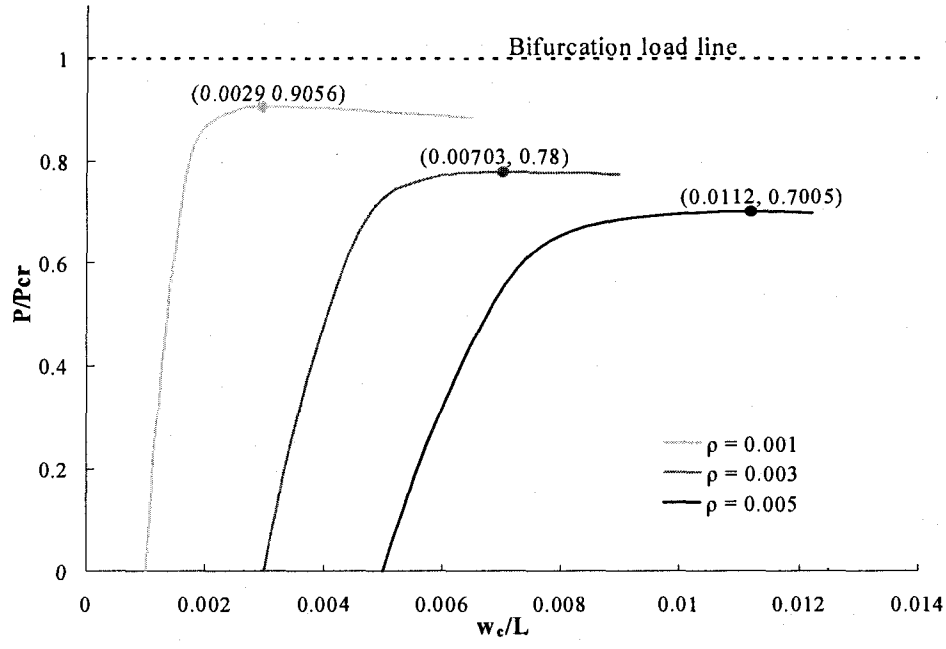

Fig. 3.9 Plastic postbuckling of columns by the deformation theory ($n = 10$)

3.8 Comparisons and Conclusions

Comparing the results from the two plasticity theories, Tables 3.5 and 3.6, one finds that the maximum load predictions are almost the same. This should not come as a surprise. In the particular case of (one dimensional) column buckling, if there is no unloading, the two theories are exactly the same despite the apparently different forms of their stress-strain relations. In particular, the bifurcation loads are the same. The small differences observed here particularly in deflections of the buckled column may be attributed to possible unloading in the incremental case. Other possible reason may be error accumulation in the incremental case due to insufficient stringency of the convergence criteria.

Table 3.5 Maximum loads predicted by the incremental and deformation theories ($n = 5$)

Imperfection	Inc. theory $\frac{P}{P_{cr}}$	Def. theory $\frac{P}{P_{cr}}$	Error $= \frac{\text{Inc} - \text{Def}}{\text{Inc}}$
$\rho = 0.001$	0.913	0.912	0.110%
$\rho = 0.003$	0.799	0.800	0.125%
$\rho = 0.005$	0.724	0.725	0.138%

Table 3.6 Maximum loads predicted by the incremental and deformation theories ($n = 10$)

Imperfection	Inc. theory $\frac{P}{P_{cr}}$	Def. theory $\frac{P}{P_{cr}}$	Error $= \frac{\text{Inc} - \text{Def}}{\text{Inc}}$
$\rho = 0.001$	0.9066	0.906	0.066%
$\rho = 0.003$	0.780	0.780	0%
$\rho = 0.005$	0.698	0.699	0.143%

The effect of initial imperfection on maximum load is shown in Fig. 3.10. These curves show sensitivity of the critical loads to imperfection magnitudes. They appreciably reduce the critical load for the occurrence of instability. A greater imperfection-sensitivity is observed for a material with low-hardening moduli ($n = 10$), i.e., with a flatter stress-strain curve, Table 3.5. For the same amount of imperfection, the maximum load is lower for a low hardening material.

Table 3.7 Reduction in maximum loads

Strain-hardening exponent	$\rho = 0.001$	$\rho = 0.003$	$\rho = 0.005$
n = 5	8.70 %	20.09 %	27.56 %
n = 10	9.34 %	21.90 %	30.03 %

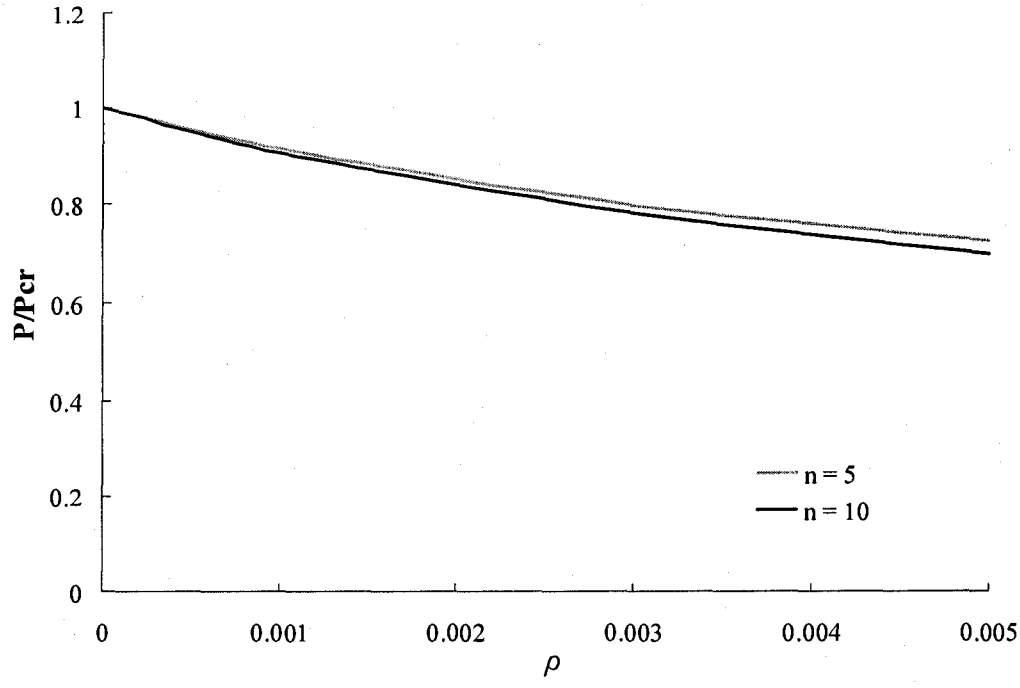

Fig. 3.10 Effect of initial imperfections on maximum loads

Based on the finite element results, one can conclude that:

1. As expected, there is no difference between the maximum load predictions of the J_2 incremental theory and the J_2 deformation theory for simply supported columns.

2. Unlike the elastic postbuckling behaviour, the plastic postbuckling path is unstable after attaining the maximum load.

3. Imperfections significantly reduce the maximum load when buckling occurs in the plastic range.

Chapter 4

Plastic Buckling and Postbuckling of Plates

In this chapter, parallel to the previous one for columns, the buckling behaviour of simply supported plates with initial imperfections, subjected to uniaxial compressive forces is examined by means of the finite element method. Again, as for the column problem, the detailed procedure describing stiffness matrix formulation, numerical integration, and stress updating for the present plate-analysis problems is given in this chapter. The two J_2 plasticity theories are used to calculate the maximum stresses of imperfect plates, and a comparison is made between their results. The load-deflection curves, before and after the maximum load, are traced by using the Newton-Raphson method of solving nonlinear algebraic equations, in conjunction with the displacement control option. Sensitivity of the buckling behaviour to imperfection magnitudes is also studied.

4.1 Strain-Displacement Relations

The thickness of plates is considered to be much smaller than the other two dimensions. Therefore, the Kirchhoff kinematic assumptions which neglect thickness strain and transverse shear strains, are assumed to hold. Physically, it is assumed that the straight lines normal to the middle surface before deformation remain straight and normal to this surface after deformation, and without any length change. The displacements used in the formulation are therefore taken as:

$$\overline{u} = u - z\frac{\partial w}{\partial x}, \quad \overline{v} = v - z\frac{\partial w}{\partial y}, \quad \overline{w} = w \tag{4.1}$$

where u, v, w are displacements of the middle plane in the x, y, z directions, respectively. Fig. 4.1 shows the plate element in xz plane before and after deformation.

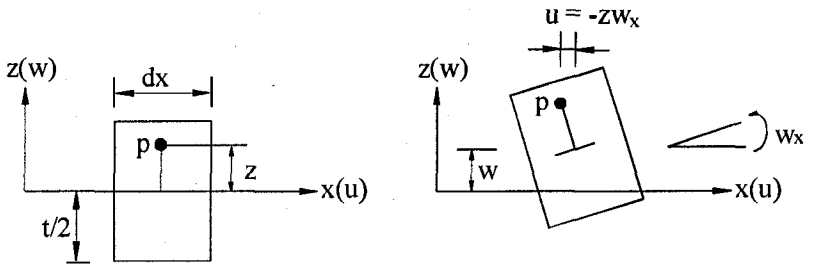

(a) Undeformed plate (b) Deformed plate

Fig. 4.1 Kirchhoff thin plate deformation model

When an initial out-of-plane imperfection, $w_o(x, y)$, is present (with $u_o(x, y) = 0$ and $v_o(x, y) = 0$), there are correspondingly initial strains present without any stress. The additional deflection $w(x, y)$ due to loading causes strains which in turn cause stress by virtue of the material resistance. Thus, the strains ε_{ij} entering the constitutive law are the differences between the total strains ε_{ij}^T and the initial strains ε_{ij}^o. In other words,

$$\varepsilon_{ij} = \varepsilon_{ij}^T - \varepsilon_{ij}^o = \varepsilon_{ij}(w + w_o) - \varepsilon_{ij}(w_o) \tag{4.2}$$

where index notation has been used, and ε_{ij} are the Green strain components involving displacement gradients with respect to undeformed coordinates. For example, in index notation, the Green strains for total displacements u_i^T are expressible as

$$\varepsilon_{ij}^T = \frac{1}{2}(u_{i,j}^T + u_{j,i}^T + u_{k,i}^T u_{k,j}^T) \tag{4.3}$$

where $u_{i,j}^T$ denotes the derivative of u_i^T with respect to coordinate directions x_j. Here, in the context of Kirchhoff theory of plates, the non-zero additional Green strains are

$$\begin{aligned}
\varepsilon_{xx} &= \frac{\partial u}{\partial x} - z\frac{\partial^2 w}{\partial x^2} + \frac{\partial w_o}{\partial x}\frac{\partial w}{\partial x} + \frac{1}{2}(\frac{\partial w}{\partial x})^2 \\
\varepsilon_{yy} &= \frac{\partial v}{\partial y} - z\frac{\partial^2 w}{\partial y^2} + \frac{1}{2}(\frac{\partial w}{\partial y})^2 + \frac{\partial w_o}{\partial y}\frac{\partial w}{\partial y} + \frac{1}{2}(\frac{\partial w}{\partial y})^2 \\
2\varepsilon_{xy} &= \frac{\partial u}{\partial y} + \frac{\partial v}{\partial x} - 2z\frac{\partial^2 w}{\partial x \partial y} + \frac{\partial w}{\partial x}\frac{\partial w_o}{\partial y} + \frac{\partial w}{\partial y}\frac{\partial w_o}{\partial x} + \frac{\partial w}{\partial x}\frac{\partial w}{\partial y}
\end{aligned} \tag{4.4}$$

In the matrix notation, one may write the above as

$$\{\varepsilon\} = \begin{bmatrix} u_x \\ v_y \\ u_y + v_x \end{bmatrix} + z \begin{bmatrix} -w_{xx} \\ -w_{yy} \\ -2w_{xy} \end{bmatrix} + \begin{bmatrix} w_x w_{ox} \\ w_y w_{oy} \\ w_x w_{oy} + w_y w_{ox} \end{bmatrix} + \frac{1}{2} \begin{bmatrix} w_x^2 \\ w_y^2 \\ 2w_x w_y \end{bmatrix} \tag{4.5}$$

4.2 Stiffness Matrix Formulation

A rectangular finite element is developed, as this shape is suitable for the present rectangular plates. As shown in Fig. 4.2, a typical element has dimensions a and b in x and y directions. Its thickness is denoted by t. The element coordinate system is oriented identical to the global plate coordinate system. Thus, the xy plane coincides with the middle plane of the perfect plate, and the z axis is perpendicular to this plane. The element has five degrees of freedom at each of its nodal points, which are the four corner points. At a node i, there are u_i, v_i, w_i as nodal displacements in x, y, z directions, and w_{xi}, w_{yi} are nodal slopes along x and y directions.

$$\{u, v, w, w_x, w_y\}$$

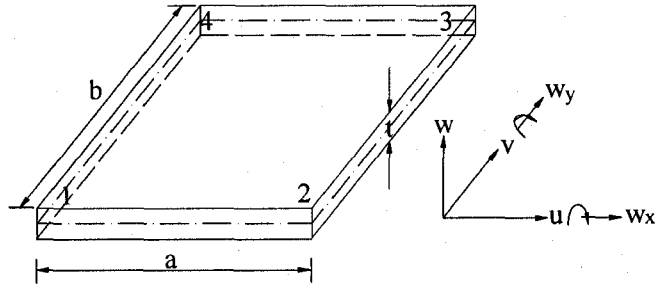

Fig. 4.2 Element geometry and nodal degrees of freedom

For finite element formulation, non-dimensional coordinates ξ and η are used, with origin at the centre of the element and $\xi = 2x/a$, $\eta = 2y/b$, Fig. 4.3. Then, in terms of $\xi\eta$ coordinates, the four nodes have the coordinates $(-1.\ -1)$, $(1,\ -1)$, $(1,1)$, $(-1,1)$.

(1) The xy displacements within the element can be interpolated in terms of the nodal degrees of freedom by bilinear functions of ξ and η (or equivalently of x and y) as

$$u = \sum_{i=1}^{4} N_i u_i, \quad v = \sum_{i=1}^{4} N_i v_i \tag{4.6}$$

where the interpolation function can be expressed succinctly, by using index notation, as

$$N_i = \frac{1}{4}(1 + \xi\xi_i)(1 + \eta\eta_i) \tag{4.7}$$

where ξ_i and η_i are the nondimensional coordinates of the nodes as mentioned above and shown below in Fig. 4.3.

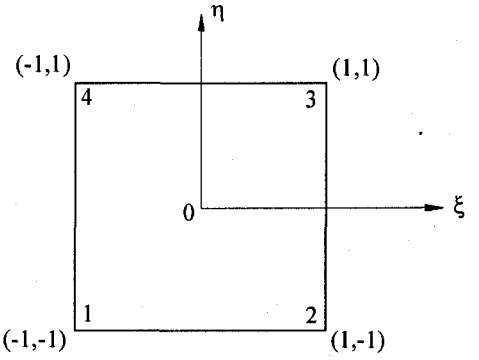

Fig. 4.3 Element nondimensional coordinate system and node numbering

(2) The additional transverse displacement w is interpolated using the Hermite interpolation functions (cubic polynomial functions) as

$$w(x, y) = \sum_{i=1}^{4}(H_{i1}w_i + H_{i2}w_{xi} + H_{i3}w_{yi}) \tag{4.8}$$

where for nodes $i = 1$ to 4, one has

$$H_{i1} = \frac{1}{8}(1 + \xi\xi_i)(1 + \eta\eta_i)(2 + \xi\xi_i + \eta\eta_i - \xi^2 - \eta^2)$$

$$H_{i2} = -\frac{a}{8}\xi_i(\xi + \xi_i)^2(1 - \xi\xi_i)(1 + \eta\eta_i) \tag{4.9}$$

$$H_{i3} = -\frac{b}{8}\eta_i(1 + \xi\xi_i)(\eta + \eta_i)^2(1 - \eta\eta_i)$$

Explicitly, one has

$$w(x,y) = < \; H_{11} \;\; H_{12} \;\; H_{13} \;\; H_{21} \;\; H_{22} \;\; H_{23} \;\; H_{31} \;\; H_{32} \;\; H_{33} \;\; H_{41} \;\; H_{42} \;\; H_{43} > \begin{pmatrix} w_1 \\ w_{x1} \\ w_{y1} \\ w_2 \\ w_{x2} \\ w_{y2} \\ w_3 \\ w_{x3} \\ w_{y3} \\ w_4 \\ w_{x4} \\ w_{y4} \end{pmatrix} \tag{4.10}$$

Thus, the 3 displacement functions within the element are expressible as

$$\begin{bmatrix} u \\ v \\ w \end{bmatrix} = [N]\{q\} \tag{4.11}$$

where $\{q\}$ is the 20×1 nodal "displacement" matrix and $[N]$ is the 3×20 matrix of shape functions.

Now, strains are connected to nodal quantities (i.e., displacements and slopes). For this purpose it is convenient to write Eq. (4.3) in the form:

$$\{\varepsilon\} = \{\varepsilon_L\} + \{\varepsilon_N\} \tag{4.12}$$

where the linear strain $\{\varepsilon_L\}$ is

$$\{\varepsilon_L\} = \begin{bmatrix} u_x \\ v_y \\ u_y + v_x \end{bmatrix} + z \begin{bmatrix} -w_{xx} \\ -w_{yy} \\ -2w_{xy} \end{bmatrix} + \begin{bmatrix} w_{ox} & 0 \\ 0 & w_{oy} \\ w_{oy} & w_{ox} \end{bmatrix} \begin{bmatrix} w_x \\ w_y \end{bmatrix} = [B_{L1}]\{q\} + z[B_{L2}]\{q\} + [B_{L3}]\{q\} \tag{4.13}$$

and the nonlinear part is

$$\{\varepsilon_N\} = \frac{1}{2} \begin{bmatrix} w_x^2 \\ w_y^2 \\ 2\,w_x w_y \end{bmatrix} = \frac{1}{2} \begin{bmatrix} w_x & 0 \\ 0 & w_y \\ w_y & w_x \end{bmatrix} \begin{bmatrix} w_x \\ w_y \end{bmatrix} = \frac{1}{2}[R][G]\{q\} = \frac{1}{2}[B_N]\{q\} \tag{4.14}$$

The matrices $[B_{L1}]$, $[B_{L2}]$ derived from the first two parts of linear strain are:

$$[B_{L1}] = \begin{bmatrix} N_{1,x} & 0 & 0 & 0 & 0 & \ldots & N_{4,x} & 0 & 0 & 0 & 0 \\ 0 & N_{1,y} & 0 & 0 & 0 & \ldots & 0 & N_{4,y} & 0 & 0 & 0 \\ N_{1,y} & N_{1,x} & 0 & 0 & 0 & \ldots & N_{4,y} & N_{4,x} & 0 & 0 & 0 \end{bmatrix} \tag{4.15}$$

$$[B_{L2}] = \begin{bmatrix} 0 & 0 & -H_{11,xx} & -H_{12,xx} & -H_{13,xx} & \ldots & 0 & 0 & -H_{41,xx} & -H_{42,xx} & -H_{43,xx} \\ 0 & 0 & -H_{11,yy} & -H_{12,yy} & -H_{13,yy} & \ldots & 0 & 0 & -H_{41,yy} & -H_{42,yy} & -H_{43,yy} \\ 0 & 0 & -2H_{11,xy} & -2H_{12,xy} & -2H_{13,xy} & \ldots & 0 & 0 & -2H_{41,xy} & -2H_{42,xy} & -2H_{43,xy} \end{bmatrix} \tag{4.16}$$

$$[B_{L3}] = [R_o][G] \tag{4.17}$$

The matrix $[R_o]$ is constructed from the derivatives of the known initial imperfection $w_o(x, y)$ as

$$[R_o] = \begin{bmatrix} w_{ox} & 0 \\ 0 & w_{oy} \\ w_{oy} & w_{ox} \end{bmatrix} \tag{4.18}$$

The matrix $[G]$ connects the derivatives w_x and w_y to the nodal displacements:

$$\begin{bmatrix} w_x \\ w_y \end{bmatrix} = [G]\{q\} = \begin{bmatrix} < G_x > \\ < G_y > \end{bmatrix}\{q\} \tag{4.19}$$

where $< G_x >$ and $< G_y >$ are row vectors obtained by differentiating $w(x, y)$. Thus,

$$[G] = \begin{bmatrix} 0 & 0 & H_{11,x} & H_{12,x} & H_{13,x} & \ldots & 0 & 0 & H_{41,x} & H_{42,x} & H_{43,x} \\ 0 & 0 & H_{11,y} & H_{12,y} & H_{13,y} & \ldots & 0 & 0 & H_{41,y} & H_{42,y} & H_{43,y} \end{bmatrix} \tag{4.20}$$

where the comma indicates differentiation with respect to x or y as indicated, The matrix $[R]$ is

$$[R] = \begin{bmatrix} w_x & 0 \\ 0 & w_y \\ w_y & w_x \end{bmatrix} = \begin{bmatrix} < G_x > \{q\} & 0 \\ 0 & < G_y > \{q\} \\ < G_y > \{q\} & < G_x > \{q\} \end{bmatrix} \tag{4.21}$$

and therefore

$$[B_N] = [R][G] = \begin{bmatrix} < G_x > \{q\} & 0 \\ 0 & < G_y > \{q\} \\ < G_y > \{q\} & < G_x > \{q\} \end{bmatrix} \begin{bmatrix} < G_x > \\ < G_y > \end{bmatrix} \tag{4.22}$$

Thus, in summary, the total strain is expressible in terms of the nodal quantities as

$$\{\varepsilon\} = [B_{L1}]\{q\} + z[B_{L2}]\{q\} + [B_{L3}]\{q\} + \frac{1}{2}[B_N]\{q\} \tag{4.23}$$

The incremental stains arising from increments $\{dq\}$ are therefore expressible as

$$\{d\varepsilon\} = [B_{L1}]\{dq\} + z[B_{L2}]\{dq\} + [B_{L3}]\{dq\} + [B_N]\{dq\} \tag{4.24}$$

where the multiplying factor to $[B_N]$ is changed from $\frac{1}{2}$ to 1 in view of the quadratic nature of the nonlinear strain, and evident from the fact that $[B_N]\{q\} = [R][G]\{q\}$ is quadratic in $\{q\}$. The element matrices $[B_{L1}]$, $[B_{L2}]$, $[B_{L3}]$, $[B_N]$ are all of size 3×20.

4.2.1 Stiffness Matrix for Incremental Analysis — J_2 Incremental Theory

For the incremental analysis, necessary for the J_2 incremental theory, the constitutive relations are the incremental ones derived in Chapter 2. The applicable moduli are the tangent moduli, expressing stress increments in terms of strain increments. Denoting the matrix of these moduli in a general way as a 3×3 matrix $[D_t]$, one may recall the expressions for the tangent stiffness matrix for a general element as:

$$[K_T] = [K_L] + [K_N] + [K_\sigma] \tag{3.35}$$

where

$$[K_L] = \int_{V_o} [B_L]^T [D_t][B_L]\, dV_o \tag{2.55}$$

$$[K_N] = \int_{V_o} \Big([B_L]^T [D_t][B_N] + [B_N]^T [D_t][B_L] + [B_N]^T [D_t][B_N] \Big) dV_o \tag{2.56}$$

$$[K_\sigma] = \int_{V_o} [G]^T [\sigma][G] dV_o \tag{2.57}$$

where $[\sigma] = \begin{bmatrix} \sigma_{xx} & \sigma_{xy} \\ \sigma_{xy} & \sigma_{yy} \end{bmatrix}$ is the matrix of current stress.

For the plate element, presently under consideration, one has

$$[B_L] = [B_{L1}] + [B_{L2}] + [B_{L3}] \tag{4.25}$$

where $[B_{L1}]$, $[B_{L2}]$, $[B_{L3}]$ have been defined above by Eqs. (4.15), (4.16), and (4.17) respectively. The matrix $[B_N]$ needed for evaluating $[K_N]$ has been defined by Eq. (4.22). The matrix $[G]$ required for determining $[K_\sigma]$ has been defined by Eq. (4.20).

4.2.2 Stiffness Matrix for Total Analysis — J_2 Deformation Theory

The analysis based on the J_2 deformation theory can either be done incrementally, by using the incremental relations similar to those employed for the incremental theory and derived in Chapter 2, or by using the total relations again as given in Chapter 2. Here the easier option of using the total relations was adopted. The matrix of the applicable moduli is therefore $[D_s]$ the secant moduli. The secant stiffness matrix $[K_S]$, as may be recalled from Chapter 2, may be constructed by the following formulas:

$$[K_S] = [K_L] + \frac{1}{2}[N_1] + \frac{1}{3}[N_2] \tag{2.43}$$

where

$$[K_L] = \int_{V_o} [B_L]^T [D_s][B_L] dV_o \tag{2.40}$$

$$[N_1] = \int_{V_o} [B_L]^T [D_s][B_N] + [B_N]^T [D_s][B_L] + [G]^T [\sigma_L][G] dV_o \tag{2.41}$$

$$[N_2] = \int_{V_o} [B_N]^T [D_s][B_N] + [G]^T [\sigma_N][G] dV_o \tag{2.42}$$

$$\{\sigma_L\} = [D_s][B_L]\{q\},\ \{\sigma_N\} = \frac{1}{2}[D_s][B_N]\{q\} \tag{2.36}$$

The matrices $[B_{L1}]$, $[B_{L2}]$, $[B_{L3}]$, $[B_N]$, $[G]$ are exactly the same as above for the incremental theory. Note that although $\{\sigma_L\}$ and $\{\sigma_N\}$ are obtained as column vectors of size 3×1, they are changed to 2×2 symmetric matrices in Eqs. (2.41) and (2.42).

4.3 Numerical Integration

The formulation of the element stiffness matrices and the internal load vector requires integration through the volume of the plate. In the present nonlinear analysis, the stiffness matrix of an element is a function of the element nodal degrees of freedom, and the stress and strain at different positions along the length, width and depth of the element. Since only parts of the element volume will be plastic, the formulation requires separate integration over the elastic and plastic volumes. We must determine the applicable D_t and D_s values from the stored stresses, stored elastic and plastic strains, and also if need be their increments at the integration points.

The Gauss quadrature method of numerical integration has been adopted here. The stiffness matrix contains terms up to degree twelve in x and y. An exact integration of the highest order terms present in the stiffness matrix, would require 7×7 integration points in each element is strictly required. This was considered prohibitively time-consuming. Therefore, for efficiency reasons, a 2×2 'mesh' was adopted for the present work [43]. For through the thickness integration, 3 Gauss points were considered sufficient, same as for the column problems of Chapter 3. Thus, a $2 \times 2 \times 3$ integration mesh through the volume of the element was chosen for the Gauss integration. The validity of this mesh will be demonstrated in a later section by comparing the results with those from $2 \times 2 \times 5$ and $3 \times 3 \times 5$ meshes.

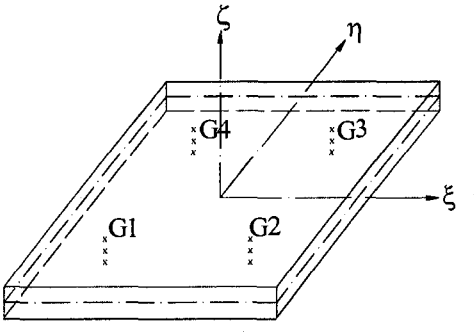

G1 (ξ_1, η_1, ζ_i), **G2** (ξ_2, η_2, ζ_i), **G3** (ξ_3, η_3, ζ_i), **G4** (ξ_4, η_4, ζ_i), $i = 1, 2, 3$

Fig. 4.4 Location of Gauss points in an element

Fig. 4.4 shows the location of the Gauss points in the volume of the element. Their coordinates and the associated weights are listed in Tables 4.1 and 4.2. The Gauss quadrature I of a quantity $Q(\xi, \eta, \zeta)$ over the element volume is then obtained as

$$I = \frac{a\,b\,t}{8}\sum_{i=1}^{2}\sum_{j=1}^{2}\sum_{k=1}^{3} W_i W_j W_k Q(\xi_i, \eta_j, \zeta_k) \tag{4.26}$$

Table 4.1 Abscissae and weights of 2×2 Gauss points in $\xi\eta$ plane

$i(j)$	ξ_i	W_i	η_j	W_j
1	$-\sqrt{1/3}$	1	$-\sqrt{1/3}$	1
2	$+\sqrt{1/3}$	1	$+\sqrt{1/3}$	1

Table 4.2 Abscissae and weights of Gauss points along ζ axis

k	ζ_k	W_k
1	$-\sqrt{3/5}$	5/9
2	0	8/9
3	$+\sqrt{3/5}$	5/9

4.4 Solution Procedures

Solution procedures are outlined, for the incremental load-deformation analyses, as well as those for the total load- deformation. As mentioned before, the former are required for imperfection analyses using the constitutive relations of the J_2 incremental theory, while the latter are needed for analyses based on the J_2 deformation theory of plasticity.

Most of the theory required for the above analyses has been covered in Chapter 2. Therefore here the emphasis is on explaining the sequence of the steps required in implementing the theory.

4.4.1 Solution Procedure for Incremental Load-Displacement Method

The equilibrium equation of the incremental method may be expressed as

$$[K_T]^G \{\Delta q\}^G = \{\Delta P\}^G + \{\Delta R\}^G \tag{3.52}$$

where $[K_T]^G$ is the global tangent stiffness matrix, and $\{\Delta R\}^G = \{P\}^G - \{\overline{P}\}^G$ may be considered as an out-of-balance force vector. $\{P\}^G$ is the total external force vector, and $\{\overline{P}\}^G$ is the corresponding internal force vector, obtained by the virtual work equality as:

$$\{\overline{P}\}^G = \sum \int_{V_o} ([B_L] + [B_N])^T \{\sigma\} dV_o \tag{4.27}$$

Newton-Raphson iterative method combined with displacement control was used to solve the above nonlinear finite element equations.

In the analyses, the imposed boundary conditions are in accordance with the stressing of a simply supported plate. Symmetry is used to reduce the problem size whenever appropriate. The boundary conditions for a full simply supported plate (without using symmetry) are taken to be the following. The transverse displacements along the supported edges are specified to be zero. The inplane v displacements at all the four supported edges are allowed to be free with no applied forces, except to impose symmetry or prevent rigid body movement. The inplane u displacements are specified to be zero along the boundary $x = L$. They are allowed to be free on the other three edges, except the centre node at the $x = 0$ edge. The nodes at this edge are subjected to applied nodal forces corresponding to the uniform compressive stress $\sigma_{xx} = -\sigma$, with σ as an unknown to be found from the solution. The displacement of the centre node at this edge is controlled by specifying its incremental values. By this device of exchanging the unknowns, the compressive stress σ is obtained as a reaction stress, and the maximum load point can be negotiated without difficulty. The plate response beyond the maximum load point can also be traced quite easily. The steps by step solution procedure is as follows:

1. Before the start of the nth incremental displacement, the updated values of all necessary variables for the analysis, $\{\sigma_{n-1}\}$, $\{\varepsilon_{n-1}\}$, $[D_{t,n-1}]$, σ'_Y, and $\{q_{n-1}\}$ from the previous step have been stored for each Gauss point.

2. The global tangent stiffness matrix $[K_T]^G$ is then constructed by using the updated quantities and assuming loading behaviour at all those Gauss points where loading is possible, i.e. points with equivalent stress equal to the current yield stress. At all other Gauss points elastic behviour is assumed. These assumption, however, may not turn out

to be true as unloading (instead of loading) may occur, or the elastic loading may surpass the yield criterion.

3. The displacement increments $\{\Delta q\}^G$ at the free nodes, and the reaction forces corresponding to the specified degrees of freedom are then found provisionally by solving the above linear equations by the standard elimination methods. The displacements are then provisionally updated as $\{q_n\} = \{q_{n-1}\} + \{\Delta q\}$.

4. The strains $\{\varepsilon_n\} = ([B_L] + \frac{1}{2}[B_N])\{q_n\}$ are determined at every Gauss point, with appropriate $\{q_n\}$, to find the incremental strains $\{\Delta\varepsilon_n\} = \{\varepsilon_n\} - \{\varepsilon_{n-1}\}$, where $\{\varepsilon_{n-1}\}$ is the converged strain vector at the previous increment.

5. The stress increments $\{\Delta\sigma_n\} = [D_t]\{\Delta\varepsilon_n\}$ are calculated for Gauss points where loading was assumed, and $\{\Delta\sigma_n\} = [D]\{\Delta\varepsilon_n\}$ where elastic behaviour was assumed.

6. The increments $\{\Delta\sigma_n\}$are added to update the previous stress at all Gauss points, i.e. $\{\sigma_n\} = \{\sigma_{n-1}\} + \{\Delta\sigma_n\}$, where $\{\sigma_{n-1}\}$ is the converged stress vector at the previous increment.

7. The Mises stress $\sigma_e = (\sigma_{xx}^2 + \sigma_{yy}^2 - \sigma_{xx}\sigma_{yy} + 3\sigma_{xy}^2)^{\frac{1}{2}}$ is calculated at all Gauss points using the updated stresses of step (6). Then, σ_e is compared with the yield stress at the end of last increment, σ_Y'. If $\sigma_e - \sigma_Y' \leq 0$, the Gauss point was elastic and remains elastic, or was plastic at the $(n-1)$ th increment but unloads in the current nth increment. The appropriate moduli are elastic at all such points, and the stiffness matrices $[K_t]$ have to be corrected if loading was assumed.

8. If, however, $\sigma_e - \sigma_Y' > 0$ at a Gauss point, then there is plastic deformation. If the Gauss point was on the verge of yield, and loading was assumed, then the assumption of elastic plastic tangent moduli $[D_t]$ is correct. If, on the other hand, the Gauss point was elastic, and elastic behaviour was assumed, then there is overshoot over the current yield stress by $\sigma_e - \sigma_Y'$. One may then assume as an approximation that the behaviour from σ_{n-1}^e to σ_Y' is elastic and from σ_Y' to σ_n^e is plastic. The factor k by which the elastic behaviour should be considered as part of the total stress increment is

$$k = \frac{\sigma_Y^{'} - \sigma_{n-1}^{e}}{\sigma_n^e - \sigma_{n-1}^e} \tag{4.28}$$

and hence the matrix of the moduli to be used in revising $[K_t]$ are $(1-k)\ [D_t] + k[D]$, where $[D_t]$ corresponds to the elastic-plastic moduli at $\sigma_e = \sigma_Y'$. The stress increments are

$$\{\Delta\sigma_n\} = (1-k)\ [D_t]\{\Delta\varepsilon_n\} + k[D]\{\Delta\varepsilon_n\} \tag{4.29}$$

and the updated components are

$$\{\sigma_n\} = \{\sigma_{n-1}\} + \{\Delta\sigma_n\} \tag{4.30}$$

9. The nodal forces corresponding to the updated internal stresses are calculated by looping over all the elements

$$\{\overline{P}\}^G = \sum \int_{V_o} ([B_L] + [B_N])^T \{\sigma\} dV_o \tag{4.27}$$

10. The global unbalanced load vector $\{\Delta R\}$ is then determined as

$$\{\Delta R\}^G = \{P\}^G - \{\overline{P}\}^G \tag{4.31}$$

where $\{P\}^G$ is the external force vector.

11. Fresh $\{\Delta q\}^G$ is found by solving the equation $[K_T]^G\{\Delta q\}^G = \{\Delta P\}^G + \{\Delta R\}^G$.

12. Steps (2) through (11) are repeated until $[K_T]^G$ is consistent with $\{\Delta q\}^G$ and the following criterion is satisfied:

$$\|\Delta R\|^G \leq \epsilon \|\overline{P}\|^G \tag{4.32}$$

where ϵ denotes a preselected tolerance value. Here $\epsilon = 0.001$ to 0.0001 was used. Updating at the nth stage is performed with the converged $\{\Delta q\}^G$.

4.4.2 Solution Procedure for the Total Load-Displacement Method

Nonlinear finite element equations of the deformation theory

$$[K_S]^G \{q\}^G = \{P\}^G + \{\Delta R\}^G \tag{3.54}$$

can be solved directly by iteration as for columns. In the following, the steps of the iteration method in conjunction with the deformation theory are described:

1. In the beginning, when the load is small and linear elastic behaviour is expected everywhere, a linear elastic finite element analysis, assuming $E_s = E$ and ignoring the stress effects, may be carried out by solving $[K_S]^G\{q\}^G = \{P\}^G$ to determine $\{q\}^G$and the corresponding stresses at each Gauss point for a suitable $\{P\}^G$. Knowing an initial estimate of stresses the iteration process for solving the fully nonlinear equations can be started.

2. For every Gauss point i, the strains can be calculated as $\{\varepsilon\} = ([B_L] + \frac{1}{2}[B_N])\{q\}$ from the appropriate $\{q\}$ determined in the previous step. The equivalent strain at each Gauss point is then found using $\varepsilon_e = \sqrt{\frac{2}{3}\varepsilon_{ij}\varepsilon_{ij}}$ which is then used to determine $[D_s]$ the corresponding matrix of the secant moduli.

3. The stress at each Gauss point can then be calculated as $\{\sigma_n\} = [D_s]\{\varepsilon_n\}$.

4. At each Gauss point, calculate the Mises stress $\sigma_e = (\sigma_{xx}^2 + \sigma_{yy}^2 - \sigma_{xx}\sigma_{yy} + 3\sigma_{xy}^2)^{\frac{1}{2}}$ using the updated stresses of step (4). Compare σ_e with the yield stress σ_Y for the material. If $\sigma_e - \sigma_Y \leq 0$, the element was elastic. The matrix of the moduli is then $[D]$ the constant matrix of elastic moduli. If, however, $\sigma_e - \sigma_Y > 0$, there is plastic deformation, and the matrix of the moduli is that of stress dependent secant moduli $[D_s]$.

5. The stiffness matrices $[K_S]$ are recomputed using the updated moduli from step 4. The global stiffness matrix is then assembled appropriately as $[K_S]^G = \sum[K_S]$.

6. The internal nodal forces vector corresponding to the stresses obtained in step 3 is computed by looping over the elements as

$$\{\overline{P}\}^G = \sum \int_{V_o} ([B_L] + [B_N])^T \{\sigma\} dV_o \tag{4.27}$$

8. The assemble the structural global unbalanced load vector $\{\Delta R\}$, where

$$\{\Delta R\}^G = \{P\}^G - \sum \{\overline{P_i}\}^G \tag{4.31}$$

where $\{P\}^G$ is the external force vector.

9. Steps (1) through (8) are repeated until $[K_S]$ is consistent with $\{q\}^G$ and the following criterion is met

$$\|\Delta R\|^G \leq \epsilon \|\overline{P}\|^G \tag{4.32}$$

where ϵ denotes a preselected tolerance value. Here, as previously, $\epsilon = 0.001$ to 0.0001 was used.

4.5 Results of Imperfection Sensitivity Analyses in Plastic Range

In order to trace the postbuckling behaviour of the simply supported plate, some geometric imperfections are added to the initial perfect geometry. If the imperfections are well chosen, the equilibrium path will be continuous and can be expected to lead to a maximum stress close to the observed experimental value. As remarked previously in the case of columns, any known imperfection $w_o(x, y)$ may be considered as a linear combination of the eigenmodes of the corresponding eigenvalue problem. The amplitudes of each of these modes may be determined from the knowledge of $w_o(x, y)$. The response of the plate to $w_o(x, y)$ may therefore be considered as the resultant of the responses from each of these eigen (i.e., Fourier) components. However, as shown for columns, the dominant effect (surpassing the effect of all others) is from the component which corresponds to the critical bifurcation mode. Therefore, instead of considering a general imperfection, it may suffice to consider the one which is proportional to this critical mode. Therefore, in order to obtain such a mode, a subsidiary calculation or analysis should be performed by posing the problem as an eigenvalue (i.e., a bifurcation buckling) problem. Such an analysis may always be based on elastic material behaviour, and then used in a trial and error manner for the imperfection analysis in elastic as well as plastic cases.

In the present case of imperfection growth analysis of an axially compressed plate, the corresponding eigenvalue problem is that of bifurcation of an axially compressed perfectly plane simply supported plate. The solution of this problem for linear isotropic elastic material is well known [42]. All eigenvalues and corresponding eigenmodes are

$$\sigma_{mn} = \frac{Et^2}{12(1-\nu^2)} \frac{\left\{\left(\frac{m\pi}{L}\right)^2 + \left(\frac{n\pi}{B}\right)^2\right\}^2}{\left(\frac{m\pi}{L}\right)^2}, \quad w_{mn}(x, y) = A_{mn} \sin\frac{m\pi x}{L} \sin\frac{n\pi y}{B} \tag{4.33}$$

where m is the number of half sine waves in the longitudinal direction, and n is that in the transverse direction. The critical eigenvalue is the smallest one of σ_{mn}. For such a value, evidently $n = 1$. The value of m is determined by assuming m a continuous variable and equating to zero the derivative of σ_{mn} with respect to m. This gives

$$m_{cr} = \frac{L}{B}, \text{ and } \sigma_{cr} = \frac{\pi^2 E}{3(1-\nu^2)} \left(\frac{t}{B}\right)^2 \tag{4.34}$$

In view of the above the initial imperfection is taken as

$$w_o(x, y) = \rho t \sin\frac{m\pi x}{L} \sin\frac{\pi y}{B} \tag{4.35}$$

where m is an integer close to L/B, ρ is a nondimensional parameter, and ρt is the maximum deviation from flatness. As can be expected, an imperfection will underestimate the critical load of the perfect plate. The difference will depend on the sensitivity of the structure type to imperfections. However, if the imperfections are small enough, the prebuckling and postbuckling behaviour can be expected to be very close to that for the perfect one.

The above distribution of the initial imperfection is valid for the whole plate domain in the xy plane. For the finite element analysis, however, a local approximation, valid only for the particular element will be used. In this thesis, the imperfection within the element is assumed to vary bilinearly over the element domain

$$w_o(\xi, \eta) = N_1 w_{o1} + N_2 w_{o2} + N_3 w_{o3} + N_4 w_{o4} \tag{4.36}$$

where the interpolation function N_1, N_2, N_3, N_4 are, as before,

$$N_i = \frac{1}{4}(1 + \xi\xi_i)(1 + \eta\eta_i).\ i = 1 \text{ to } 4 \tag{4.7}$$

and w_{oi} are the values of the imperfection function at the xy coordinates of the element nodes

$$w_{oi} = \rho\, t \sin\frac{m\pi x_i}{L}\sin\frac{\pi y_i}{B},\ i = 1 \text{ to } 4 \tag{4.37}$$

4.5.1 Elastic Buckling and Postbuckling of Square Plates

Elastic buckling and postbuckling of axially compressed simply supported square and rectangular plates are well-studied problems. The treatment here is motivated for the purpose of verification of the constructed FE programs.

The postbuckling problem is intrinsically different from the linear buckling problem. As for column problems in Chapter 3, two sources of nonlinearity exist for the postbuckling problems. The first is connected with the strain-displacement equations. The second order rotation related strains exert a significant influence on the structural behaviour. The second source of nonlinearity stems from the effect of deformed geometry on equilibrium equations. It is necessary to keep track of the evolving deformed geometry when writing the equilibrium equations. This change in geometry causes these equations to become nonlinear. In the finite element method, this nonlinearity is taken into account by forcing the unbalanced forces to zero, and thus establishing equality between the external loads and the internal stresses in the deformed configuration.

For the square plate, one has $L = B$, and $m = n = 1$. Accordingly, the imperfection is taken as

$$w_o(x,\, y) = \rho\, t \sin\frac{\pi x}{B}\sin\frac{\pi y}{B} \tag{4.38}$$

The plate dimensions and properties (Aluminum) were taken as:

$L = B = 500$ mm, $B/t = 23$, $E = 70,000$ MPa, $\nu = 0.32$.

In accordance with the symmetry of the deformation mode, only one quarter of the plate needs to be modeled. Fig. 4.5 shows the chosen quarter, with 9 finite elements.

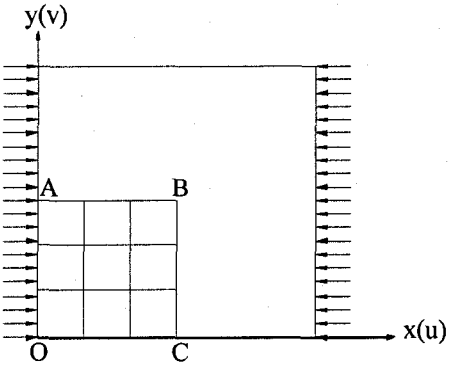

Fig. 4.5 Load condition and finite element mesh employed

To enforce w equal to zero along all edges, for example at edge $x = 0$, one must require $w = 0$ as well as $w_y = 0$. Therefore the boundary conditions on the edges are:

$$
\begin{aligned}
OA \qquad & w = 0, w_y = 0, \\
OC \qquad & w = 0, w_x = 0, \\
CB \qquad & u = 0, w_x = 0, \\
AB \qquad & v = 0, w_y = 0.
\end{aligned}
$$

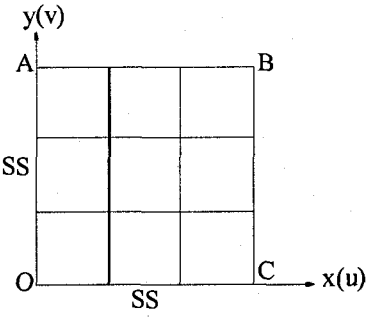

Fig. 4.6 A symmetrical quater of the simply supported plate of Fig. 4.5

Figure 4.7 shows the progress of the centre point deflection as a function of the applied stress. Graphs corresponding to initial imperfections $\rho = w_0/t$, increasing from 0.1 % to 5 % are plotted, as shown. One can infer that for very small initial imperfections, the load deflection behaviour would be close to that of a "perfect" plate with zero imperfection. For relatively large imperfections, the load deflection behaviour is initially more compliant, but with larger deformations, the graphs begin to come close together. It is

evident that the plate behaviour in elastic range is stable regardless of the initial imperfections; there is no decrease in the load as deformation progresses. This conclusion is in line with the results of other investigators of this problem. These results therefore demonstrate the validity of the present FE formulation and its implementation.

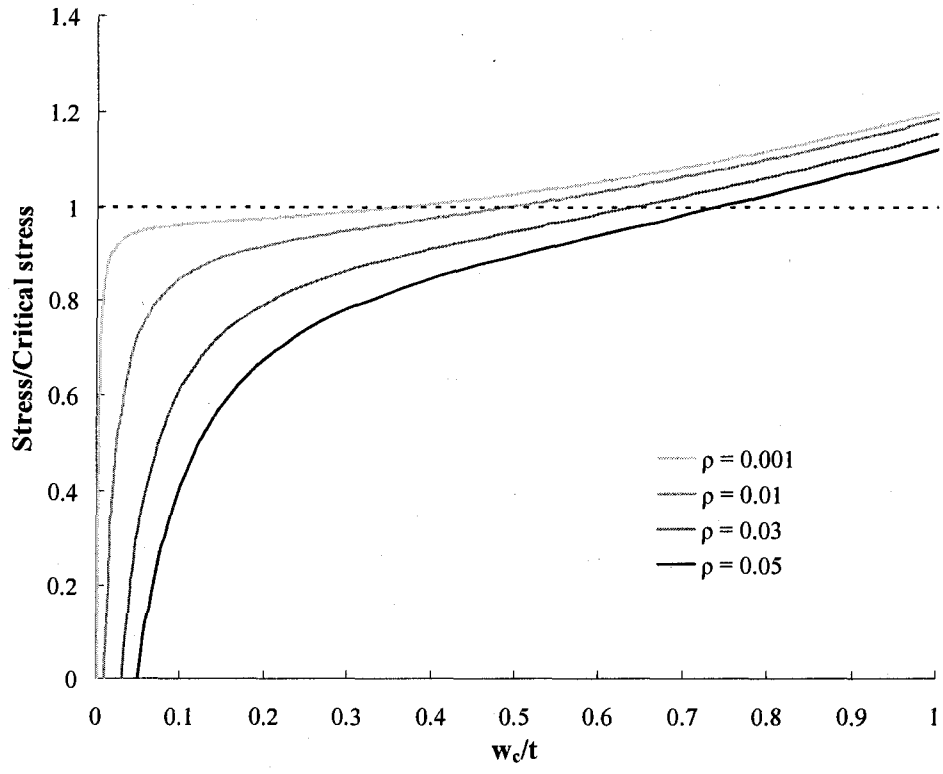

Fig. 4.7 Elastic postbuckling of a simply supported square plate

4.5.2 Elastic Buckling and Postbuckling of Rectangular Plates

Now, the elastic postbuckling behaviour of a rectangular plate is considered. For this purpose, a rectangular plate of a length 5 times the width is considered. The dimensions of the plate and (Aluminum) properties are taken as follows.

$L/B = 5$, $B/t = 23$, $E = 70,000$ MPa, $\nu = 0.32$.

Since the length over width ratio is 5, $m = 5$. The initial imperfection is therefore taken as

$$w_o(x, y) = \rho t \sin\frac{5\pi x}{L}\sin\frac{\pi y}{B} \tag{4.39}$$

The corresponding bifurcation stress is same as that of the square plate which has the same B/t ratio, and can be calculated from Eq. (4.34).

Although, the boundary conditions, the loading conditions and the geometric shapes are symmetrical about the centre lines, the buckling modes along the longitudinal direction may not symmetric (for rectangular plates with different L/B and B/t ratio). Therefore, only a widthwise symmetric half of the plate, Fig. 4.8, was used in the finite element modeling. The boundary conditions were taken as:

$$\begin{aligned} OA \qquad & w = w_y = 0, \\ OC \qquad & w = w_x = 0, \\ AB \qquad & v = w_y = 0, \\ CB \qquad & u = w = w_y = 0. \end{aligned}$$

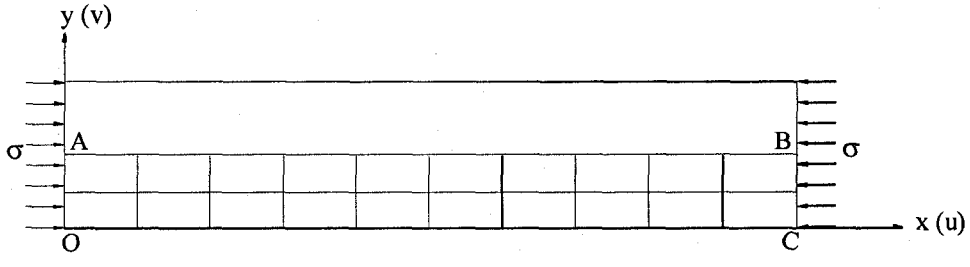

Fig. 4.8 FE mesh for elastic imperfection behaviour of a rectangular plate ($L/B = 5$)

The mesh density was chosen so as to obtain accurate results. The number of elements along the longer side was taken to be 10, while that on the shorter side was taken as 2. Figure 4.9 shows the progress of the centre point deflection as a function of the applied stress. Graphs corresponding to initial imperfections, $\rho = w_c/t$, increasing from 0.1 % to 5 % are plotted. The graphs are similar to those for the square plate. In general, there are significant differences among them, but more initially and less after the bifurcation load is crossed. As in the case of a square plate, and again in line with the expected conclusion, the plate behaviour is stable regardless of the initial imperfections. These results therefore provide a further validation of the present FE formulation.

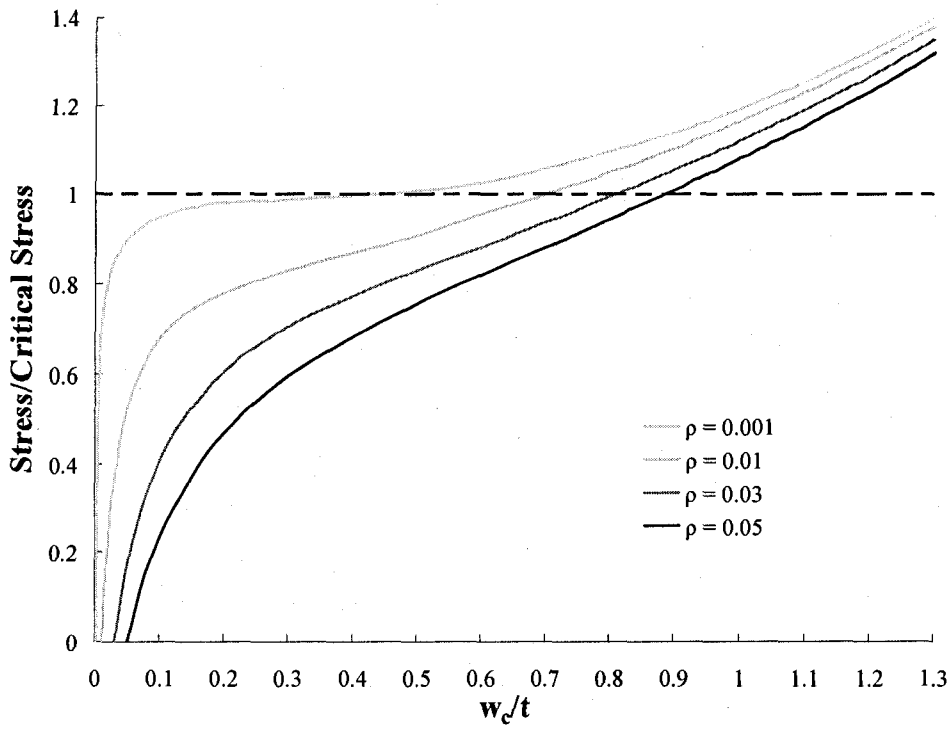

Fig. 4.9 Elastic postbuckling of a simply supported rectangular plate

In summary, it is found that elastic postbuckling behaviour of plates is almost the same as that of columns. Two main points may be reiterated.

1. The load-deflection paths for imperfect elastic plates are all stable. In other words, the load continues to increase as deformation progresses. The rate of load increase is faster for plates than for columns, and the bifurcation load in the former cases is crossed quite early by the load-deflection paths. It may be recalled that for columns, the slope of load-deflection curve is zero at bifurcation point, and increases very gradually. However, for plates, the slope is never zero, even at bifurcation.

2. The buckling behaviour of elastic plates is not very sensitive to initial imperfections. In the prebuckling range, the load-deflection curves are different depending on the imperfection magnitudes. However, these differences begin to become less after the bifurcation load is crossed.

4.5.3 Plastic Buckling and Postbuckling of Square Plates

Nonlinear effects due to plasticity have been tackled in a manner similar to that for the geometric nonlinearity. The nonlinear strain-path dependent plasticity effects are accounted for by accumulating displacements at each node, and stresses and strains at each of the Gauss points. For each increment of load, the matrix of elastic-plastic tangent moduli is determined which relates the incremental stresses to incremental strains. The yield condition at each of the Gauss points is used to determine the applicable (loading or unloading) constitutive law to determine the stress increments from strain increments by trial and error iteration process. The stresses are updated after convergence. Newton-Raphson method combined with the displacement control was used to trace the load-deflection curves up to and beyond the maximum load point.

For square plates, the critical plastic buckling mode is the same as the elastic one. Hence an initial imperfection in the shape of single half-waves in both direction, same as Eq. (4.38), was assumed. The plastic bifurcation stress [36] can be calculated from Eq. (2.65), repeated here, as

$$\sigma_{cr} = \frac{\pi^2}{12}\left(\frac{t}{B}\right)^2 \{B_1 + D_1 + 2(C_1 + 2F_1)\} \tag{2.65}$$

where B_1, C_1, D_1, F_1 are the elastic/plastic moduli defined in Chapter 2.

The material properties used are defined by a uniaxial stress-strain curve of the form

$$\varepsilon = \frac{\sigma}{E} + 0.002(\frac{\sigma}{\sigma_Y})^{20} \tag{4.40}$$

where $E = 10,700$ ksi, $\sigma_Y = 61.4$ ksi are respectively the Young's modulus, and the nominal initial yield stress. This formula represents the behaviour of 14S-T6 aluminum alloy. In this Chapter, all plates are considered to be of the same material, defined by Eq. (4.40).

Before presenting results for the plastic postbuckling behaviour, the validity of mesh $2 \times 2 \times 3$ employed in the FE plate elements is established. Three meshes of Gauss points (1) $3 \times 3 \times 3$, (2) $2 \times 2 \times 5$, and (3) $2 \times 2 \times 3$ were used in the comparison study. Three magnitudes of imperfection $\rho = 0.01, 0.03,$ and 0.05 were tried, where it may be recalled

that ρ denotes the ratio of the maximum initial out-of-plane deflection to plate thickness. The maximum loads calculated by three kinds of mesh are listed in Table 4.3.

Table 4.3 Maximum loads; effect of Gauss points in one element

Mesh Size	ρ **= 0.01**	***Error**	ρ **= 0.03**	***Error**	ρ **= 0.05**	***Error**
Mesh 3 × 3 × 3	389.46 MPa	0.477%	352.99 MPa	0.272%	337.47 MPa	0.388 %
Mesh 2 × 2 × 5	392.63 MPa	0.333%	353.22 MPa	0.337%	338.10 MPa	0.147 %
Mesh 2 × 2 × 3	391.89 MPa	0.144%	349.89 MPa	0.609%	337.23 MPa	0.108 %

$$\textbf{*Error} = \left|\frac{\text{Load}_i - \text{Av. Load}}{\text{Av. Load}}\right| \times 100\% \ (i = 1, 2, 3 \text{ refers to the meshes in listed order})$$

From Table 4.3, it is evident that an increase in Gauss points affects the maximum load predictions, rather insignificantly, less than 1%. Consequently, the use of the 2 × 2 × 3 mesh in the present investigations is justified.

4.5.3.1 Numerical Results for the Incremental Theory

The load-deflection curves for various imperfection levels are shown in Fig. 4.10 for the aluminum square plate with $B/t = 23$. The dots on these curves denote the maximum stress points, which are the critical stresses for onset of instability. Figure 4.11 shows similar graphs for another square plate with $B/t = 18$.

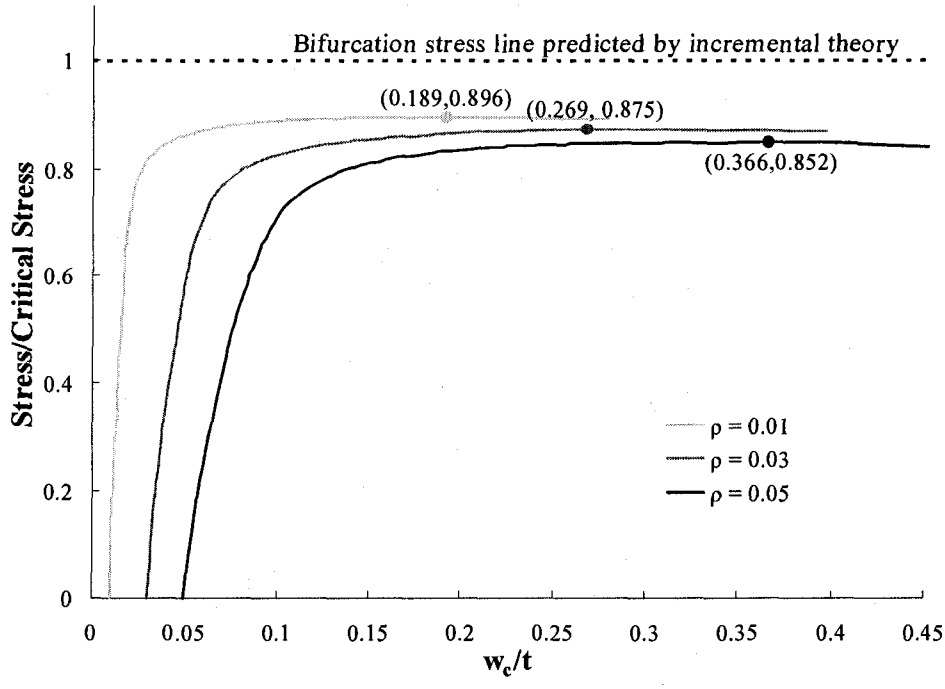

Fig. 4.10 Plastic postbuckling of square plates ($B/t = 23$) by incremental theory

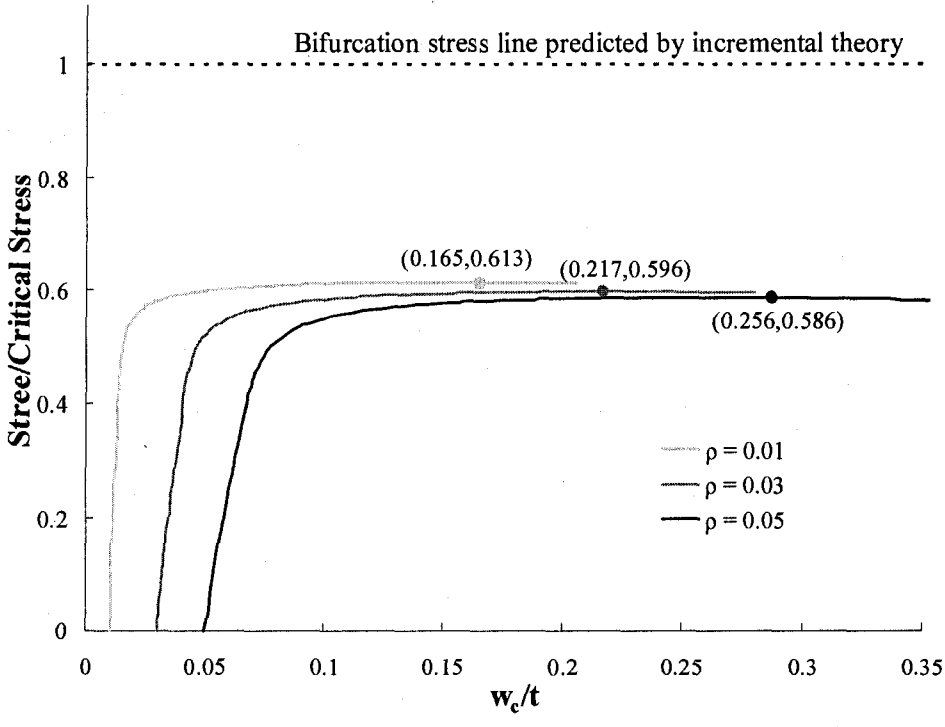

Fig. 4.11 Plastic postbuckling of square plates ($B/t = 18$) by incremental theory

One can see that the plastic postbuckling behaviour is completely different from elastic postbuckling behaviour, the load-deflection curves descend after reaching the maximum loads. The maximum loads are all smaller than the bifurcation load and increasingly decreased as the magnitude of initial imperfection increases.

4.5.3.2 Numerical Results for the Deformation Theory

The parallel results using the constitutive relations of the deformation theory are now presented. The graphs in Fig. 4.12 show the load-deflection behaviour for various imperfection levels for the aluminum square plate with $B/t = 23$. The dots on these curves indicate the critical stresses for onset of instability. Figure 4.13 shows similar graphs for this theory for another square plate with $B/t = 18$.

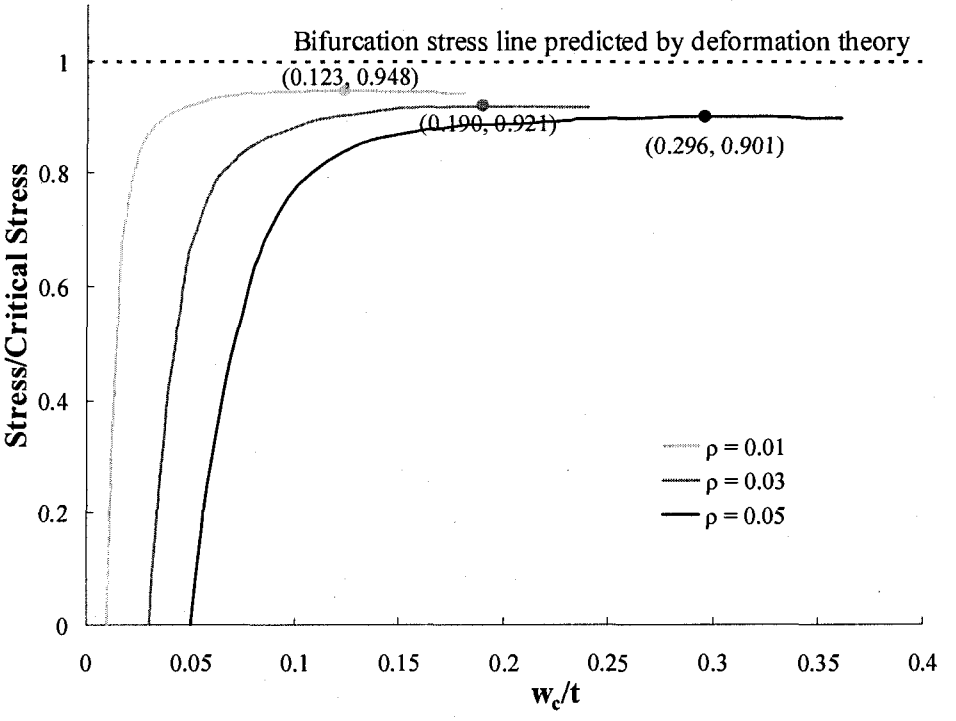

Fig. 4.12 Plastic postbuckling of square plates ($B/t = 23$) by deformation theory

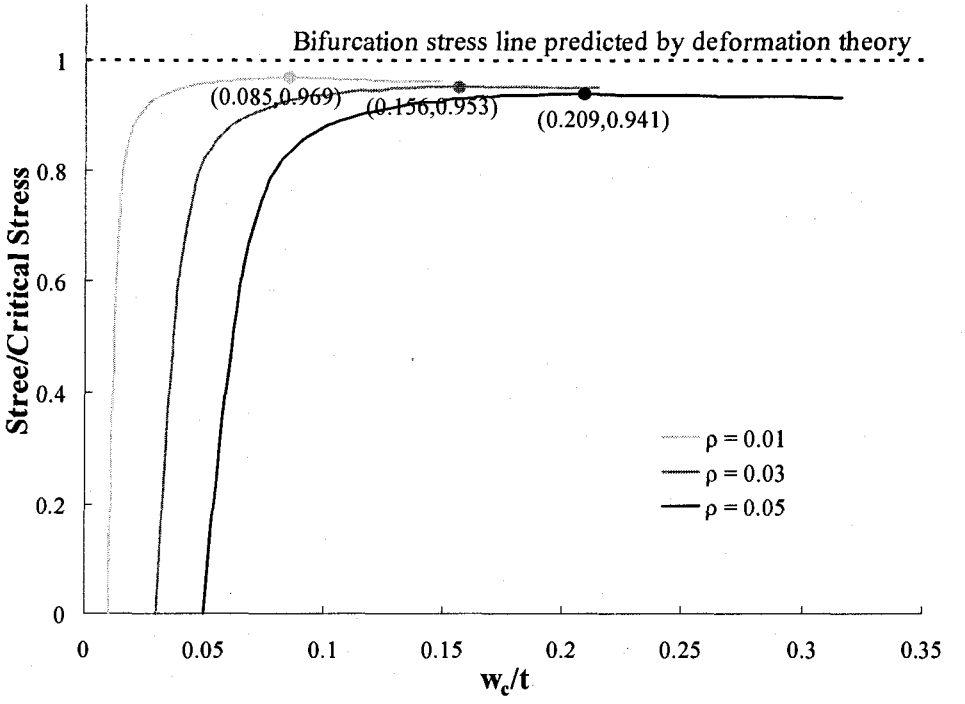

Fig. 4.13 Plastic postbuckling of square plates ($B/t = 18$) by deformation theory

4.5.4 Plastic Buckling and Postbuckling of Rectangular Plates

Now the plastic postbuckling behaviour of rectangular plates is pursued. The plastic bifurcation modes for rectangular plates are different from those of the elastic plates. The number of half waves m along the longitudinal direction is not equal to the length over width ratio. The number is now given by [36]

$$(mB/L)^2 = \sqrt{D_1/B_1} \tag{2.67}$$

and the plastic bifurcation stress [36] is that given by Eq. (2.66), repeated here

$$\sigma_{cr} = \frac{\pi^2 t^2}{12B^2}[2\sqrt{B_1 D_1} + 2(C_1 + 2F_1)] \tag{2.66}$$

where B_1, C_1, D_1, and F_1 are the elastic/plasticity moduli defined in Chapter 2.

4.5.4.1 Numerical Results for the Incremental Theory

Based on the given material, plate dimension and incremental theory, m is equal to 6.673 for the rectangular plate $(L/B = 5, B/t = 23)$ and 7.071 for the plate $(L/B = 5,$ $B/t = 18)$ respectively. The initial imperfection is taken approximately as $m = 7$ sine waves for both plates. The mesh density was chosen as 14×2 for the half plate, Fig. 4.14.

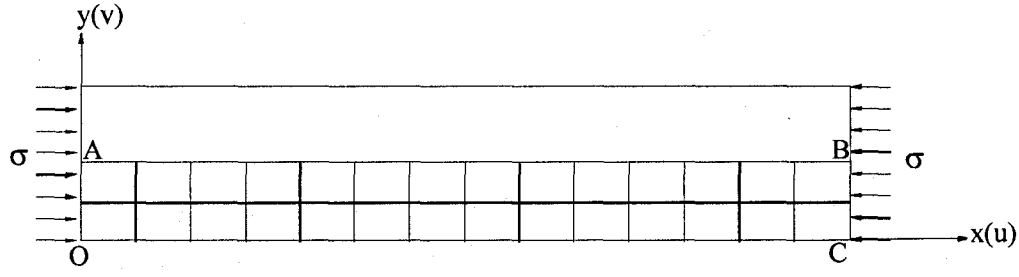

Fig. 4.14 FE mesh for plastic imperfection behaviour of a rectangular plate $(L/B = 5)$

Figures 4.15 and 4.16 show the progress of the centre point deflection as a function of applied stress for the two rectangular plates. Graphs corresponding to initial imperfections w_c/t increasing from 0.01 to 0.05 are plotted. One can observe that the load-deflection behaviour is close to that of a perfect plate for small initial imperfections. The load-deflection curves descend after reaching the maximum loads. As expected, the maximum loads are decreased as the magnitudes of the initial imperfection increase.

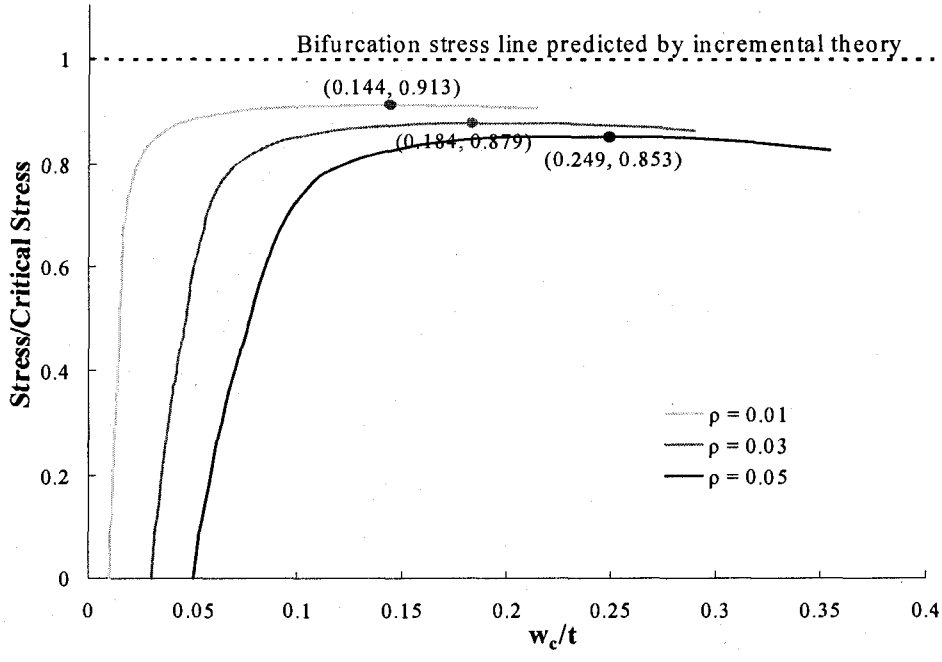

Fig. 4.15 Plastic postbuckling of rect. plates $(L/B = 5, B/t = 23)$, incremental theory

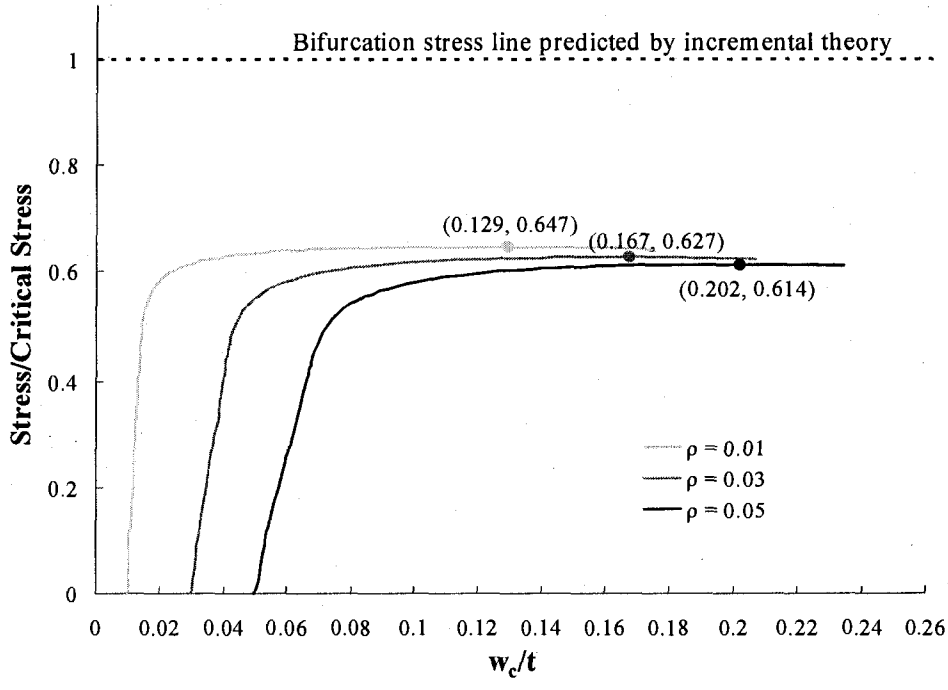

Fig. 4.16 Plastic postbuckling of rect. plates ($L/B = 5, B/t = 18$), incremental theory

4.5.4.2 Numerical Results for the Deformation Theory

Based the material, plate dimension and deformation theory, $m = 6.031$ for the rectangular plate $(L/B = 5, B/t = 23)$ and $m = 6.565$ for the rectangular plate $(L/B = 5, B/t = 23)$. Accordingly, in the initial imperfection specification, the approximation is made that $m = 6$ sine waves for the first (thinner) plate, and $m = 7$ for the second plate. The mesh densities were chosen as 14×2 and 12×2 for the two plates. The load-deflction graphs for different magnitudes of imperfections for this theory are shown in Figs. 4.17 and 4.18 for the two plates.

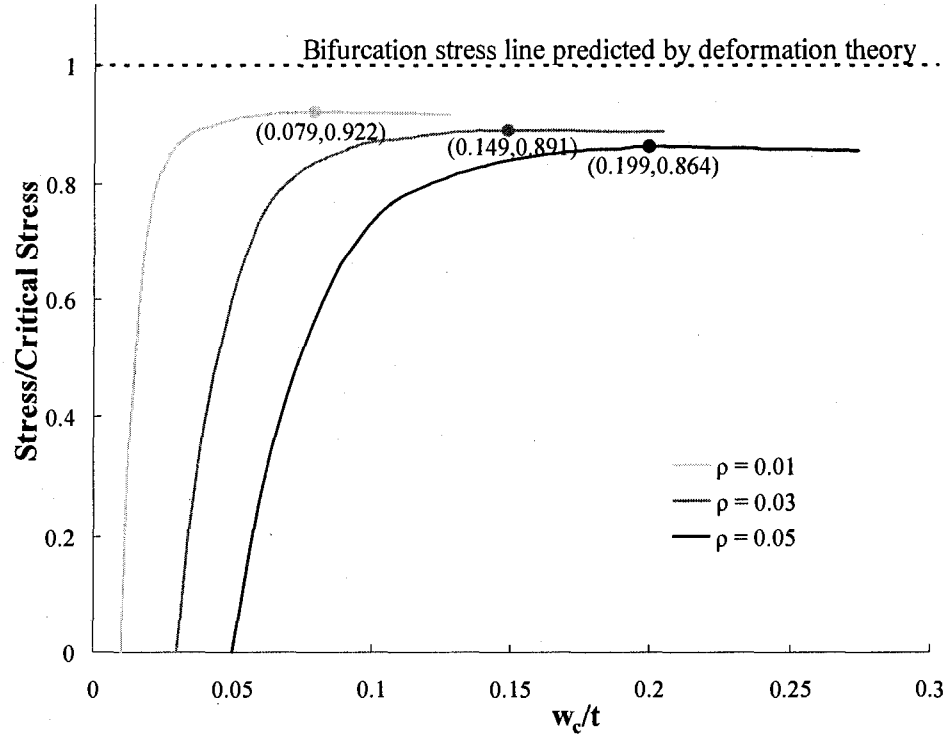

Fig. 4.17 Plastic postbuckling of rect. plates ($L/B = 5$, $B/t = 23$), deformation theory

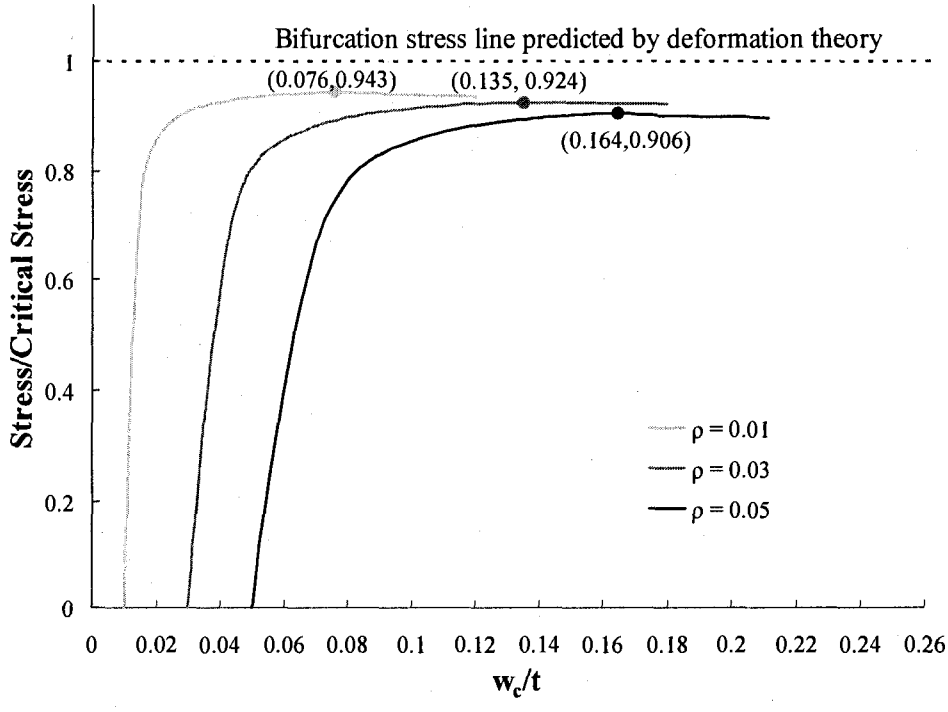

Fig. 4.18 Plastic postbuckling of rect. plates ($L/B = 5$, $B/t = 18$), deformation theory

4.6 Comparison and Conclusion

The load-deflection behaviours predicted by the two J_2 plasticity theories are shown together in Figs. 4.19 to 4.22. The triangular symbols denote the maximum stress points predicted by the incremental theory, whereas the diamond symbols denote the maximum stress points predicted by the deformation theory. Also shown are the bifurcation stress lines predicted by the two theories; the higher line is that from the J_2 incremental theory, and the lower one is that from the J_2 deformation theory.

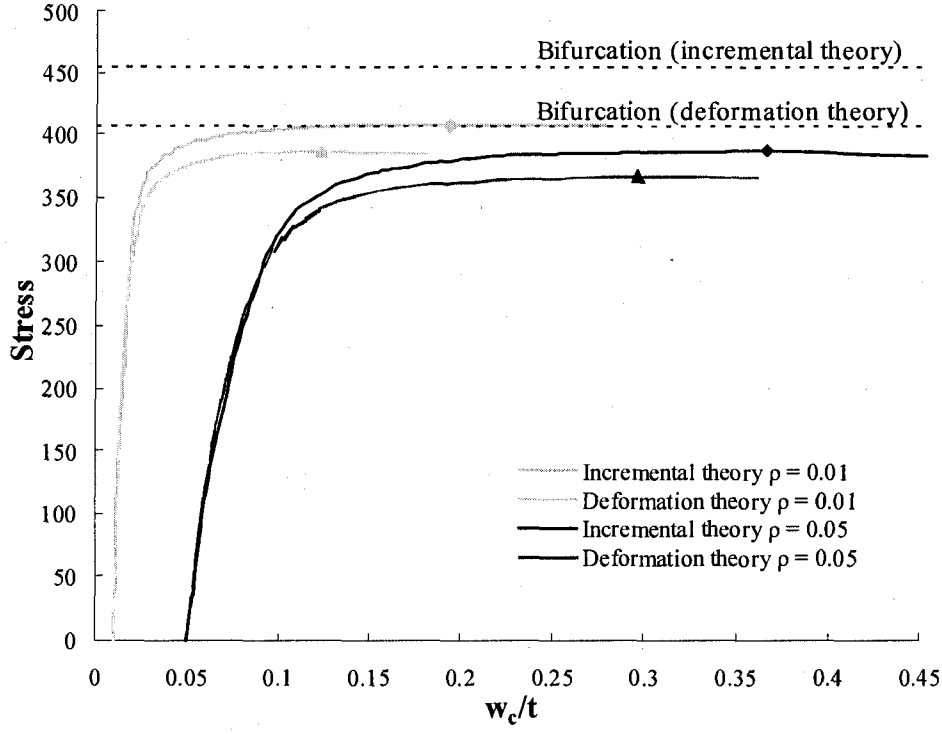

Fig. 4.19 Numerical result comparison of square plate ($B/t = 23$)

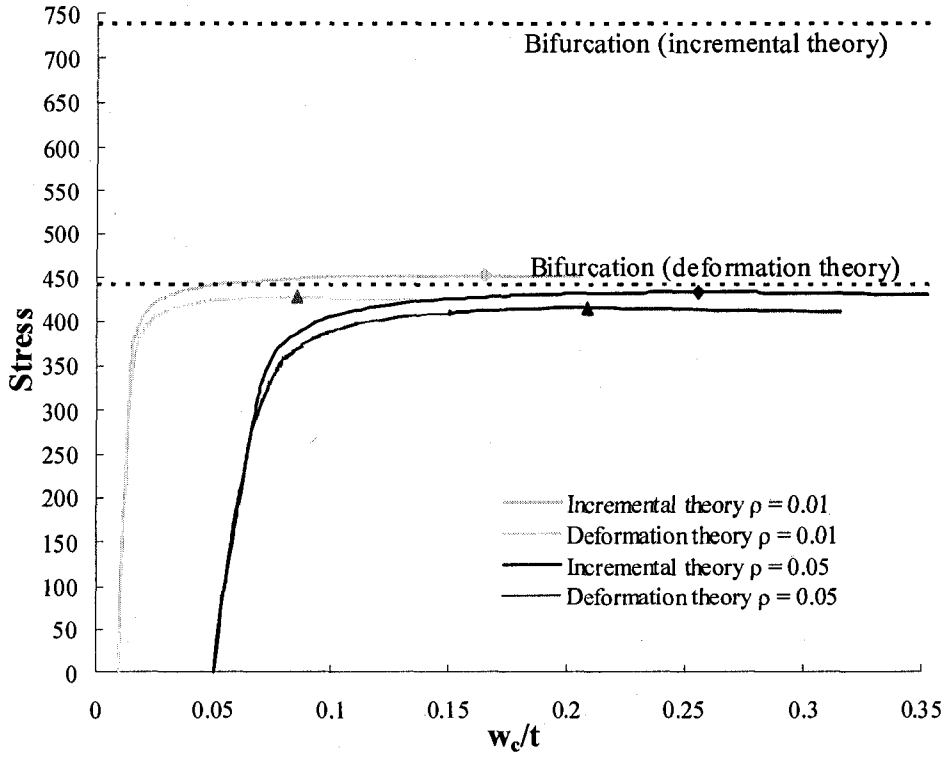

Fig. 4.20 Numerical result comparison of square plate ($B/t = 18$)

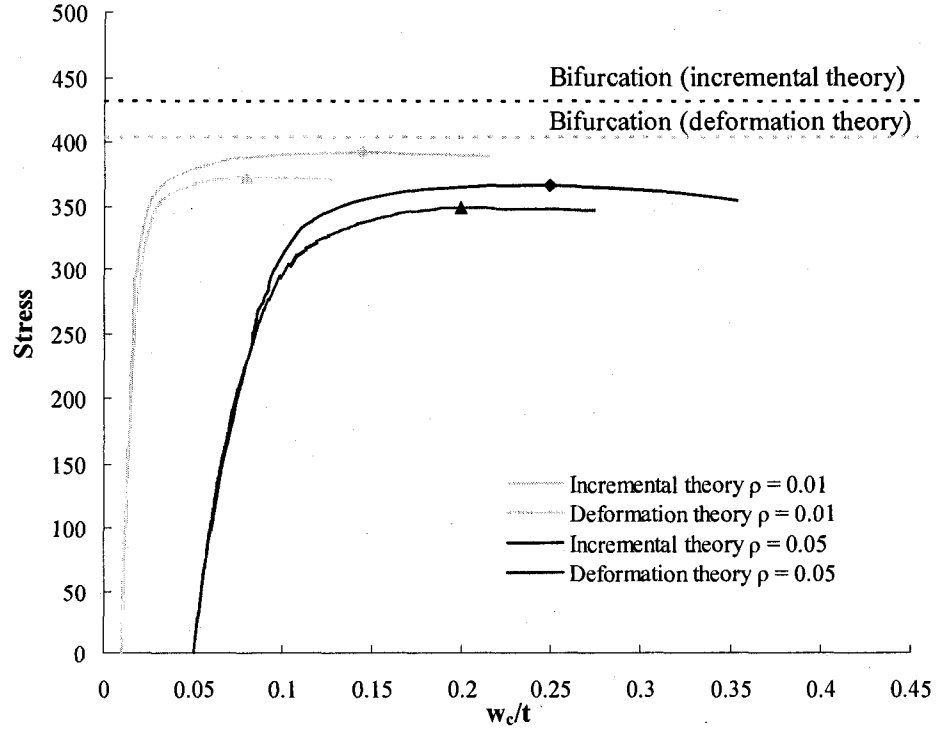

Fig. 4.21 Numerical result comparison of rectangular plate ($L/B = 5,\ B/t = 23$)

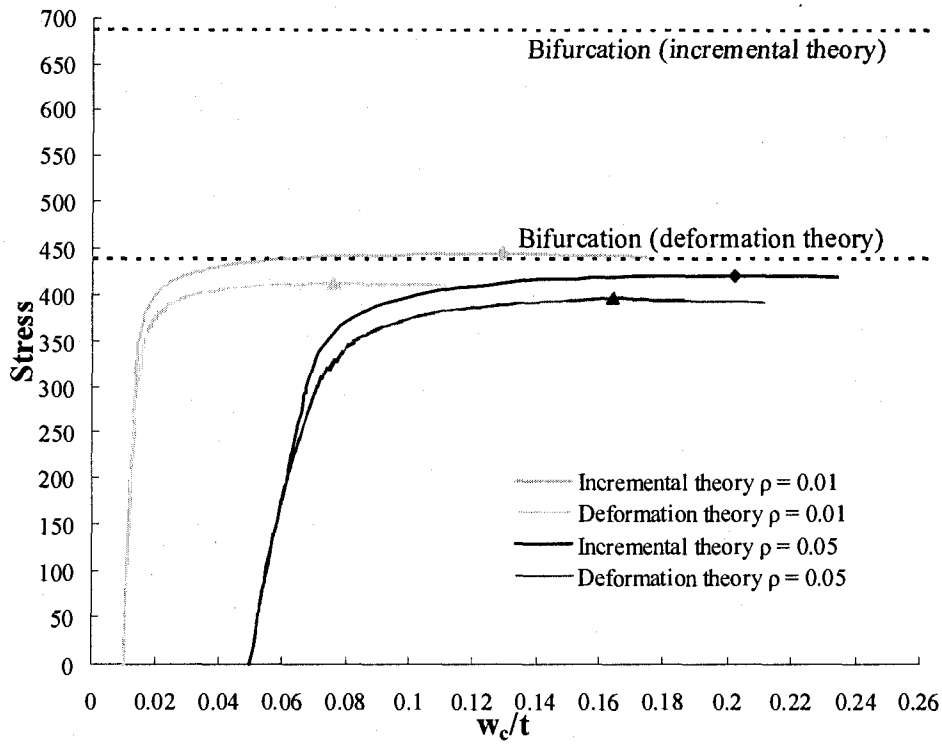

Fig. 4.22. Numerical result comparison of rectangular plate ($L/B = 5$, $B/t = 18$)

A numerical comparison between the results of the two theories is presented in Tables 4.4 to 4.7 below.

Table 4.4 Maximum stress comparison (square plates: $B/t = 23$)

Imperfection	σ_{max}^{inc} **(MPa)**	σ_{max}^{def} **(MPa)**	***Error**
$\rho = 0$	454.36	407.13	10.96 %
$\rho = 0.01$	407.16	386.12	4.88%
$\rho = 0.03$	397.38	375.09	5.17 %
$\rho = 0.05$	387.03	366.81	4.97 %

$$*\text{Error} = \frac{2(\sigma_{max}^{inc} - \sigma_{max}^{def})}{(\sigma_{cr}^{inc} + \sigma_{cr}^{def})}$$

Table 4.5 Maximum stress comparison (square plates: $B/t = 18$)

Imperfection	σ_{max}^{inc} **(MPa)**	σ_{max}^{def} **(MPa)**	***Error**
$\rho = 0$	739.22	441.33	50.47 %
$\rho = 0.01$	452.97	427.49	4.317 %
$\rho = 0.03$	440.70	420.59	3.406 %
$\rho = 0.05$	433.22	415.08	3.073 %

Table 4.6 Maximum stress comparison (rectangular plates: $B/t = 23$, $L/B = 5$)

Imperfection	σ_{max}^{inc} **(MPa)**	σ_{max}^{def} **(MPa)**	***Error**
$\rho = 0$	432.56	403.92	6.848 %
$\rho = 0.01$	394.94	372.33	5.406 %
$\rho = 0.03$	376.88	359.91	4.058 %
$\rho = 0.05$	365.73	348.88	4.029 %

Table 4.7 Maximum stress comparison (rectangular plates: $B/t = 18$, $L/B = 5$)

Imperfection	σ_{max}^{inc} **(MPa)**	σ_{max}^{def} **(MPa)**	***Error**
$\rho = 0$	686.51	438.47	44.10 %
$\rho = 0.01$	444.09	413.70	5.401 %
$\rho = 0.03$	430.52	405.43	4.462 %
$\rho = 0.05$	421.42	397.15	4.314 %

Based on the above finite element results, one can conclude that :

1. The postbuckling paths are unstable, load decreases after attaining the maximum.

2. There are significant differences between the bifurcation stress predictions of the J_2 incremental theory and the J_2 deformation theory for simply supported plates (which is well known). However, if the buckling is considered as an initial imperfection growth

phenomenon, the differences between the maximum stress predictions by the two plasticity theories can be reduced to a much smaller extent, less than 6%. More importantly, the maximum loads predicted by the incremental theory growth analysis can be brought down lower than the bifurcation loads of the deformation theory

3. For the J_2 incremental theory, the thicker plates are more imperfection sensitive than the thinner ones. This means that for the J_2 incremental theory, the imperfection sensitivity is increased with plastic buckling strains. The deformation theory, on the other hand, is found not to be very imperfection sensitive.

Chapter 5

Simulation of Experiments and Comparison of Results

An experimental study of the plastic buckling of rectangular aluminum plates under uniaxial compression and simply supported edge conditions was performed by Kamal Berrada in 1985 at McGill University [12]. The results showed that the bifurcation loads of neither the J_2 incremental theory nor the J_2 deformation theory of plasticity provided a close correlation with experiments. It therefore appears that in order to find some agreement with the test results, imperfection analyses using both plasticity theories are needed. As mentioned previously, the objective of the present study is to perform such analyses. The FE programs developed in accordance with the theory presented in Chapter 4 are now applied to the task of imperfection analyses of the specimens tested by Berrada. Two FE programs were constructed for this purpose using the *Mathematica* software. The program PPBP-INC and PPBP-DEF perform the imperfection analyses using respectively the J_2 incremental and J_2 deformation theories of plasticity. Load-deflection paths, up to and beyond the maximum loads, are calculated using the measured initial imperfections of the test specimens. These maximum load predictions for the two theories are compared with the experimental results, as well as with the predictions of the bifurcation buckling loads of the two theories.

5.1 Finite Element Simulation of Experimental Cases

Ideally, to compare the numerical results with the experimental ones, one should simulate the experimental conditions in the finite element programs as accurately as possible. However, some experimental conditions are not known, or are not easy to simulate. One must therefore make some reasonable assumptions in accordance with the theoretical requirements. Some aspects of these requirements are explained below.

5.1.1 Material Properties

All experiments were done on Aluminum tubes of square sections of centreline width B. Such tubes when compressed in the longitudinal direction, simultaneous stressing of 4 identical simply supported plates. The local buckling of such tubes is equivalent to

simultaneous buckling of four simply supported plates. Tubes of several different B/t ratio were tested to obtain a wide range of buckling load magnitudes.

The plasticity theories used in the formulations require the material to be an isotropic and homogeneous continuum initially, and to remain so during the deformation. Furthermore, the theories postulate that the material undergoes isotropic hardening resulting in a uniform expansion of the von Mises yield surface in the stress space. In order to ensure that the specimen material did approximate the above postulated properties, all specimen tubes were annealed at 420° C for 2 hours, to minimize or eliminate some defects, e.g. preexisting plastic strains (due to cold work) and residual stresses. In finite element program, the material was assumed have satisfied all theoretical requirements.

5.1.2 Stress-Strain Relation

In finite element programs, the uniaxial stress-strain relations are based on a bilinear approximation to average stress-strain curves of specimens in experiments, as shown below in Fig. 5.1.

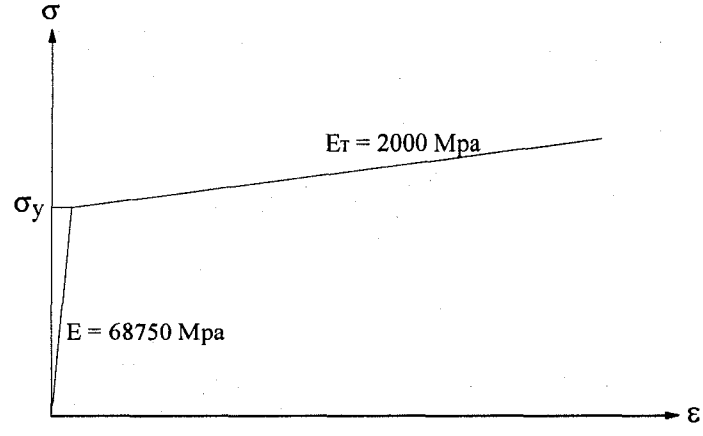

Fig. 5.1 Bilinear stress-strain relation

The Young's modulus is that of Aluminum, $E = 68,750$ MPa. The tangent modulus is taken as $E_t = 2,000$ MPa. The yield stress σ_Y changes from one specimen to other [12].

The vertical axis on the graph represents the nominal average compressive stress equal to the axial force divided by the initial area ($\sigma = P/A_o$). The horizontal axis represents the nominal average compressive strain equal to the shortening of the specimen length

divided by original length ($\varepsilon = 1 - L/L_o$). For relatively moderate strains ($\varepsilon < 5\%$), only negligible difference exist between these nominal measures and the Kirchhoff stress and the Lagrangian strain of the theory.

5.1.3 Initial Geometrical Imperfections

The specimens used in the experiment contain geometrical imperfections, some of these can be listed as follows:

(1) Variations in thickness over the cross-section and length
(2) Variations in width along the length
(3) Variations of the corner angles from 90°
(4) Variation in flatness
(5) Deviation from a plane end surface
(6) Twist along the length.

In the experiments, only some of these imperfections were measured. The maximum error in cross-sectional width, in longitudinal width, and longitudinal thickness were all very small (< 2%) [12]. These imperfections are therefore neglected in the finite element modeling. The error in cross-sectional thickness is up to 9%, which probably should have been considered in the FE model to render it more realistic. However, this would require a large number of elements, and for highly nonlinear problems like the present ones, the large number will reduce the calculation speed significantly, and also may not be allowed by the capacity of the computing software. Hence in the present finite element simulations, only the out-of-flattness imperfections were considered, and all other imperfections were neglected.

5.1.4 Boundary Conditions

As mentioned previously, in the experiments, square tubes were chosen to simulate the simple support condition at the unloaded longitudinal edges. The reason for this is that a square tube of uniform thickness will buckle under uniform compression as shown in Fig. 5.2.

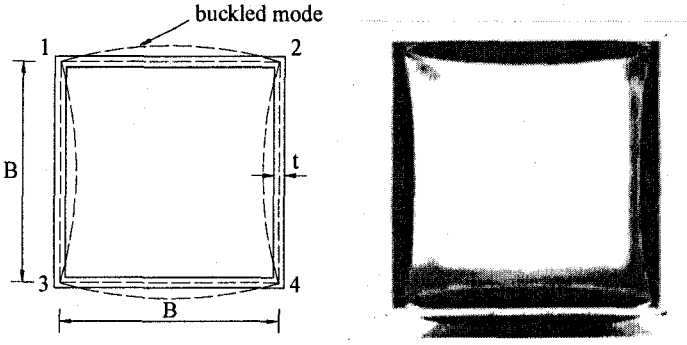

Fig. 5.2 Cross-section of a buckled square tube

By symmetry, the corners do not undergo any buckling displacement. A corner angle will keep at 90° as its initial angle, but can rotate bodily during the buckling deformations as shown in the figure. Therefore, the moments at the corners in such a deformation mode are zero. Thus, the condition at the tube corner can be identified as that of a simple support for a single plate. At the loaded edges, i.e., at the flat ends roller supports were used to simulate the simply supported conditions, by reducing inplane friction forces between the loading plates and the specimens.

The boundary conditions required in plasticity theory are as follows:

$$\begin{aligned} w(0,y) &= w_y(0,y) = 0 \\ w(x,0) &= w_x(x,0) = 0 \\ w(L,y) &= w_y(L,y) = 0 \\ w(x,B) &= w_x(x,B) = 0 \end{aligned} \tag{5.1}$$

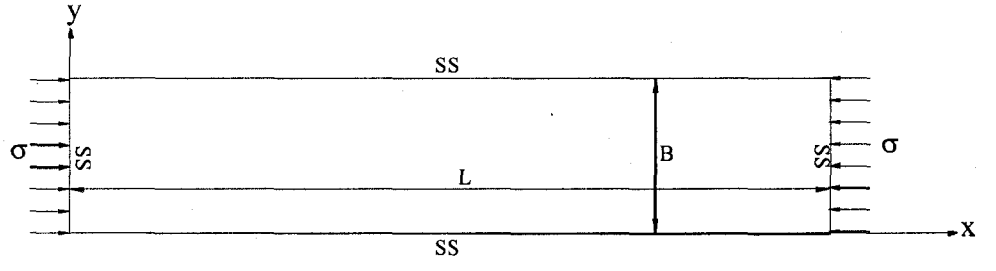

Fig. 5.3 Simply supported plate under uniform compression

The boundary conditions used in the FE models were the same as the above, except that the axial displacements were constrained at $x = L$:

$$u(L,y) = 0 \tag{5.2}$$

to develop the reaction forces corresponding to the axial forces applied at the $x = 0$ edge.

5.1.5 Load Application

In experiments, a ball joint between the machine loading head and the specimen was used to eliminate any eccentricity of loading which might have been caused by imperfect contact between the machine loading head and the loading plates. Loading plates were used to reduce the bending effect and assure uniform transfer of load to the specimen. To assure coincidence of the loading axis and the specimen axis, the geometric centres of the specimens, the loading plates and the ball joint were aligned with the geometrical centre of the machine loading head as accurately as possible. In the finite element analysis, based on the theoretical postulates and the experimental conditions, the compressive stresses are assumed as uniformly distributed through the thickness of plate and the resultant is assumed to lie in the middle plane of the plate.

5.2 Representation of Initial Imperfections

As for the columns, the actual imperfection function should be represented as a series in terms of the eigenfunctions of the related eigenvalue problem. In general these eigenfunctions or eignmodes will have to be determined, either analytically or numerically, before the imperfection analysis is carried out. The related eigenvalue in the present case is the bifurcation buckling of a perfectly plane simply supported rectangular plate stressed uniformly in the x direction. As mentioned before, the solution of this eigenvalue problem is well known for elastic and plastic cases, The eigenmodes for this problem (whether elastic or plastic) are of the form $K_{mn}\sin\frac{m\pi x}{L}\sin\frac{n\pi y}{B}$, i.e. of a Fourier series form, where m and n are numbers of half sine waves in x and y directions respectively. For the critical bifurcation mode there is only one half sine wave in the y direction, i.e., $n = 1$. Therefore, for an imperfection growth analysis, the imperfection should be expressed in the form:

$$w_o(x, y) = (\sum_{m=1}^{\infty} A_m \sin\frac{m\pi x}{L}) \sin\frac{\pi y}{B} \tag{5.3}$$

where the coefficients A_m can be determined from the experimental data as explained below.

In the experiments the imperfection profiles were obtained from measurements on the sides of the tubular specimens. Out-of-plane deviations were measured along the longitudinal centre lines of the four sides of the tubular specimens, and were then averaged. Thus, if for a specimen, the averaged deviations along the longitudinal centre lines are expressed as $\phi(x)$, then the initial imperfections as functions of x and y are expressible as

$$w_o(x,\, y) = \phi(x)\psi(y) \tag{5.4}$$

where $\psi(y)$ is a function related to these deviations in the transverse direction. In the absence of any widthwise measurements of the imperfections, the function $\psi(y)$ is assumed here a half sine wave, i.e., $\psi(y) = \sin\frac{\pi y}{B}$, which is a reasonable assumption, since the imperfections must be zero at the ends $y = 0, B$, and should be maximum near or at the centre line $y = B/2$. Thus,

$$w_o(x,\, y) = \phi(x)\, \sin\frac{\pi y}{B} \tag{5.5}$$

The function $\phi(x)$ represents the initial imperfections as a continuous function of x, although in fact, it is known only at discrete measurement points. The transition from discrete to continuous is accomplished here by using the Lagrange interpolation polynomials. For each specimen, nine measurements were made, excluding the two end points, corresponding to $\phi(0) = \phi(L) = 0$. Let the sets of experimentally measured values be denoted as (x_1, ϕ_1), $(x_2, \phi_2), \ldots (x_{10}, \phi_{10})$, (x_{11}, ϕ_{11}). Then by assuming $\phi(x)$ to be a tenth degree polynomial, one may represent it as

$$\phi(x) = N_1\phi_1 + N_2\phi_2 + \ldots + N_{10}\phi_{10} + N_{11}\phi_{11} \tag{5.6}$$

where N_i are the standard Lagrange's interpolation polynomials.

$$N_1 = \frac{(x-x_2)(x-x_3)(x-x_4)(x-x_5)(x-x_6)(x-x_7)(x-x_8)(x-x_9)(x-x_{10})(x-x_{11})}{(x_1-x_2)(x_1-x_3)(x_1-x_4)(x_1-x_5)(x_1-x_6)(x_1-x_7)(x_1-x_8)(x_1-x_9)(x_1-x_{10})(x_1-x_{11})}$$

$$N_2 = \frac{(x-x_1)(x-x_3)(x-x_4)(x-x_5)(x-x_6)(x-x_7)(x-x_8)(x-x_9)(x-x_{10})(x-x_{11})}{(x_2-x_1)(x_2-x_3)(x_2-x_4)(x_2-x_5)(x_2-x_6)(x_2-x_7)(x_2-x_8)(x_2-x_9)(x_2-x_{10})(x_2-x_{11})}$$

...

In this thesis, 5 typical specimens with different B/t ratio and different initial imperfection were chosen. The smoothened imperfection profiles $\phi(x)$ for these specimens are shown in Figs. 5.4 to 5.8.

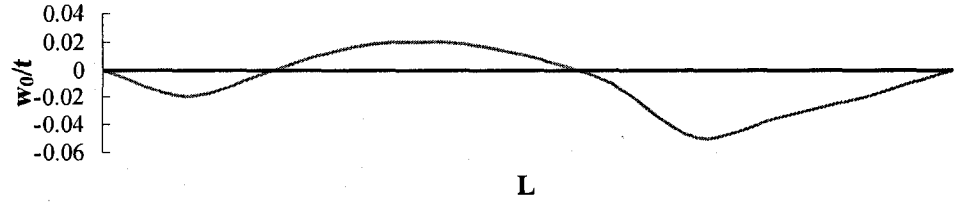

Fig. 5.4 Initial imperfection profile of specimen 03 ($L/B = 5$, $B/t = 40.38$)

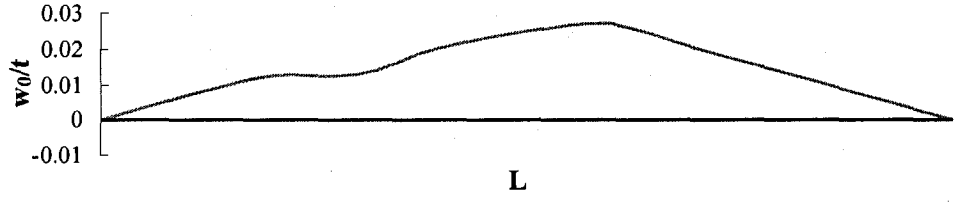

Fig. 5.5 Initial imperfection profile of specimen 04 ($L/B = 5$, $B/t = 27.88$)

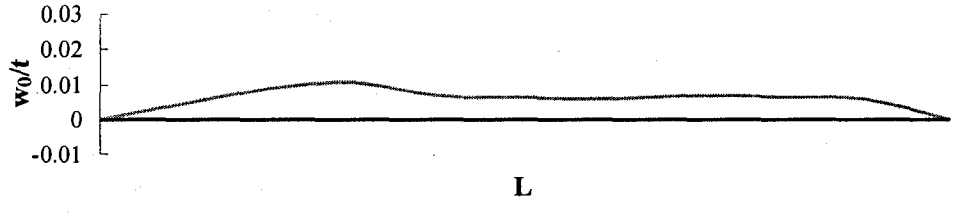

Fig. 5.6 Initial imperfection profile of specimen 08 ($L/B = 5$, $B/t = 23.95$)

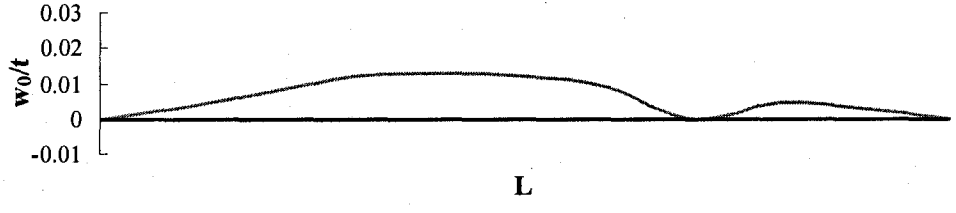

Fig. 5.7 Initial imperfection profile of specimen 11 ($L/B = 5$, $B/t = 20.21$)

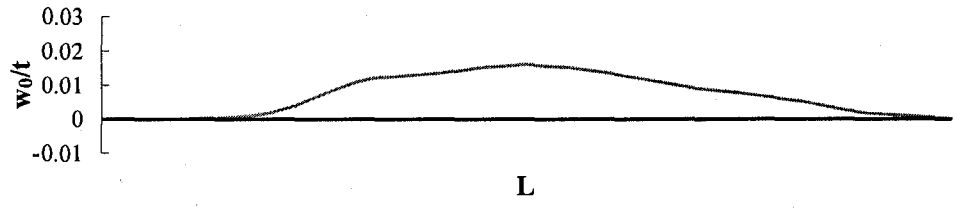

Fig. 5.8 Initial imperfection profile of specimen 14 ($L/B = 5$, $B/t = 17.01$)

Having obtained $\phi(x)$ as a continuous function, the coefficients A_m, i.e., the amplitudes of the sine waves of different wavelengths can be determined from the standard formula

$$A_m = \frac{2}{L}\int_0^L \phi(x) \sin\frac{m\pi x}{L} dx \tag{5.7}$$

Thus, the imperfections are known in the desired form:

$$w_o(x, y) = (\sum_{m=1}^{\infty} A_m \sin\frac{m\pi x}{L}) \sin\frac{\pi y}{B} \tag{5.8}$$

Although in the analysis, one may use several eigenmodes starting with m equal to 1, the mode which grows fastest is that corresponding to the critical (i.e., the lowest) bifurcation load. Therefore, as demonstrated in the case of columns, it was considered sufficient to consider only that one mode of the imperfection.

Based on the experimental stress-strain relation and the dimensions of the specimens, the critical bifurcation mode [36] was found to consists of 7 half waves along the longitudinal coordinate for both the incremental and deformation theories of plasticity. Therefore $m = 7$ in the above formula, and for the growth analysis

$$w_o(x, y) = A_7 \sin\frac{7\pi x}{L} \sin\frac{\pi x}{L} \tag{5.9}$$

where

$$A_7 = \frac{2}{L}\int_0^L \phi(x) \sin\frac{7\pi x}{L} dx \tag{5.10}$$

5.3 Numerical Results

The load-deflection curves corresponding to the J_2 incremental and J_2 deformation plasticity theories were computed by using the constructed programs for the chosen specimens. They are shown in the same figure for easy and explicit comparison with corresponding bifurcation stresses, Fig. 5.9 to Fig. 5.13.

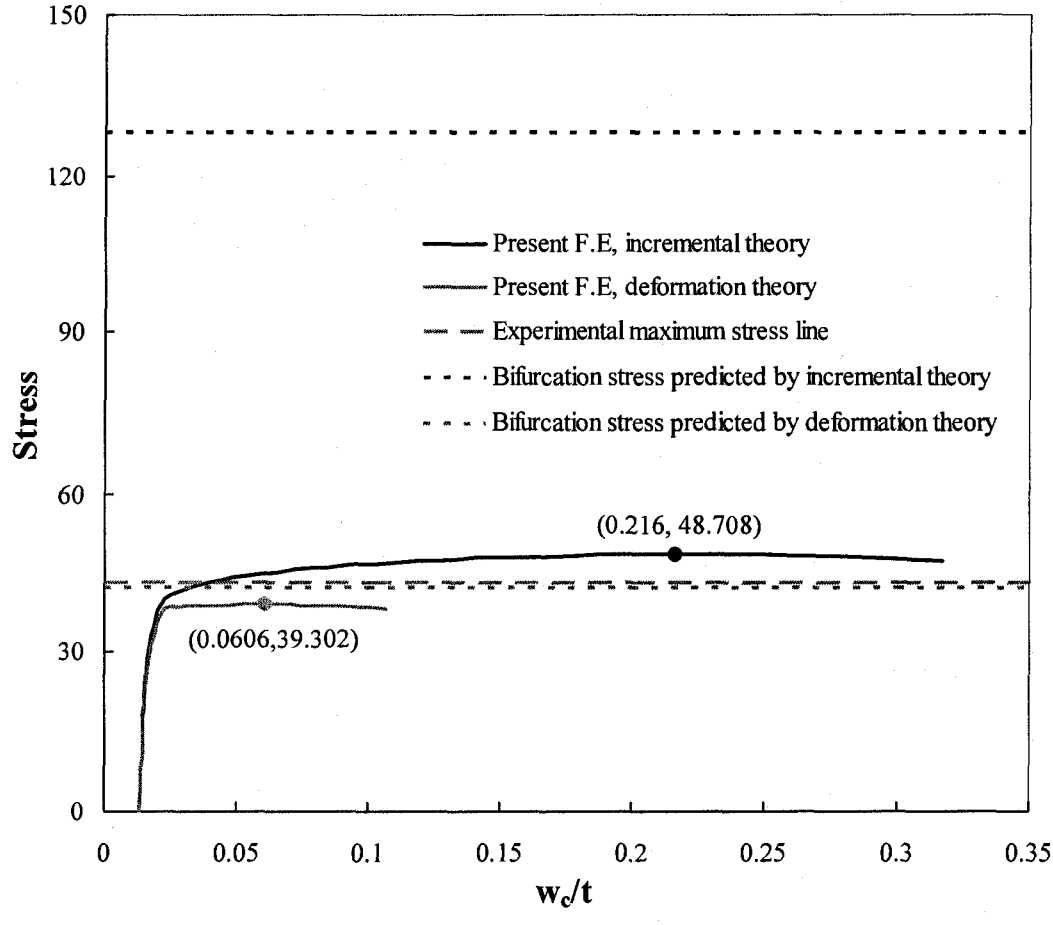

Fig. 5.9 Imperfection growth curves for specimen 03

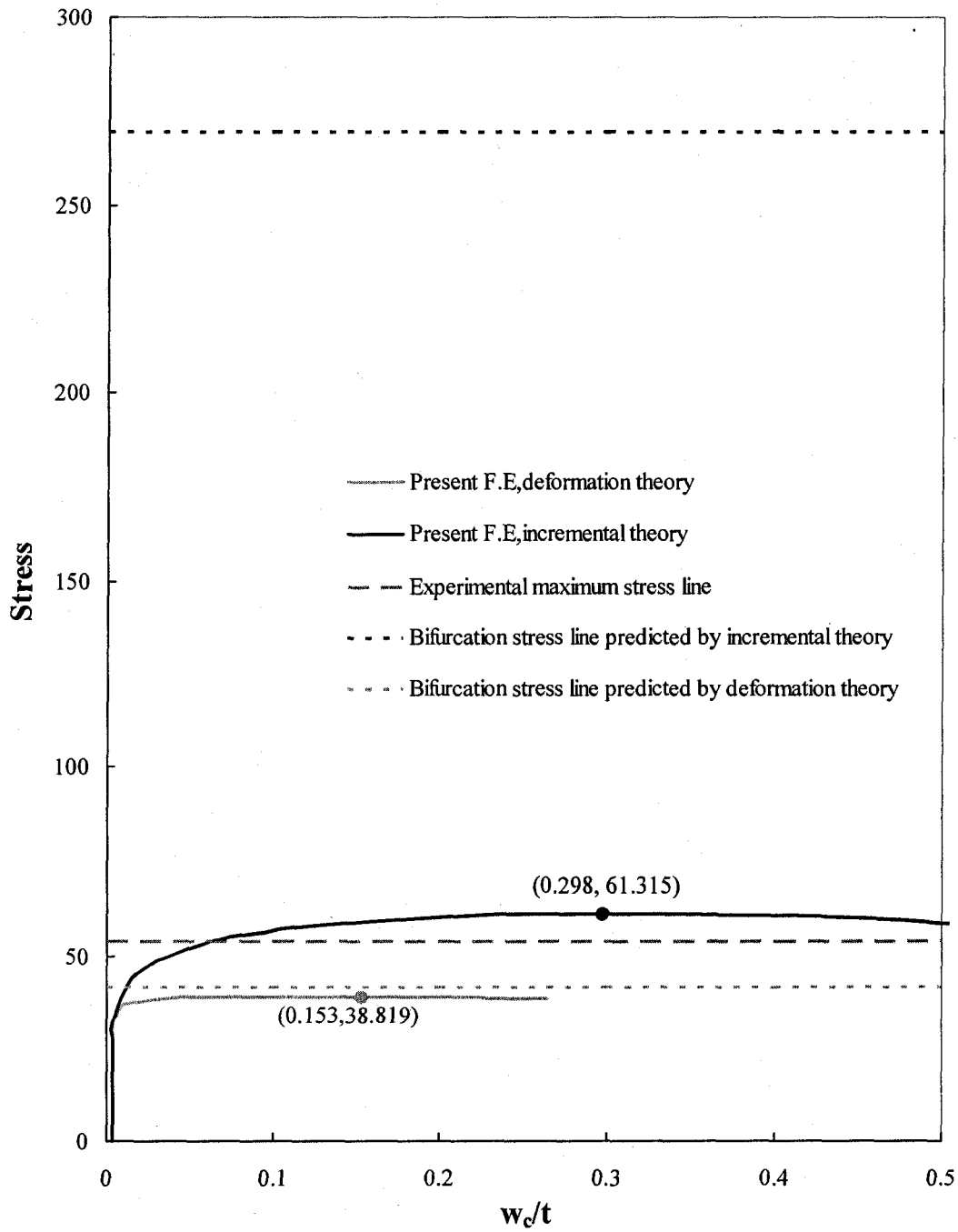

Fig. 5.10 Imperfection growth curves for specimen 04

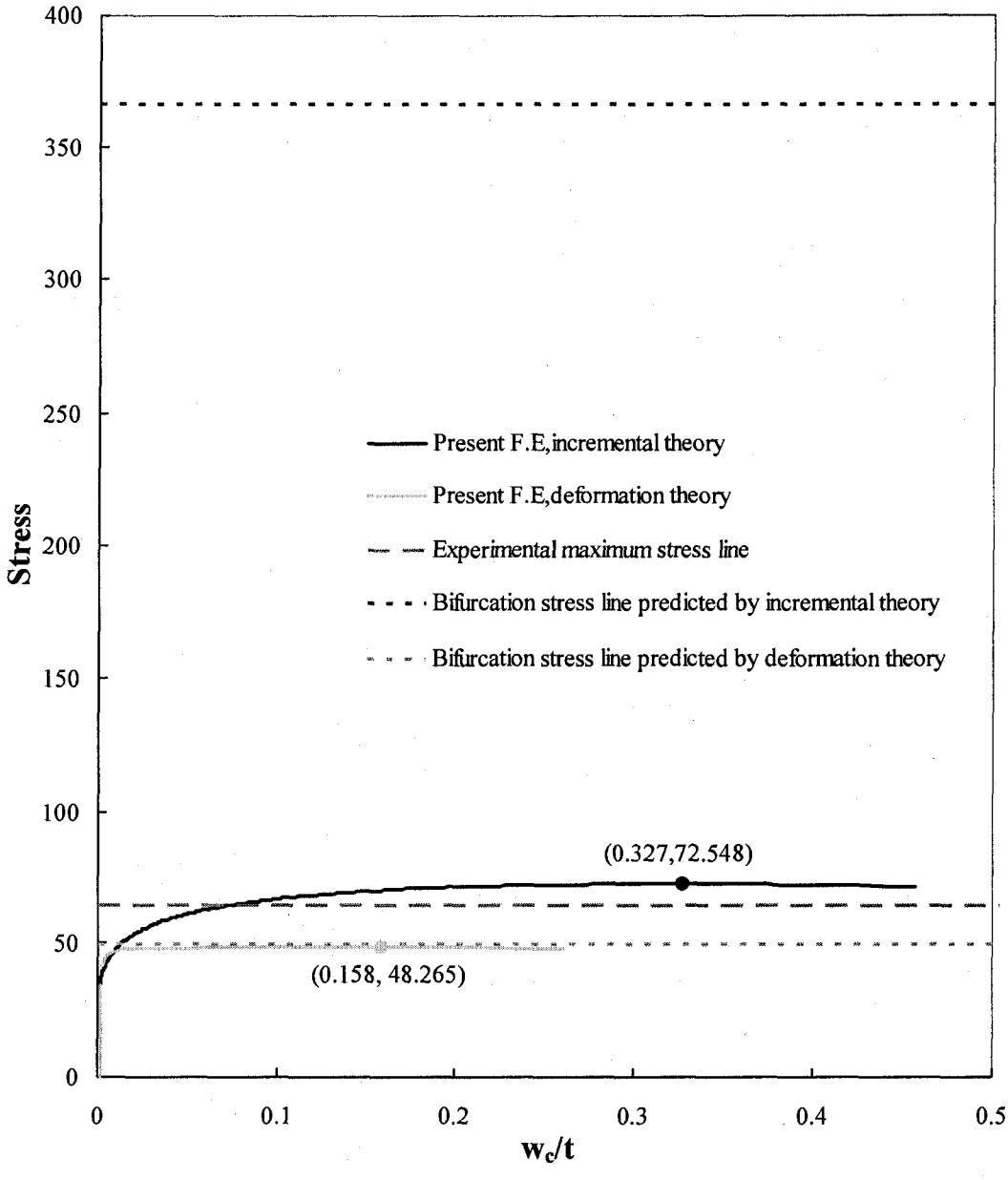

Fig. 5.11 Imperfection growth curves for specimen 08

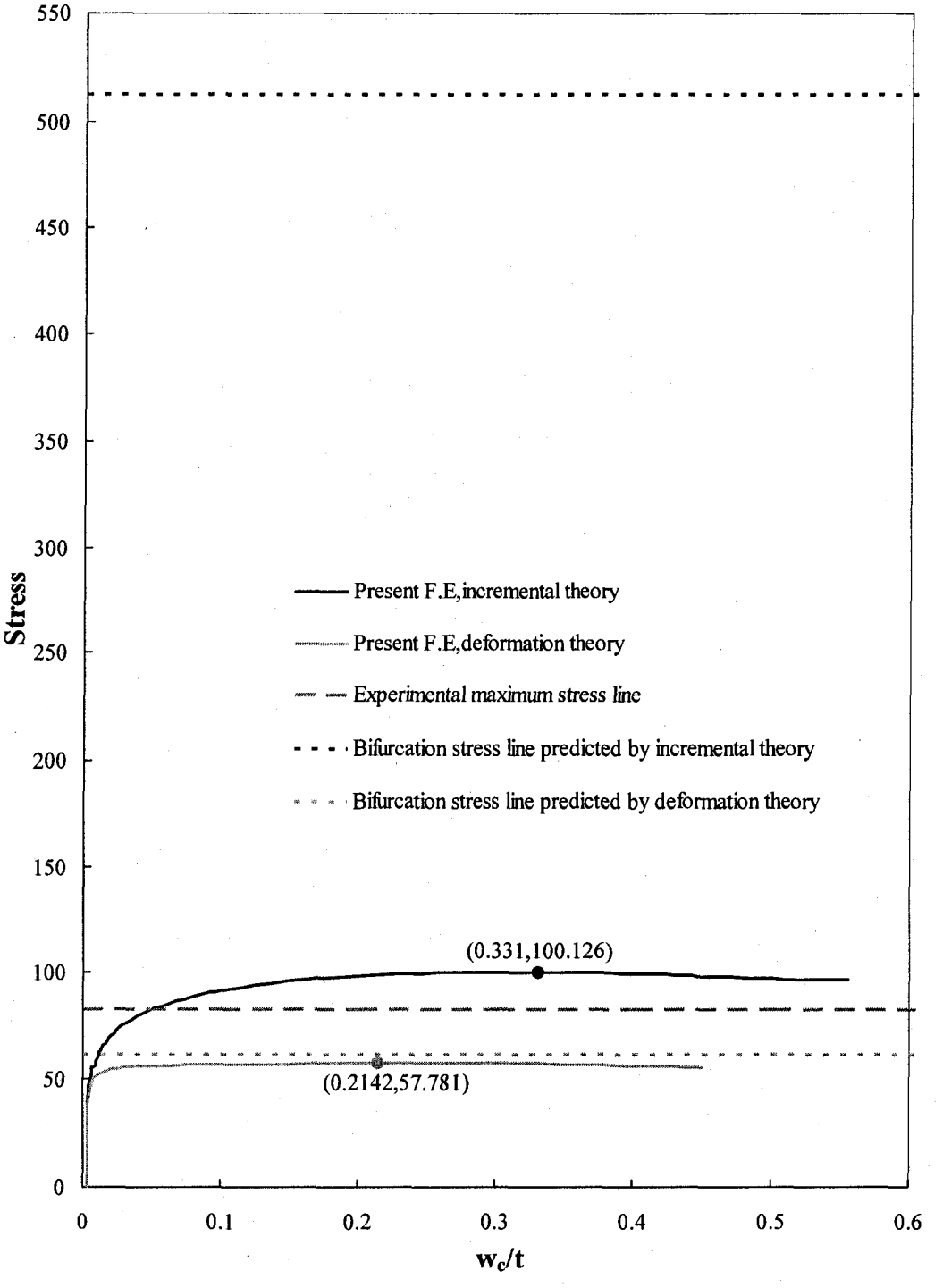

Fig. 5.12 Imperfection growth curves for specimen 11

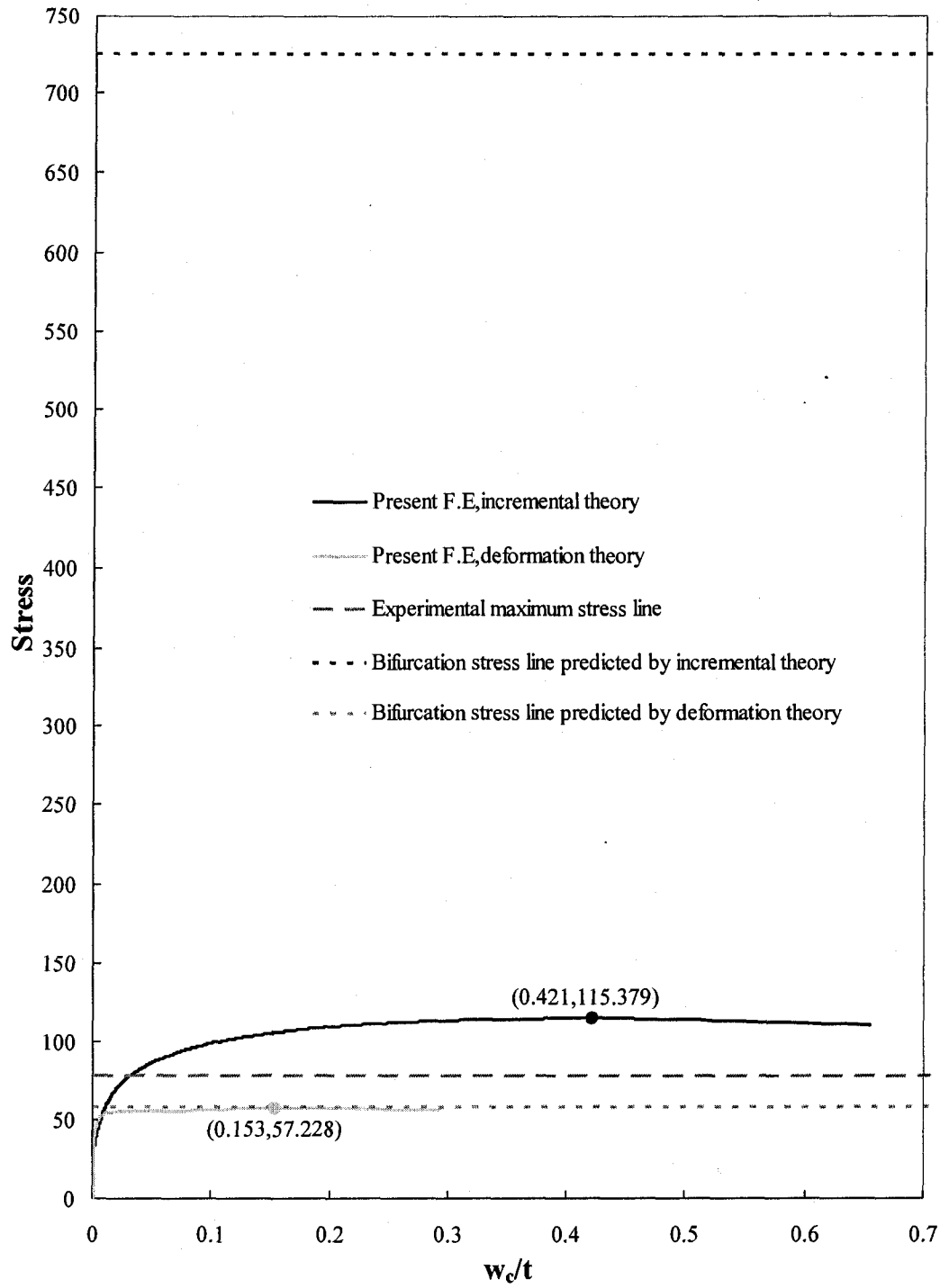

Fig. 5.13 Imperfection growth curves for specimen 14

The above results are summarized in a tabular form in Tables 5.1 and 5.2.

Table 5.1 Comparison of the J_2 incremental theory maximum stresses with experimental results

Specimen	B/t	L/B	σ_{cr}^{inc}(MPa)	σ_{max}^{exp} (MPa)	σ_{max}^{inc}(MPa)	$\frac{\sigma_{max}^{inc}}{\sigma_{cr}^{inc}}$	$\frac{\sigma_{max}^{inc}}{\sigma_{max}^{exp}}$
03	40.38	5	128.4	43.24	48.708	0.379	1.126
04	27.88	5	269.3	54.13	61.315	0.228	1.132
08	23.95	5	366.0	64.48	72.548	0.198	1.125
11	20.21	5	512.6	82.49	100.126	0.195	1.214
14	17.01	5	725.7	78.09	115.379	0.159	1.478

Table 5.2 Comparison of the J_2 deformation theory maximum stresses with experimental results

Specimen	B/t	L/B	σ_{cr}^{def}(MPa)	σ_{max}^{exp} (MPa)	σ_{max}^{def}(MPa)	$\frac{\sigma_{max}^{def}}{\sigma_{cr}^{def}}$	$\frac{\sigma_{max}^{def}}{\sigma_{max}^{exp}}$
03	40.38	5	42.3	43.24	39.302	0.929	0.909
04	27.88	5	41.6	54.13	38.819	0.933	0.717
08	23.95	5	49.7	64.48	48.954	0.985	0.759
11	20.21	5	61.7	82.49	57.781	0.936	0.700
14	17.01	5	58.6	78.09	57.228	0.983	0.733

From these five figures and the two tables, the following conclusions may be drawn:

(1) The imperfections significantly reduce the maximum loads which can be attained. The maximum stresses based on the J_2 incremental theory are much less than their corresponding bifurcation stresses. However, these maximum stresses are close (but still above), the experimental results. The maximum load predicted for specimen 14 is significantly high. Perhaps a different value of m (other than 7), or an imperfection representation with several sine terms starting with $m = 1$, could bring the maximum load value lower. Also, a refined mesh might bring down the maximum loads. However, in view of the time and resource constraints, these suggestions were not tried. The point

has already been made in Chapter 4 that the maximum loads of the incremental theory can be brought down below the bifurcation loads of the deformation theory which, as reiterated below, are generally lower than the experimental buckling (i.e., maximum) loads.

(2) The maximum stresses calculated by using the J_2 deformation theory are also lower than the corresponding bifurcation stresses, but not dramatically, Moreover these maximum stresses are lower than the experimental results. The deformation theory gives conservative estimates of the maximum loads.

(3) Comparing the ratios of the maximum stress to the bifurcation stresses, it is clear that the J_2 incremental theory is much more imperfection sensitive than is the case with the J_2 deformation theory. Thus, a known theoretical conclusion has now been proved by the experimental data.

5.4 Discrepancy Analysis

Having presented a full discussion of the numerical results in section 5.2, the purpose of the present section is to seek reasons for discrepancies among the maximum load predictions based on the numerically obtained theoretical results and the experiments. The theoretical results are based on certain ideal assumptions of material behaviour, perfect support conditions, and imperfections derived from experimental data. The experiments, on the other hand, do not entirely fulfill these ideal conditions.

5.4.1 Effect of Material Properties

Although all specimens were annealed at 420° C for 2 hours to minimize or eliminate some defects, the material might still not have been ideally isotropic and homogeneous as the theoretical postulates require.

The annealing process might not have been identical from one batch to the next due to the fact that the oven size was small, and that not all samples could be annealed at the same time. Therefore, conceivably, the specimens ended up possessing different material characteristics despite the fact that the nominal conditions for annealing were identical. Thus, no unique stress-strain curve for the material could be defined for the compression behaviour.

5.4.2 Geometric Imperfections

In the theoretical bifurcation analysis, the plates are assumed to have uniform thickness and be perfectly plane and rectangular. In finite element analysis, only the out of plane imperfections were simulated, and possible thickness, width, and length variations were neglected. However, as recorded in Berrada's thesis [12], the maximum cross-sectional thickness variations were up to 9%. These imperfections might have affected the maximum stresses reached in experiments,.

5.4.3 Effects of Boundary Conditions

Hollow square tubes were chosen in the experiment to simulate the simple support condition at the unloaded edges. However, the success of this method greatly depends on the magnitude and type of imperfections present in the tube, and also on the adequate provision of simple supports along the loaded edge of the plates. Imperfections such as thickness and width variations, out-of-plane deviations, and lack of square-ness at the corners can all cause discrepancies from the ideal behaviour.

The friction forces between the loading plates and specimens, Fig. 5.14, causes the prebuckling state of stress to be strictly not of pure compression at the loaded edges. This effect can be quite significant if the specimen undergoes large plastic strains prior to buckling.

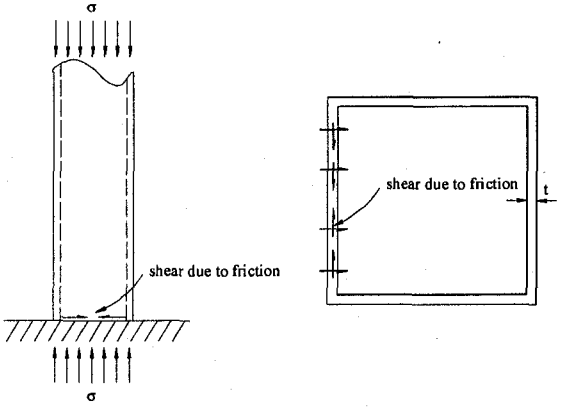

Fig. 5.14 Friction force along the loaded edges

In the majority of experimental cases, the imperfect boundary conditions (created by the presence of friction and lack of freedom for expansion of the tubes) might have had much more effect on the buckling shapes than that of the out-of-plane deviations. It may be difficult to simulate the same boundary conditions as the experimental ones, because it is difficult to know the real boundary conditions during loading of the specimens.

5.4.4 Effects of Eccentricity

In theory and in finite element analyses, pure compression is required for loading. In experiments, despite the efforts to keep the loading axis coincident with the geometric centre line of the tubular specimens, eccentricities might still have existed because the mass centres might not have been the same as the geometric centres due to imperfections.

Chapter 6

Conclusions and Future Work

6.1 Conclusions

Imperfection growth analyses, taking into account the experimentally measured initial out-of-plane imperfections, and the elastic-plastic behaviour based on the von Mises yield criterion with isotropic strain-hardening, have been carried out for axially compressed simply supported plates. The FE programs constructed by the author for this purpose, are based on the standard kinematic assumptions of the thin plate theories, and the constitutive laws of the J_2 incremental and J_2 deformation theories of plasticity. Results are obtained for both plasticity theories in order to compare them against each other, and with experiments.

As a forerunner to the plate buckling problems, the elastic-plastic postbuckling behaviour of columns is studied in chapter 3. As expected, there is virtually no difference between the maximum load predictions of the two plasticity theories for simply supported columns obeying the Bernoulli-Euler kinematic assumption. In the particular case of (one dimensional) column buckling, if there is no unloading, the two theories are exactly the same despite the apparently different forms of their constitutive relations.

The plates are treated in a parallel fashion in Chapter 4. The treatment is necessarily more complex than that for columns. The FE programs constructed by the author, were used in predicting the buckling and the postbuckling behaviours of 14S-T6 aluminum alloy square plates with $B/t = 18$, 23, and rectangular plates with $L/B = 5$, $B/t = 18$, 23. Both geometric and material nonlinearities are considered in the imperfection growth analyses. Incremental load-displacement method is used for the incremental theory, and the total one for the deformation theory. It is found that unlike the elastic postbuckling paths, the plastic postbuckling paths are invariably unstable. In other words, the displacements increase under decreasing load.

Also, the two plasticity theories gave quite different predictions for the maximum load. The J_2 incremental theory is much more imperfection sensitive than the J_2 deformation

theory. In contrast to the large differences between the bifurcation loads, the differences between the maximum load predictions can be reduced to less than 6% if imperfections are considered in the FE programs. In addition, results of the incremental theory are more imperfection sensitive for thicker plates; the plate with $B/t = 18$ is more imperfection sensitive than that with $B/t = 23$. This means that for this theory the imperfection sensitivity is increased with the increased buckling strains. For most cases considered in this chapter the maximum loads of the incremental theory were lower than the bifurcation loads of the deformation theory. The deformation theory, in contrast, is found to be not as imperfection sensitive, and the maximum loads predicted by this theory for the imperfect plates are not very much lower than the bifurcation loads.

Chapter 5 is concerned with the experimental validation of the two competing theories. Finite element simulations of the buckling experiments of Berrada [12] were performed in this study. Based on the measured initial out-of-plane imperfections, and the stress-strain curves (load versus end-shortening curves) recorded for each specimen, the load-deflection behaviour of five specimens for $L/B = 5$ and $B/t = 40.38$, 27.88, 23.95, 20.21, 17.01 were traced by the constructed FE programs. The FE results for the J_2 incremental theory are dramatically lower than the bifurcation stresses, but quite close to the experimental results (Table 5.1). If other geometric imperfections, material imperfections, and realistic boundary conditions were to be taken into account, it is reasonable to say that the maximum stresses by incremental theory could be lowered to the experimental results.

The maximum stresses calculated by the J_2 deformation theory are also lower than the corresponding bifurcation stresses, but not dramatically. Moreover these maximum stresses are lower than the experimental results. Therefore, there is substantial disagreement between the maximum stress prediction of the J_2 deformation theory and the experimentally observed maximum stresses, particularly for specimens buckling at large plastic strains (Table 5.2). This means that insofar as the buckling of simply supported rectangular plates in uniaxial compression is concerned, the so called "Plastic Buckling Paradox" does not exist since it has been shown that the maximum stresses predicted by the correct theory, the incremental theory, can be brought in close agreement with the experimental results by taking into account the small imperfections of the real plates. The maximum stresses predicted by the deformation theory are lower than the experimentally observed values, and cannot be increased to match them.

6.2 Future Work

For the sake of firmly establishing the above conclusions which are based on the experimental results and FE simulations, more realistic material imperfections and geometric imperfections should be included in the FE programs, for example, the residual stresses, variations in width, cross-sectional thickness, and the presence of the friction forces along the loaded edges, etc.

On the experimental side, one needs to make every effort to implement the proper boundary conditions, since they seem to play an important role in influencing the buckling behaviour of the specimens.

REFERENCES

[1] Pride, R. A. and G. J. Heimerl, Plastic buckling of simply supported compressed plates, NACA, Tech. Note No.1817 (1949).

[2] Gerard, G. and H. Becker, Handbook of structural stability: Part1- Buckling of flat plates, NACA, Tech. Note No. 3781 (1957).

[3] Shanley, F. R., Inelastic Column Theory, Journal of the Aeronutical Sciences, Vol. 14, pp. 261-267 (1947).

[4] Hutchinson, J. W., Plastic buckling, Advances in Applied Mechanics, Vol. 14, pp. 67-144. Academic Press, New York (1974).

[5] Onat, E. T. and D. C. Drucker, Inelastic instability and incremental theories of plasticity. Journal of the Aeronutical Sciences, Vol. 20, pp. 181-186 (1953).

[6] Sewell, M. J., A general theory of elastic and inelastic plate failure-I. Journal of the Mechanics and Physics of Solids. Vol. 11, pp. 377-393 (1963).

[7] Sewell, M. J., A general theory of elastic and inelastic plate failure-II. Journal of the Mechanics and Physics of Solids. Vol. 12, pp. 279-279 (1964).

[8] Sewell, M. J., A yield-surface corner lowers the buckling stress of an elastic-plastic plate under compression. Journal of the Mechanics and Physics of Solids. Vol. 21, pp. 19 (1973).

[9] Neale, K. W., Journal of Applied Mechanics. Vol. 47, pp. 115-116 (1975).

[10] Needleman, A. and V. Tvergaard, An analysis of the imperfection-sensitivity of square elastic-plastic plates under axial compression. Inteernational Journal of Solids and Structures, Vol.12, pp.185-201 (1976).

[11] Hutchinson, J. W., Postbifurcation behaviour in the plastic range, Journal of the Mechanics and Physics of Solids. Vol. 21, pp. 163-190 (1973).

[12] Berrada, K, An experimental investigation of the plastic buckling of aluminum plates. M.Eng thesis, McGill University, Montreal (1985).

[13] Turner, M. J., E. H. Dill, H. C. Martin, and R. J. Melosh, Large deflections of structures subjected to heating and external loads, Journal of Aerospace Sciences, Vol. 17 (1960).

[14] Gallagher, R. J. and J. Padlog, Discrete element approach to structural stability. AIAA Journal, Vol.1, No.6, pp. 1437-1439 (1963).

[15] Gallagher, R. H., Stability of plates using the finite element method, Proceedings, Journal of the Engineering Mechanics Division, ASCE, Vol. 93, No. EM1, pp. 80-83, (1967).

[16] Hartz, B. J., Matrix formulation of structural stability problems, Proceedings, Journal of the Structural Division, ASCE, Vol. 91, No. 6, pp. 141-157 (1965).

[17] Kapur, K. K., and B. J. Hartz, Stability of plates using the finite element method, Proceedings, Journal of the Engineering Mechanics Division, ASCE, Vol. 93, No. EM2, Paper 4790 (1966).

[18] Yang, T. Y., Finite displacement plate flexure by the use of matrix incremental approach. International Journal for Numerical Methods in Engineering, Vol. 4, pp. 415-432 (1972).

[19] Mallet, R. H. and P. V. Marcal. Finite element analysis of non-linear structures. Journal of the Structural Division, ASCE, Vol. 94, No. ST9, pp. 2081-2105 (1968).

[20] Dupius, G. A., H. D. Hibbit, S. F. Mcnamara and P. V. Marcal. Non-linear material and geometric behaviour of shell structurs. Computers and Structures, Vol.1, pp 223-239 (1971).

[21] Oden, J. T. Numerical formulation of non-linear elasticity problems. Journal of the Structural Division, ASCE, Vol.93, No.ST3 (1967).

[22] Murray, D. W. and E. L. Wilson, Finite element postbuckling analysis of thin elastic plates, AIAA Journal, Vol. 7, pp. 1915-1930 (1969).

[23] Brebbia, C. and J. Connor, Geometrically non-linear finite element analysis. Journal of the Engineering Mechanics Division, ASCE, Paper 6516 (1969).

[24] Zienkiewicz, O. C. The finite element in engineering science. Mcgraw-Hill, London (1971).

[25] Nayak, G. C. and O. C. Zienkiewicz, Elasto-plastic analysis. As generation for various constitutive relationships including strain softening. International Journal for Numerical Methods in Engineering, Vol. 5, pp.113-135 (1972).

[26] Zienkiewicz, O. C., S. Valliapan and I. P. King, Elasto-plastic solutions of engineering problems. Initial stress, finite element approach. International Journal for Numerical Methods in Engineering, Vol. 1, pp. 75-100 (1969).

[27] H. A. El-Ghazaly and A. N. Sherbourne, Deformation theory for elasto-plastic buckling analysis of plates under nonproportional planar loading, Computers and Strucrures, Vol. 22, pp. 131-149 (1986).

[28] Terazawa, K., Y. Ueda and M. Matsuishi, Elasto-plastic buckling of plates by finite element method. ASCE Annual Meeting and National Meeting on Water Resouces Engineering, New Orleans, La., Paper 845 (1969).

[29] Harris, H. G. and A. B. Pifko, Elastoplastic buckling of stiffened rectangular plates. Proc. Symp. on Application of Finite Element methods in Civil Eng., School of Engineering, Vanderbilt University, ASCE, pp. 207-253 (1969).

[30] Stowell, E. Z., A unified theory of plastic buckling of columns and plates. Tech. Note-1556, NASA (1948).

[31] Ilyushin, A. A., The elasto-plastic stability of plates. NACA Technical Memorandum No. 1188 (1947).

[32] Murry, D. W. and E. L. Wilson, An approximate non-linear analysis of thin plates. Air Force 2nd Conf. on Matrix Meth. in Struct. Mech., Wright-Patterson Air Force Base, Ohio (1968).

[33] Stricklin, J. A., W. E. Haisler and W. A. Von Riesemann, Computation and solution procedures for non-linear analysis by conbined finite element-finite difference methods. Computers and Structures., Vol. 2, pp. 995-974 (1972).

[34] M. A. Crisfield, Large deflection elastoplastic buckling analysis of plates using finite elements. Rep. LR 593 TRRL. U.K (1973).

[35] Hill, R. The mathematical theory of plasticity. Oxford University Press (1950).

[36] Shrivastava, S.C., Inelastic buckling of plates including shear effects. International Journal of Solids Structures, Vol. 15, pp.567-575 (1979).

[37] Wood, R.D. and B. Schrefler, Geometrically nonlinear analysis---a correlation of finite element notations. International Journal for Numerical Methods in Engineering Vol. 12, pp. 635-642 (1978).

[38] Zienkiewicz, O. C. and R.L. Taylor. The finite element method, 5th ed. Butterworth-Heinemann (2000).

[39] Tvergaard, V. and A. Needleman, On the buckling of elasticplastic columns with asymmetric cross-sections. International Journal of Mechanical Sciences. Vol. 17, pp. 419-424 (1975).

[40] Burgoynne, C. and M. A. Crisfield, Numerical integration strategy for plates and shells, International Journal for Numerical Methods in Engineering, pp. 105-121 (1990).

[41] Cook, R. D., D. S. Malkus, M. E. Plesha and R. J. Witt. Concepts and applications of finite element analysis, 4th ed. John Wiley & Sons, New York (2002).

[42] Timoshenko, S. P. and J. M. Gere, Theory of elastic stability, 2nd ed. McGraw-Hill, New York (1961).